EVALUATING THE EFFECTS OF HISTORICAL LAND COVER CHANGE ON SUMMERTIME WEATHER AND CLIMATE IN NEW JERSEY

By

PAUL STUART WICHANSKY

A dissertation submitted to the

Graduate School-New Brunswick

Rutgers, the State University of New Jersey

In partial fulfillment of the requirements

For the degree of

Doctor of Philosophy

Graduate Program in Environmental Sciences

Written under the direction of

Christopher P. Weaver

And approved by

New Brunswick, New Jersey

May 2008

ABSTRACT OF THE DISSERTATION

EVALUATING THE EFFECTS OF HISTORICAL LAND COVER CHANGE ON SUMMERTIME WEATHER AND CLIMATE IN NEW JERSEY

By

PAUL STUART WICHANSKY

Dissertation Director:
Christopher P. Weaver

The 19th-century agrarian landscape of New Jersey (NJ) and the surrounding region has been extensively transformed to the present-day land cover by urbanization, reforestation, and localized areas of deforestation. This study used a mesoscale atmospheric numerical model to investigate the sensitivity of the warm season climate of NJ to these land cover changes. Reconstructed 1880s-era and present-day land cover datasets were used as surface boundary conditions for a set of simulations performed with the Regional Atmospheric Modeling System (RAMS). Three-member ensembles with historical and present-day land cover were compared to examine the sensitivity of surface air and dewpoint temperatures, rainfall, the individual components of the surface energy budget, horizontal and vertical winds, and the vertical profiles of temperature and humidity to these land cover changes.

Mean temperatures for the present-day landscape were 0.3-0.6°C warmer than for the historical landscape over a considerable portion of NJ and the surrounding region, with daily maximum temperatures at least 1.0°C warmer over some of the highly urbanized locations. Reforested regions in the present-day landscape, however, showed a slight cooling. Surface warming was generally associated with repartitioning of net radiation from latent to sensible heat flux, and conversely for cooling. Reduced evapotranspiration from much of the present-day land surface led to dewpoint temperature decreases of 0.3-0.6°C. While urbanization was accompanied by strong surface albedo decreases and increases in net shortwave radiation, reforestation and potential changes in forest composition have generally increased albedos and also enhanced landscape heterogeneity. The increased deciduousness of forests may have further reduced net downward longwave radiation.

These land cover changes have modified boundary-layer dynamics by increasing low-level convergence and upper-level divergence in the interior of NJ, especially where sensible heat fluxes have increased for the present-day landscape, hence enhancing uplift in the mid-troposphere. The mesoscale circulations that developed in the present-day ensemble were also more effective at lifting available moisture to higher levels of the boundary layer, lowering dewpoints near the surface but increasing them aloft. Likewise, the sea breeze in coastal areas of NJ in the present-day ensemble had stronger uplift during the afternoon and enhanced moisture transport to higher levels.

ACKNOWLEDGEMENTS / DEDICATION

This research was sponsored by a grant from the New Jersey Agricultural Experiment Station (NJAES), as part of the 2001 NJAES Graduate Scholar Program. The research and preparation of this study have also been supported by a grant from the NASA Goddard Space Flight Center, Biospheric Sciences Branch, through their Landsat Data Continuity Mission project. I thank David Robinson, Peter Wacker, and Mark Demitroff for their knowledge of New Jersey land cover, and James Irons for his support. Finally, I extend an appreciation to Dr. George H. Cook and Cornelius C. Vermeule, because without their true commitment and dedication to mapping New Jersey in the late 19th century, my land cover change project would likely have proved much more difficult, if not impossible.

I owe a huge debt of gratitude to my graduate advisor Christopher Weaver for his strong and unwavering guidance and support in my pursuit of the doctorate degree in addition to his constant encouragement to refine my analytical and critical-thinking skills that are essential in the field. It has also been an honor for me to work with Louis Steyaert and Robert Walko, as they have both motivated me to appreciate the scope of interpreting land cover datasets as well as master one of the main numerical tools designed to evaluate the effects of land cover change. In this regard, Chris, Lou, and Bob have become my role models and Heroes, because I want to one day be able to inspire and encourage future meteorology students with the same contagious passion that each of them have instilled in me. I also thank Alan Robock and Anthony Broccoli for serving on my Ph.D committee and for offering guidance, in addition to Anthony's constructive critiques during my internship at the Geophysical Fluid Dynamics Laboratory all those

years ago. Though I was officially a meteorologist when I graduated Cook College, I feel that I have not intellectually earned this title until I had written my Masters thesis on northeastern snowstorms as well as the Ph.D. thesis you are about to read.

This dedication would not be complete without first thanking the faculty and administrators at Rutgers, including Barbara Sirman, Robert Hills, and Carol Rutgers, for their inspiration and positive reinforcement over the years. Nathan Reiss and Roni Avissar deserve mention too, as they always believed in my academic success, which helped me believe in myself. My numerous friends and fellow graduate students were always there when I needed them through the good times and the bad times as well. Nevertheless, the most important people in my life have been my parents, my sister Suzanne, and my little brothers Ian and Alex, and for this reason, I am dedicating the thesis to them. They have provided constant love and emotional support in my academic and personal growth at Rutgers here during the last 19 years, so they deserve a hearty thank-you for helping me in the transition from the Paul that I know (the learner/student of today) so that I can confidently become the leader of tomorrow.

It is true that realizing my dream of walking has been one of the proudest moments in my life, convincing me that each one of us can be heroes: ordinary people who triumph over extraordinary circumstances. My graduation with a doctorate degree from Rutgers University is also a significant milestone and it is in this proud moment that I reflect upon my nearly two decades at this school and the friends and family that have encouraged me to be the best Paul I can be! Some of them are no longer with us, but they deserve special recognition. I am also proud to still be living on the Rutgers campus that bears the name of the pioneer who documented New Jersey land cover: George H. Cook.

TABLE OF CONTENTS

TABLE OF CONTENTS *(continued)*

TABLE OF CONTENTS *(continued)*

PAGE

TABLE OF CONTENTS *(continued)*

PAGE

TABLE OF CONTENTS *(continued)*

LIST OF FIGURES

[1] The differences between the ensemble with present-day land cover minus the ensemble with historical land cover, for each grid 3 cell or a composite of grid 3 cells, for this and all subsequent figures as noted.

LIST OF FIGURES *(continued)*

LIST OF TABLES

CHAPTER 1 – Overview of Land Use and Land Cover Change Studies

1.1. Introduction

Although humans have continually shaped the landscape for centuries, it has only been within the past two decades that land use and land cover change (LULCC) has been widely recognized as a key proximate driving force of global environmental change [*Turner*, 2001]. With the clearing of native forests and wetlands, the expansion and shifts of agriculture, and the rise of urbanization, the human use of the land has produced a heterogeneous and fragmented global mosaic of semi-natural and manmade surfaces [*Meyer and Turner*, 1994; *Ramankutty and Foley*, 1999; *Klein Goldewijk*, 2001]. The physical modification of the landscape that accompanies land cover change, e.g., shifts in surface roughness, albedo, and leaf area index (LAI), alters the key land surface processes (radiation, energy, and soil moisture budgets) that modulate fluxes of heat and moisture at the surface and exchanges between the surface and lower atmosphere [e.g., *Segal and Arritt*, 1992], thereby influencing the biogeochemical cycles of water and carbon [*Claussen et al.*, 2001]. These changes may also affect surface air temperatures, atmospheric boundary-layer properties, convective rainfall, and soil moisture, which can influence surface weather and climate across a range of space and time scales [*Pielke*, 2001]. These changes can, in turn, exert controls on vegetation conditions and ecosystem structure and function, which may lead to feedbacks on land surface processes and interactions at the atmosphere-terrestrial interface [*Pielke et al.*, 1998; *Oleson et al.*, 2004].

During the past three decades, numerical studies and field programs have revealed that the variation in surface properties, most notably those related to vegetation and moisture, exerts a more controlling influence upon local and regional climate than once believed. The fractional vegetative cover first used in a numerical model by *Deardorff* [1978] provided the impetus to design and implement field experiments, such as the International Satellite Land Surface Climatology Project and its component, the Boreal Ecosystem-Atmosphere Study [*Sellers et al*., 1997]. These experiments were designed to improve our understanding of the energy and moisture exchange occurring between the lower atmosphere and the existing vegetation, allowing for the development of improved land surface parameterizations (at various spatial scales) in numerical models. The ongoing effort to more precisely quantify subgrid-scale vegetative processes reflects a drive to refine the surface representation in numerical models that would realistically simulate the mesoscale fluxes of heat, moisture, and momentum [*Avissar and Pielke*, 1989; *Avissar and Chen*, 1993; *Walko et al.*, 2000].

The landscape change that has occurred over historical time is expected to continue, and even accelerate, into the future, driven primarily by the effects of a rapidly growing world population and the anthropogenic pressures exerted on environmental and ecological systems by technological advances and economic development, with corresponding impacts on the physical climate system [*Feddema et al.*, 2005]. Though recent government-sponsored collaborative efforts, including the International Geosphere-Biosphere Program [IGBP; *Turner et al.*, 1993] and the Strategic Plan for the U.S. Climate Change Science Program [*CCSP*, 2003], have identified LULCC as a principal driver of regional and global climate, we need to document and understand the past drivers of LULCC [*NRC*, 2005] to better understand the range of potential impacts arising from current and possible future land use changes. Many empirical and numerical studies, as summarized in the following sections, have been designed to give us a better understanding of the effects of LULCC and its multi-scale interactions with the overlying atmosphere [*Pitman et al.*, 1999]. Land use planning strategies can then be incorporated to minimize the impacts of anticipated land use changes in this and other regions, effects that may be comparable regionally to those associated with increasing global concentrations of carbon dioxide [*Hansen et al.*, 1988; *Pielke*, 2001; *IPCC*, 2007].

In the following sections, I briefly review principal findings in the area of landscape change impacts on the atmosphere on a variety of scales, with a primary focus on model-based approaches.

1.2. Review of global- and continental-scale studies

The large-scale conversion of one type of land cover to another can modify the biophysical properties of the land surface, with the potential to affect atmospheric processes over similarly large scales, thereby leading to weather and climate shifts. Examples of model- (and some observation-) based studies of large-scale alterations of biophysical parameters due to LULCC include warming and rainfall pattern shifts resulting from deforestation in tropical regions [*Dickinson and Henderson-Sellers*, 1988; *Walker et al.*, 1995; *Claussen et al.*, 2001; *Chagnon et al.*, 2004; *Chagnon and Bras*, 2005] and cooling associated with mid-latitude reforestation (i.e., the change from grassland or mixed agriculture to deciduous forest) [*Sellers*, 1992; *Pitman*, 2003; *Beltrán*, 2005]. In addition, some numerical studies have suggested potential cooling due to replacement of pre-settlement vegetation with agriculture and other modern land cover types (e.g., pasture) [*Bonan*, 1997; *Betts*, 2001; *Zhao et al.*, 2001; *Bounoua et al.*, 2002; *Matthews et al.*, 2003; *Mahmood et al.*, 2004]. However, *Bonan et al.* [2007] found that simulated large-scale cooling associated with the mid-latitude conversion of forest to cropland was robust but its magnitude can be sensitive to the quality of the land surface datasets as well as the model physics. As computational power increases in the future, and model physics continue to be refined, the use of improved parameterizations of the land surface in large-scale numerical models, as well as studies that increasingly employ nested grids, would help us better understand the interactions between changes in albedo, evapotranspiration, and other regional land-atmosphere processes on large-scale climate.

1.3. Review of regional-scale studies

Regional climate modeling studies have also been used to investigate the potential consequences of land cover change on regional land-atmosphere interactions in particular areas [*Copeland et al.*, 1996; *Pielke*, 2001]. These empirical studies have investigated soil moisture depletion and warming due to overgrazing in the Sonoran desert [*Bryant et al.*, 1990; *Balling*, 1988]; changes in local cloudiness and rainfall due to landscape changes in Germany [*Mölders*, 2000]; reductions in summer rainfall, mesoscale circulation changes, and increased severity of winter freeze events due to historical LULCC in South Florida [*Pielke et al.*, 1999; *Marshall et al.*, 2003; *Marshall et al.*, 2004a, 2004b]; and the sensitivity of the lower atmosphere to changes in the fractional vegetation as estimated from the satellite-derived normalized difference vegetation index

(NDVI) [*Bounoua et al.*, 2000; *Zeng et al.*, 2000], roughness length [*Sud et al.*, 1988], and LAI [*Chase et al.*, 1996].

In addition to altering mean biophysical properties in a region, LULCC can also influence weather and climate due to changes in the spatial heterogeneity of the land cover and corresponding impacts on mesoscale circulations that affect surface temperatures, clouds, and rainfall. Empirical and numerical modeling studies have shown that the thermodynamic properties of the boundary layer can be affected by changes in the surface heterogeneity [*Anthes*, 1984; *Pielke et al.*, 1991; *Pielke and Avissar*, 1990; *Weaver and Avissar*, 2001] due to landscape patches on the order of 5–100 km which can induce the development of mesoscale circulations [*Avissar and Schmidt*, 1998; *Baidya Roy and Avissar*, 2000; *Baidya Roy et al.*, 2003a]. Numerical studies have examined the surface flux heterogeneities that induce the formation of these circulations [*Segal et al.*, 1988; *André et al.*, 1989; *Pielke et al.*, 1991; *Chen and Avissar*, 1994; *Lynn et al.*, 1995] and their effects on surface air temperatures, clouds, and rainfall [*Cutrim et al.*, 1995; *Avissar and Liu*, 1996; *Brown and Arnold*, 1998; *Weaver and Avissar*, 2001].

Many of these studies emphasize the importance of designing land surface schemes that can parameterize these impacts of subgrid-scale landscape heterogeneity in global-scale climate models. To date, however, it is only the influence of surface heterogeneity on the grid-cell mean land-atmosphere fluxes that is parameterized (e.g., via "mosaic of tiles" approaches as introduced in *Avissar and Pielke*, 1989) and not the full range of dynamical impacts on the boundary layer and lower free troposphere, which is a topic of ongoing research. Recent advances in multi-scale modeling frameworks (e.g., the so-called "superparameterization" approach, as described in *Randall et al.* [2003]) hold some promise for addressing this issue as well.

1.4. Urban growth and related landscape change effects

Urbanization is an extreme conversion of land cover within highly populated regions [*Taha*, 1997; *Arnfeld*, 2003]. The replacement or reduction of vegetated surfaces with pavement, buildings, and roofing materials, in addition to other land uses associated with population growth, modifies surface albedo and moisture availability to the soil and lower atmosphere, generally creating atmospheric islands of higher air temperature relative to the surrounding rural areas. Empirical studies have documented how urban growth during the 20th century has led to observed increases in the mean and diurnal minimum temperature in developed areas, and decreases in the diurnal temperature range [*Karl et al.*, 1988, 1993; *Gallo et al.*, 1996; *Gedzelman et al.*, 2003], creating the "urban heat island" (UHI) effect. *Kalnay and Cai* (2003) concluded that a significant portion of the temperature increase during the last several decades in the land-surface observational record may have resulted from urbanization and other land use changes, though there is not widespread agreement with this viewpoint. The removal of vegetative cover and expansion of impervious urban surfaces combine to reduce surface evaporative cooling and lead to additional warming. Other impacts of urbanization can include enhanced rainfall amounts over and downwind of major cities [*Bornstein and Lin*, 2000; *Shepherd et al.*, 2002; *Shepherd and Burian*, 2003]. Numerical studies [*Sanders*, 1986; *Grimmond and Oke*, 1995; *Sailor*, 1995; *Avissar*, 1996; *Xiao et al.*, 1998; *McPherson et al.*, 2000] have shown that latent heat flux increases from urban vegetation can have a moderating influence upon the local metropolitan climate. In coastal regions, the meteorological impact of a city interacts with the sea breeze circulations, contributing to the ventilation of elevated urban temperatures [*Yoshikado*, 1990, 1992; *J. Nielsen-Gammon*, 2000]. The interactions of these climate change impacts on the urban atmosphere are highly nonlinear and still not well understood [*Rosenzweig and Solecki*, 2001; *Shepherd*, 2005], emphasizing the need for more research, including into improved land surface parameterizations in urban climate models [*Grimmond and Oke*, 1999; *Niyogi et al.*, 2006].

1.5. Synopsis of thesis and principal objectives

Although several mesoscale modeling studies have investigated the potential consequences of LULCC in North America from the natural vegetation prior to European settlement to the present-day semi-natural land cover [see *Copeland et al.*, 1996; *Pielke et al.*, 1999; *Eastman et al.*, 2001; *Baidya Roy et al.*, 2003b; *Marshall et al.*, 2004a, 2004b; *Schneider et al.*, 2004], few modeling studies to date have examined in detail the potential effects of land use change within a highly populated, urban region that was once primarily agricultural and forested in the late 19th century. The northeastern United States is among those regions of the world that has witnessed dramatic changes in land use resulting from extensive agricultural, silvicultural, urban, and industrial development during the last century. This project evaluates the sensitivity of weather and climate to historical changes in land use and land cover for the entire state of New Jersey (NJ) and surrounding regions, a heavily urbanized area that has seen pronounced surface changes.

To accomplish this, we take advantage of a high-resolution dataset of 1880s-era land cover that I digitally reconstructed from detailed topographical maps [*Vermeule*, 1889]. I applied this reconstruction [also *U.S. Bureau of the Census*, 1960], along with present-day land cover derived from Landsat Thematic Mapper (TM) imagery [*Vogelmann et al.*, 2001], in simulations of a summertime drought period using the Regional Atmospheric Modeling System (RAMS) [*Walko and Tremback*, 2000].

The primary objectives of this study are:

- To document and describe the direction and magnitude of land cover change over a roughly century-long period (1880s to 1992) for a highly urbanized region that was once predominantly agricultural and forested, and
- To identify and quantify the impact and sensitivity to these land cover changes of surface air and dewpoint temperatures, rainfall, surface heat and radiative fluxes, and mesoscale atmospheric dynamics and thermodynamics during an extreme climatological episode (i.e., a prolonged drought).

I show how landscape conversions in NJ may have modified surface climate by altering albedo and other components of the land surface energy budget. Three land cover change themes within this region are identified (urbanization, reforestation, and deforestation) to demonstrate how each theme could have modified surface climate over the mean diurnal cycle. In addition, I also examine the effects of land cover change, in both mean properties and spatial heterogeneity, on the thermodynamics and dynamics of the boundary layer and evaluate the impacts on the development of mesoscale atmospheric circulations such as the sea breeze.

Chapter 2 describes the reconstruction of historical and present-day land cover datasets for NJ and its surrounding states and discusses the experimental design, including describing the RAMS model and its configuration for the simulations I have performed. Chapter 3 presents a comparison of documented land cover changes between the 19th and 20th centuries for this region. Chapter 4 describes the simulated changes in surface climate and the land surface energy budget, while Chapter 5 discusses the simulated changes in atmospheric dynamics and the vertical profiles of thermodynamic variables. Chapter 6 provides a summary and describes avenues for future research.

1.6. Chapter summary

During the past two decades, many numerical and empirical studies have shown the impacts of LULCC have been recognized as one of the principal drivers of climate on a variety of scales [*Turner*, 2001; *Feddema*, 2005]. These scales cover the full spatial and temporal spectrum: from continental scales [*Matthews et al.*, 2003; *Betts*, 2001] to regional scales [*Pielke*, 2001; *Weaver*, 2004a, b] and even local scales [*Bornstein and Lin,* 2000; *Rosenzweig and Solecki*, 2001], and likewise, from the five-year model integration of *Bonan* [1997] to the diurnal changes as described by *Mölders* [2000]. Sensitivity analyses have also assessed the significance of regional LULCC impacts on regional weather and climate [i.e., *Pielke et al.*, 1999; *Marshall et al.*, 2003, 2004a; *Wichansky et al.*, 2006; *Georgescu et al.*, 2007], which help us separate the effects of global-scale climate change (e.g., increasing concentrations of atmospheric carbon dioxide, as described in *Hansen et al.* [1988]) from those at the regional scales (such as LULCC).

Historical land use change, especially within urban and suburban regions, is primarily driven by continued population growth [*Arnfeld*, 2003; *Jin and Shepherd*, 2005] and may have long-term effects on land surface-atmosphere heat and moisture exchange, which can, in turn, directly (and indirectly) impact the quality of life within human communities. In effect, LULCC has the potential to affect many facets of human health and welfare, including water quality and availability, air quality, agriculture and food production, energy supply and demand, wetlands and sensitive ecosystems, and even the further expansion of urban areas. In a broader context, the anthropogenic influences on globally-averaged temperatures and the global-scale radiative budget as described in *IPCC* [2007] are presently recognized as the primary consensus on global climate change, but the studies described in this chapter have shown that the impacts of regional LULCC still remain among the most uncertain (and perhaps among the most important) factors affected by regional and global climate change.

The results presented in my thesis attempt to separate the land cover change effects from other anthropogenic forcing factors that could also alter regional climate, such as the increase in concentration of atmospheric greenhouse gases. As the land use has dramatically changed in NJ and the surrounding states during a roughly century-long time period, my use of a mesoscale numerical model with an unusually high spatial resolution (as compared with other LULCC studies) will help quantify the sensitivity of the regional warm-season climate signal to the conversion of a predominantly agrarian 19th-century landscape to a highly urban 20th-century metropolis and surrounding regions. As the landscape continues to be transformed in many other areas of the country and world into the 21st century and beyond, I believe that my results will help us gain a better understanding of the far-reaching impacts of LULCC on regional climate trends, especially within an agricultural region that has the potential to be converted to extensive urban land use in the next 50 to 100 years.

References

Anthes, R. A. (1984), Enhancement of convective precipitation by mesoscale variations in vegetative covering in semiarid regions, *J. Clim. Appl. Meteorol.*, *23*, 541-554.

Arnfeld, A. J. (2003), Two decades of urban climate research: A review of turbulence, exchanges of energy and water, and the urban heat island, *Int. J. Climatol.*, *23*, 1-26.

Avissar, R. (1996), Potential effects of vegetation on the urban thermal environment, *Atmos. Environ.*, *30*, 437-448.

Avissar, R. and F. Chen (1993), Development and analysis of prognostic equations for mesoscale kinetic energy and mesoscale (subgrid scale) fluxes for large-scale atmospheric models, *J. Atmos. Sci*., *50*, 3751-3774.

Avissar, R., and Y. Liu (1996), Three-dimensional numerical study of shallow convective clouds and precipitation induced by land surface forcing, *J. Geophys. Res.*, *101*, 7499-7518.

Avissar, R., and R. A. Pielke (1989), A parameterization of heterogeneous land surfaces for atmospheric numerical models and its impact on regional meteorology, *Mon. Weather Rev.*, *117*, 2113-2136.

Avissar, R., and T. Schmidt (1998), An evaluation of the scale at which ground-surface heat flux patchiness affects the convective boundary layer using large-eddy simulations, *J. Atmos. Sci.*, *55*, 2666-2689.

Balling, R. C., Jr. (1988), The climatic impact of a Sonoran vegetation discontinuity, *Clim. Change*, *13*, 99-109.

Baidya Roy, S., and R. Avissar (2000), Scales of response of the convective boundary layer to land surface heterogeneity, *Geophys. Res. Lett.*, *27*, 533-536.

Baidya Roy, S., C. P. Weaver, D. S. Nolan, and R. Avissar (2003a), A preferred dynamical scale for landscape-forced mesoscale circulations? *J. Geophys. Res.*, *108*, 8808, doi:10.1029/2002JD003097.

Baidya Roy, S., G. C. Hurtt, C. P. Weaver, and S. W. Pacala (2003b), Impact of historical land-use/land-cover change on the July climate of the United States, *J. Geophys. Res.*, *108*, 4793, doi:10.1029/2003JD003565.

Beltrán, A. (2005), Using a coupled atmospheric-biospheric modeling system (GERRAMS) to model the effects of land-use/land-cover changes on the near-surface atmosphere, Ph.D dissertation, 186 pp., Colorado State University, Boulder, Colorado.

Betts, R. A. (2001), Biogeophysical impacts of land use on present-day climate: near-surface temperature change and radiative forcing, *Atmos. Sci. Lett.*, *1*, doi:10.1006/asle.2001.0023.

Bonan, G. B. (1997), Effects of land use on the climate of the United States, *Clim. Change*, *37*, 449-486.

Bonan, G. B., S. Levis, K. Oleson, and P. Lawrence (2007), Do mid-latitude croplands cool climate?, presentation at the Detecting the Atmospheric Response to the Changing Face of the Earth: A Focus on Human-Caused Regional Climate Forcings, Land-Cover/Land-Use Change, and Data Monitoring workshop, National Science Foundation, Boulder, CO, 27-29 Aug.

Bornstein, R., and Lin, Q. (2000), Urban heat islands and summertime convective thunderstorms in Atlanta: three case studies, *Atmos. Environ.*, *34*, 507-516.

Bounoua, L., G. J. Collatz, S. O. Los, P. J. Sellers, D. A. Dazlich, C. J. Tucker, and D. A. Randall (2000), Sensitivity of climate to changes in NDVI, *J. Clim.*, *13*, 2277-2292.

Bounoua, L., R. Devries, G. J. Collatz, P. J. Sellers, and H. Kahn (2002), Effects of land cover conversion on surface climate, *Clim. Change*, *52*, 29-64.

Brown, M. E., and D. L. Arnold (1998), Land-surface-atmosphere interactions associated with deep convection in Illinois, *Int. J. Climatol.*, *18*, 1637-1653.

Bryant, N. A., L. F. Johnson, A. J. Brazel, R. C. Balling, C. F. Hutchinson, and L. R. Beck (1990), Measuring the effect of overgrazing in the Sonoran desert, *Clim. Change*, *17*, 243-264.

Chagnon, F. J. F., and R. L. Bras (2005), Contemporary climate change in the Amazon, *Geophys. Res. Lett.*, *32*, L13703.

Chagnon, F. J. F., R. L. Bras, and J. Wang (2004), Climatic shift in patterns of shallow clouds over the Amazon, *Geophys. Res. Lett.*, *31*, L24212, doi:10.1029/2004GL021188.

Chase, T. N., R. A. Pielke Sr., T. G. F. Kittel, R. Nemani, and S. W. Running (1996), Sensitivity of a general circulation model to global changes in leaf area index, *J. Geophys. Res.*, *101*, 7393-7408.

Claussen, M., V. Brovkin, and A. Ganopolski (2001), Biogeophysical versus biogeochemical feedbacks of large-scale land cover change, *Geophys. Res. Lett.*, *28*, 1011-1014.

Climate Change Science Program, [U.S.] (CCSP) (2003), Strategic Plan for the U.S. Climate Change Science Program *Final Report*, CCSP, Washington, D.C., available online at www.climatescience.gov

Copeland, J. H., R. A. Pielke, and T. G. F. Kittel (1996), Potential climatic impacts of vegetation change: A regional modeling study, *J. Geophys. Res.*, *101*, 7409-7418.

Cutrim, E., D. W. Martin, and R. Rabin (1995), Enhancement of cumulus clouds over deforested lands in Amazonia, *Bull. Am. Meteorol. Soc.*, *76*, 1801-1805.

Deardorff, J. W. (1978), Efficient prediction of ground surface temperature and moisture with inclusion of a layer of vegetation, *J. Geophys. Res.*, *83*, 1889-1903.

Dickinson, R. E., and A. Henderson-Sellers (1988), Modeling tropical deforestation: a study of GCM land-surface parameterizations, *Q. J. R. Meteorol. Soc.*, *114*, 439-462.

Eastman, J. L., M. B. Coughenour, and R. A. Pielke, Sr. (2001), The regional effects of CO_2 and landscape change using a coupled plant and meteorological model. *Global Change Biol.*, *7*, 797-815.

Feddema, J. J., K. W. Oleson, G. B. Bonan, L. O. Mearns, L. E. Buja, G. A. Meehl, and W. M. Washington (2005), The importance of land-cover change in simulating future climates, *Science*, *9*, 1674-1678.

Gallo, K. P., D. R. Easterling, and T. C. Peterson (1996), Notes and correspondence: The influence of land use/land cover on climatological values of the diurnal temperature range, *J. Clim.*, *9*, 2941-2944.

Gedzelman, S. D., Austin, S., Cermak, R., Stefano, N., Partridge, S., Quesenberry, S., and D. A. Robinson (2003), Mesoscale Aspects of the Urban Heat Island around New York City, *Theor. Appl. Climatol.*, *75*, 29-42.

Georgescu, M., G. Miguez-Macho, L. T. Steyaert, and C. P. Weaver (2007), Sensitivity of summer climate to land cover change over the Greater Phoenix, AZ, area. *J. Arid Env.*, submitted.

Grimmond, C. S. B., and T. R. Oke (1999), Heat storage in urban areas: Local-scale observations and evaluation of a simple model, *J. Appl. Meteorol.*, *38*, 922-940.

Hansen, J., I. Fung, A. Lacis, D. Rind, Lebedeff, R. Ruedy, G. Russell, and P. Stone (1988), Global climate changes as forecast by Goddard Institute for Space Studies three-dimensional model, *J. Geophys. Res.*, *93*, 9341-9364, doi:10.1029/88JD00231.

IPCC (Intergovernmental Panel on Climate Change) (2007), *Climate Change 2007: The Physical Science Basis. Contribution of Working Group I to the Fourth Assessment Report of the Intergovernmental Panel on Climate Change* [Solomon, S., D. Qin, M. Manning, Z. Chen, M. Marquis, K. B. Averyt, M. Tignor and H. L. Miller (Eds.)], 996 pp., Cambridge University Press, Cambridge, United Kingdom and New York, NY, USA.

Jin, M. and J. M. Shepherd (2005), On including urban landscape in land surface model - How can satellite data help? *Bull. Am. Meteorol. Soc.*, 86, 681-689.

Kalnay, E., and M. Cai (2003), Impact of urbanization and land-use change on climate, *Nature*, *423*, 528-531.

Karl, T. R., H. F. Diaz, and G. Kukla (1988), Urbanization: its detection and effect in the United States climate record, *J. Clim.*, *1*, 1099-1123.

Karl, T. R., P. D. Jones, R. W. Knight, G. Kukla, N. Plummer, V. Razuvayev, K. P. Gallo, J. Lindseay, R. J. Charlson, and T. C. Peterson (1993), A new perspective on recent global warming: Asymmetric trends of daily maximum and minimum temperature, *Bull. Am. Meteorol. Soc.*, *74*, 1007-1023.

Klein Goldewijk, K. (2001), Estimating global land use change over the past 300 years: the HYDE database, *Global Biochem. Cycl.*, *15*, 415-433.

Lynn, B. H., D. Rind, and R. Avissar (1995), The importance of mesoscale circulations generated by subgrid-scale landscape heterogeneities in general circulation models, *J. Clim.*, *8*, 191-205.

Marshall, C. H., Jr., R. A. Pielke Sr., and L. T. Steyaert (2003), Crop freezes and land-use change in Florida, *Nature*, *426*, 29-30.

Marshall, C. H., Jr., R. A. Pielke, L. T. Steyaert, and D. A. Willard (2004a), The impact of anthropogenic land-cover change on the Florida peninsula sea breezes and warm season sensible weather, *Mon. Weather Rev.*, *132*, 28-52.

Marshall, C. H., Jr., R. A. Pielke Sr., and L. T. Steyaert (2004b), Has the conversion of natural wetlands to agricultural land increased the incidence and severity of damaging freezes in South Florida?, *Mon. Weather Rev.*, *132*, 2243-2258.

Matthews, H. D., A. J. Weaver, M. Eby, and K. J. Meissner (2003), Radiative forcing of climate by historical land cover change, *Geophys. Res. Lett.*, *30*, 27:1-27:4, 1055, doi: 10.1029/2002GL016098.

McPherson, G., J. R. Simpson, P. J. Peper, S. E., Maco, and Q. Xiao (2000), Benefit-cost analysis of Fort Collins' municipal forest. *Internal Tech. Rep.*, 38 pp., Center for

Urban Forest Research, USDA Forest Service, Pacific Southwest Research Station, Davis, California.

Meyer, W. B., and B. L. Turner II (Eds.) (1994), *Changes in Land Use and Land Cover: A Global Perspective*, 537 pp., Cambridge Univ. Press, Cambridge England; New York, New York, USA.

Mölders, N. (2000), Similarity of microclimate as simulated in response to landscapes of the 1930s and the 1980s, *J. Hydrometeorol.*, 1, 330-352.

Nielsen-Gammon, J. W. (2000), The Houston heat pump: modulation of a land-sea breeze by an urban heat island, Preprints, *11th Joint Conf. on the Applications of Air Pollution Meteorology with the A&WMA*, Long Beach, Calif., Amer. Meteorol. Soc., 65-69.

NRC (National Research Council) (2005), *Radiative Forcing of Climate Change: Expanding the Concept and Addressing Uncertainties* [Jacob, D.J., R. Avissar, G. C. Bond, S. Gaffin, J. T. Kiehl, J. L. Lean, U. Lohmann, M. E. Mann, R. A. Pielke, Sr., V. Ramanathan, and L. M. Russell (Eds.)], 207 pp, The National Academies Press, Washington, DC.

Oleson, K. W., G. B. Bonan, S. Levis, and M. Vertenstein (2004), Effects of land use change on North American climate: impact of surface datasets and model biogeophysics, *Clim. Dyn.*, *23*, 117-132.

Pielke, R. A. (2001), Influence of the spatial distribution of vegetation and soils on the prediction of cumulus convective rainfall, *Rev. Geophys.*, *39*, 151-177.

Pielke, R. A., and R. Avissar (1990), Influence of landscape structure on local and regional climate, *Landscape Ecology*, *4*, 133-155.

Pielke, R. A., G. Dalu, J. S. Snook, T. J. Lee, and T. G. F. Kittel (1991), Nonlinear influence of mesoscale land use on weather and climate, *J. Clim.*, *4*, 1053-1069.

Pielke, R. A., R. Avissar, M. Raupach, A. J. Dolman, X. Zeng, and A. S. Denning (1998), Interactions between the atmosphere and terrestrial ecosystems: Influence on weather and climate, *Global Change Biol.*, *4*, 461-475.

Pielke, R. A., R. L. Walko, L. T. Steyaert, P. L. Vidale, G. E. Liston, W. A. Lyons, and T. N. Chase (1999), The influence of anthropogenic landscape changes on weather in south Florida, *Mon. Weather Rev.*, *127*, 1663-1673.

Pitman, A. (2003), The evolution of, and revolution in, land surface schemes designed for climate models, *Int. J. Clim*., *23*, 479-510.

Pitman, A., R. A. Pielke Sr., R. Avissar, M. Claussen, J. Gash, and H. Dolman (1999), The role of the land surface in weather and climate: does the land surface matter?, in *Global Change Newsletter*, *39*, 4-11.

Ramankutty, N., and J. A. Foley (1999), Estimating historical changes in global land cover: Croplands from 1700 to 1992, *Global Biochem. Cycl.*, *13*, 997-1027.

Randall, D. A., M. Khairoutdinov, A. Arakawa, and W. Grabowski (2003), Breaking the cloud-parameterization deadlock, *Bull. Am. Meteorol. Soc.*, *84*, 1547-1564.

Rosenzweig, C., and W. D. Solecki (2001), Climate change and a global city: Learning from New York, *Environment*, *43*, 2-12.

Sailor, D. J. (1995), Simulated urban climate response to modifications in surface albedo and vegetative cover, *J. Appl. Meteorol.*, *34*, 1694-1704.

Sanders, R. A. (1986), Urban vegetation impacts on the hydrology of Dayton, Ohio, *Urban Ecology*, *9*, 361-376.

Schneider, N., W. Eugster, and B. Schichler (2004), The impact of historical land-use changes on the near-surface atmospheric conditions on the Swiss Plateau, *Earth Interactions*, *8*, 1-27.

Segal, M., and R. W. Arritt (1992), Non-classical mesoscale circulations caused by surface sensible heat-flux gradients, *Bull. Am. Meteorol. Soc.*, *73*, 1593-1604.

Segal, M., R. Avissar, M. C. McCumber, and R. A. Pielke (1988), Evaluation of vegetation effects on the generation and modification of mesoscale circulations, *J. Atmos. Sci.*, *45*, 2268-2292.

Sellers, P. J. (1992), Biophysical models of land surface processes, in *Climate System Modeling*, edited by K. E. Trenberth, pp. 451-490, Cambridge University Press, New York, New York.

Sellers, P., F. Hall, R. Kelly, A. Black, D. Baldocchi, J. Berry, M. Ryan, K.J. Ranson, P. Crill, D. Lettenmaier, H. Margolis, J. Cihlar, J. Newcomer, D. Fitzjarrald, P. Jarvis, S.T. Gower, D. Halliwell, D. Williams, B. Goodison, D. Wickland and F. Guertin (1997), BOREAS in 1997: Experiment overview, scientific results, and future directions. *J. Geophys. Res.*, 102**,** 28731–28769.

Shepherd, J. M. (2005), A review of current investigations of urban-induced rainfall and recommendations for the future. *Earth Interactions*, *9*, 1-27.

Shepherd, J. M., and S. J. Burian (2003), Detection of urban-induced rainfall anomalies in a major coastal city, *Earth Interactions*, *7*, 1-17.

Shepherd, J. M., H. F. Pierce, and A. J. Negri (2002), Rainfall modification by major urban areas: Observations from spaceborne rain radar on the TRMM satellite, *J. Appl. Meteorol.*, *41*, 689-701.

Stone, D. A., and A. J. Weaver (2003), Factors contributing to diurnal temperature range trends in twentieth and twenty-first century simulations of the CCCma coupled model, *Clim. Dyn.*, *20*, 435-445.

Sud, Y. C., J. Shukla, and Y. Mintz (1988), Influence of land surface-roughness on atmospheric circulation and precipitation: A sensitivity study with a general circulation model, *J. Appl. Meteorol.*, *27*, 1036-1054.

Taha, H. (1997), Urban climates and heat islands: albedo, evapotranspiration, and anthropogenic heat, *Energy and Buildings*, *25*, 99-103.

Turner, B. L. II (2001), Land-use and land-cover change: Advances in 1.5 decades of sustained international research, *GAIA - Ecological Perspectives in Science, Humanities, and Economics*, *10*, 269-272.

Turner, B.L. II, R. H. Moss and D. L. Skole (1993), Relating land use and global land-cover change: A proposal for IGBP-HDP core project. *International Geosphere-Biosphere Programme (IGBP), IGBP Report No. 24*, Secretariat, Stockholm, Sweden.

U.S. House, Bureau of the Census (1960), *Historical statistics of the United States: colonial times to 1957, a statistical abstract supplement*, p. 789, The Social Science Research Council, United States Bureau of the Census, Washington, D.C.

Vermeule, C. C. (1889), Topographical Atlas Sheets 1-17, *Atlas of New Jersey, Geological Survey of New Jersey*, 62 x 88 cm, 1883-1889, Julius Bien and Company, New York, NY, Special Collections and University Archives, Rutgers University Libraries.

Vogelmann, J. E., S. M. Howard, L. M. Yang, C. R. Larson, B. K. Wylie, and N. Van Driel (2001), Completion of the 1990s National Land Cover Dataset for the Conterminous United States from Landsat Thematic Mapper Data and Ancillary Data Sources, *Photogrammetric Engineering and Remote Sensing*, *67*, 650-662.

Walker, G. K., Y. C. Sud, and R. Atlas (1995), Impact of ongoing Amazonian deforestation on local precipitation: A GCM simulation study, *Bull. Am. Meteorol. Soc.*, *76*, 346-361.

Walko, R. L., and C. J. Tremback (2000), Regional Atmospheric Modeling System Users Guide: Version 4.2MRC, ASTeR internal report, ASTeR Div., Mission Research Corporation, Fort Collins, Colorado.

Walko, R. L., L. E. Band, J. Baron, T. G. F. Kittel, R. Lammers, T. J. Lee, D. Ojima, R. A. Pielke, C. Taylor, C. Tague, C. J. Tremback, and P. L. Vidale (2000), Coupled atmosphere-biophysics-hydrology models for environmental modeling, *J. Appl. Meteorol.*, *39*, 931-944.

Weaver, C. P. (2004a), Coupling between large-scale atmospheric processes and mesoscale land-atmosphere interactions in the U.S. Southern Great Plains during summer: Part I. Mesoscale case studies, *J. Hydrometeorol.*, *5*, 1223-1246.

Weaver, C. P. (2004b), Coupling between large-scale atmospheric processes and mesoscale land-atmosphere interactions in the U.S. Southern Great Plains during summer: Part II. Large-scale-mean impacts of the mesoscale, *J. Hydrometeorol.*, *5*, 1247-1258

Weaver, C. P., and R. Avissar (2001), Atmospheric disturbances caused by human modification of the landscape, *Bull. Am. Meteorol. Soc.*, *82*, 269-281.

Wichansky, P. S., C. P. Weaver, L. T. Steyaert, and R. L. Walko (2006), Evaluating the effects of historical land cover change on summertime weather and climate in New Jersey, p. 128-163, in *New Jersey's Environments: Past, Present, and Future*, edited by Neil M. Maher, Rutgers University Press, New Brunswick, New Jersey.

Xiao, Q., E. G. McPherson, J. R. Simpson, and S. L. Ustin (1998), Rainfall interception by Sacramento's urban forest, *J. Arboric.*, *24*, 235-244.

Yoshikado, H. (1990), Vertical structure of the sea breeze penetrating through a large urban complex, *J. Appl. Meteorol.*, *29*, 878–891.

Yoshikado, H. (1992), Numerical study of the daytime urban effect and its interaction with the sea breeze, *J. Appl. Meteorol.*, *31*, 1146-1164.

Zeng, X., R. E. Dickinson, A. Walker, M. Shaikh, R. S. DeFries, and J. Qi (2000), Derivation and evaluation of global 1-km fractional vegetation cover data for land modeling, *J. Appl. Meteorol.*, *39*, 836-839.

Zhao, M., A. J. Pitman, and T. N. Chase (2001), The impact of land cover change on the atmospheric circulation, *Clim. Dyn.*, *17*, 467-477.

CHAPTER 2: Datasets, Numerical Model, and Experimental Design

2.1. Introduction

As I prepared for this study, my objective was to find high-quality and spatially-accurate historical land cover data that were reasonably comparable to the resolution and thematic detail of modern satellite imagery. My search led me to a highly-detailed late 19th-century topographical map series of New Jersey (NJ) land cover that is stored at the New Jersey Special Collections and University Archives at Rutgers University. This chapter describes the meticulous gathering, interpretation, and digitization of the 1880s-era land cover data on these maps, which were combined with supplementary historical land cover data for the surrounding states. Once my historical land cover reconstruction was completed, the comparison of this late 19th-century landscape with present-day land cover derived from satellite imagery for the same region allowed me to document the land use changes that have occurred. Following some data reconciliations, I used these datasets in a mesoscale numerical model to examine the sensitivity of local weather and climate to regional landscape change. The numerical model is also described in this chapter.

The numerical model that I used was the Regional Atmospheric Modeling System (RAMS) [*Cotton et al.*, 2003]. RAMS is coupled to a land surface model [*Walko et al.*, 2000] that estimates vertical energy and moisture exchanges between the surface and the atmosphere for multiple land cover types within individual grid cells. Several RAMS simulations were then performed that provided a framework by which we could begin to understand the warm-season weather and climate impacts in a region where land use changes in some areas of NJ have transformed a relatively homogeneous and predominantly agrarian 19th-century landscape into a fragmented and highly urban late 20th-century landscape.

2.2. Historical land cover reconstruction

The 19th-century land cover dataset for NJ used in this study was reconstructed from a series of topographical maps that were created under the direction of Dr. George H. Cook, a renowned state geologist and educator. As the first director of the New Jersey Agricultural College Experiment Station in 1880, Dr. Cook, along with his colleagues, created a detailed topographical atlas of the entire state, thereby documenting the distribution of wetlands, forests, and other land cover types that described a relatively rural landscape in the circa 1880 time period [*Vermeule*, 1889]. New Jersey thus became the first state in the nation to have its official geological survey completed with the mapping of 19th-century land cover information [*Sidar*, 1976] on a scale of one inch to one statute mile, or 1:63,360 [*Letts*, 1905]. This topographical atlas was mapped to a rectangular polyconic projection, which was a projection derived and used by the U.S. Coast and Geodetic Survey in the latter half of the 19th century [*Schott*, 1882]. Figure 1 shows a representative portion of the map series (hereafter referred to as the Cook map series) which was mapped at a sufficiently detailed spatial resolution to conduct my historical land cover change analysis.

I interpreted and manually digitized the information contained in the Cook map series to create a high-resolution, gridded land cover database of the state's vegetation, wetlands, surface water, and built-up areas during the 1880s era.[1] For all 17 maps in the series, I manually estimated and aggregated the fractional percentages of 14 semi-natural land cover types depicted on these maps, in increments of 10 percent, within 2.0-arcminute latitude-longitude grid cells[2] [*Wichansky et al.*, 2006]. This translated the state into a gridded domain of 51 x 74 cells; for the mean latitude of NJ (40°N), the approximate zonal (west-east) and meridional (north-south) cell widths were 3.71 km and 2.84 km, respectively. Estimating the fractional areas of land cover in increments finer than 10 percent was not feasible. Table 1 lists these 14 land cover types. Appendix A describes in more detail the procedures I used to identify these and other historical land cover types on the Cook map series (e.g., urban areas, agricultural land), as well as estimate their corresponding fractional areal percentages within each grid cell.

As will be discussed in section 2.5, the boundaries of my model simulation domain encompass not only NJ, but also parts of adjacent states or regions that include Pennsylvania (PA), New York (NY) / Long Island (LI), Delaware (DE), and Connecticut (CT). Louis Steyaert of the U.S. Geological Survey (USGS) supplied me with a reconstructed historical land cover dataset for this broader region. He based this reconstruction on county-level data from the 1880 U.S. Census, which represents the best existing regional land cover information available to reconstruct the historical landscape for the states adjacent to NJ. The county-level census data include observed estimates on the total acreage of improved and unimproved farmland in each county where improved

---

[1] The flatbed scanners available to me at the time of my historical landscape reconstruction had too small a total image scan area relative to the size of each of the maps of the Cook map series (62x88 cm), which made it necessary to manually estimate the NJ land cover data.

[2] Within a given grid cell, I estimated the land cover type with the largest area in total fractional coverage, then estimated the land cover type with the second-largest area in total coverage, and so on. Also, the relative location of each land cover type within a grid cell was ignored.

farmland was further delineated as either tilled land or meadow-pasture land, while unimproved farmland corresponds to forests and woodlots [*U.S. Bureau of the Census*, 1960; *Waisanen and Bliss*, 2002]. The fractional areal percentages derived from these acreage estimates for the surrounding states were then binned into four broad land cover categories: mixed agriculture, deciduous broadleaf forest, pasture, and an “other” category for non-farmland types such as towns or, in some cases, semi-natural vegetation types. Appendix B describes the data adjustments that were required to ensure that my census-based reconstruction was reasonably consistent with known historical land use.

Once I gridded these county-wide averages of interpreted land cover to the same 2.0-arcminute mesh as that of the Cook map series, and then merged it with the NJ land cover data, I was able to reconstruct a continuous 1880s-era land cover dataset for the entire region.

2.3. Present-day land cover reconstruction

My present-day land cover dataset was adapted from the USGS 1992 National Land Cover Dataset (NLCD) [*Vogelmann et al.*, 2001]. Based on Landsat Thematic Mapper (TM) data from 1992 and 1993, this 30-m resolution dataset was designed for use in environmental, land management, and regional modeling applications. Its land cover classification consists of 21 hierarchical classes in a modified Anderson Level II scheme [*Anderson et al.*, 1976]. For this study, Louis Steyaert assisted me by aggregating the 30-m NLCD to a 1-km grid according to the dominant land cover class, and further aggregating the resulting data to a 2.0-arcminute grid (i.e., a grid spacing of 3.7 km). This aggregation technique is similar to that used by *Steyaert and Pielke* [2002].

Because the land cover categories defined by the Cook map series (and in the 1880 census data) differ from those of the NLCD Anderson II classification, I reconciled the historical and present-day datasets and re-mapped each to a common, simplified set of eight land cover classes. These simplified classes are: (1) combined agricultural and pasture land; (2) deciduous broadleaf (DBL) forest; (3) evergreen needleleaf (ENL) forest; (4) mixed DBL and ENL forest; (5) marshes and other treeless wetlands; (6) forested wetlands; (7) urban areas; and (8) surface water. Each of these eight categories represent (with minor modifications) a standard land cover type (or mixture of two types) in the RAMS land-surface scheme, described in section 2.4. I carried out this reconciliation and re-mapping to avoid introducing any spurious land cover changes into my surface datasets, as might arise, for example, from classifying the same land cover into two different categories. This strategy helped me isolate, within this multi-state region, the actual land use changes from the late 19th century to the late 20th century.

Because water can be an important land cover class at the regional scale, I made assumptions about the relative distributions of lakes and other inland surface water bodies between the various datasets. The census does not have a land cover category to represent inland water, so I overlaid all lakes, rivers, and inland water that were present in the NLCD (using the final 2.0-arcminute grid resolution, or a grid spacing of 3.7 km) onto the census data for those states that surrounded NJ. This adjustment made the 1880 census and NLCD inland water distributions virtually identical, ensuring that inland water bodies did not abruptly shift their locations between these two time-slices of the same region. Therefore, outside NJ, there is no change in the distribution of inland surface water from the 1880s to the 1990s in my landscape reconstructions. Within historical NJ, however, I used the inland water data from the Cook map series.

One of the key characteristics of the Cook map series data is the rough correspondence of the level of detail between the 1880s-era topographical maps and the aggregated 1-km present-day land cover that was derived from satellite data analysis. The relatively fine spatial details of these datasets for NJ make interpretation of probable shifts in land cover features much easier.[3] For those areas outside NJ, however, some of the differences between my historical and present-day reconstructions (e.g., in the degree of fragmentation of the landscape) are likely artifacts due to differences in effective resolution between the 1-km NLCD data and the county-level census data. The interpretation of observed land cover changes within the broader region should also consider these differences in mapping scales.

2.4. RAMS model description

The simulations presented in this study were performed using the three-dimensional atmospheric RAMS model, version 4.3, in its non-hydrostatic mode [*Walko and Tremback*, 2000; *Cotton et al.*, 2003]. My simulations were configured to include the parameterizations for subgrid-scale transport [*Mellor and Yamada*, 1982], convection [*Kain and Fritsch*, 1992], microphysics [*Walko et al.*, 1995], and radiative transfer [*Harrington*, 1997]. RAMS was coupled to the Land Ecosystem-Atmosphere Feedback Model, version two (LEAF-2) [*Walko et al.,* 2000], a module that estimates vertical energy and water exchange between the soil, vegetation, canopy, and overlying

---

[3] To minimize potential degradation that comes with resampling my land cover data to another projection, I did not apply any geometric map corrections to the historical landscape reconstruction.

atmosphere for multiple patches of land cover within a single grid cell. These four components interact dynamically with each other and with the RAMS atmosphere and soil surface, allowing the land surface state and vertical soil water movement to respond to changing atmospheric conditions. LEAF-2 assimilates land cover datasets to define the surface-atmosphere boundary. Land surface parameters (LSPs), including surface albedo, leaf area index, fractional vegetative cover, roughness length, and displacement height, can be prescribed according to land cover type and time of year. The values assigned to these LSPs generally correspond to those of the standard Biosphere-Atmosphere Transfer Scheme (BATS) vegetation categories [*Dickinson et al.*, 1993].

To simulate the effects of 19th- vs. 20th-century land cover in RAMS, I initialized LEAF-2 with my historical and present-day datasets, as mapped to the eight categories described earlier in section 2.3. Table 2 provides a cross-reference that matches each of the Cook-Census reconstructed and NLCD classes with the corresponding LEAF-2 categories. Because some NLCD classes with small spatial coverage, including bare rock and sand, were not explicitly mapped during the late 19th century, I reclassified them in my model as agricultural and pasture land.

The LEAF-2 categories were initialized with the LSPs shown in Table 3. Each land cover type is parameterized by the assigned LSPs, which help modulate the physical soil and land processes at the lower boundary as well as the interaction between this lower boundary in LEAF-2 and the RAMS atmosphere. For example, according to the LSPs in Table 3, if the forest composition within a given area changed from mixed to DBL between the 19th and 20th centuries, the surface albedo would increase from 0.15 to 0.20 in the model. In addition, I made two modifications to the standard LSPs in LEAF-2 to more realistically reflect the surface characteristics of semi-natural land cover types in the region. First, I modified the displacement height of trees in the mixed forest class. Second, I also specified the vegetation and soil moisture properties that characterize the forested and non-forested wetlands that are prevalent in NJ. Refer to Appendix C for a more detailed description of these modifications.

2.5. RAMS model configuration

My simulation domain was centered over NJ at 40.1°N and 74.6°W. I configured RAMS with three nested grids (Figure 2): grid 1, 1600 km x 1800 km with 32-km horizontal grid spacing, covering much of eastern North America and adjacent ocean (50 x 56 points); an intermediate grid 2, 560 km x 624 km with 8-km spacing (70 x 78 points); and grid 3, 284 km x 284 km with 2-km spacing, covering NJ and portions of its surrounding states (142 x 142 points). This nested grid configuration allows RAMS to downscale the time-varying large-scale (synoptic) forcing into appropriate lateral boundary conditions for the fine-grid domain, on which we can more faithfully capture the details of the small-scale atmospheric dynamics (e.g., sea breezes and inland mesoscale circulations) that respond most closely to the surface forcing. I used a 60-s time step on grid 1 with progressively shorter time step intervals on the two inner grids. Each grid used the same, stretched vertical coordinate (38 levels), ranging from $\Delta z = 50$ m at the surface to $\Delta z = 1500$ m at and above 14 km to the model top at 22 km. I also defined 11 soil layers down to a depth of 2.5 m, with soil layer thicknesses, descending from the surface, of 5, 5, 10, 10, 10, 20, 20, 20, 50, 50, and 50 cm. Convection was parameterized using the *Kain-Fritsch* [1992] scheme on the two outermost grids, but not on the innermost. Thus, convective-scale dynamic processes were modeled explicitly, to the extent possible, on the finest grid (grid 3). While schemes such as *Kain-Fritsch* have been designed to operate at coarser grid scales than the 8 km of grid 2, the model dynamics alone cannot resolve convection at this grid scale, and so employing a cumulus scheme on grid 2 is the best choice currently available. Note that there is no double counting of precipitation in RAMS when both cumulus parameterization and bulk microphysics are operating, so this is not an issue when using the *Kain-Fritsch* scheme on grid 2.

I performed two sets of RAMS simulations – one with 1880s-era land cover for NJ and its immediate surroundings, and one with present-day land cover. To isolate the atmospheric response to land cover changes in the region, both sets of model simulations were initialized using identical large-scale atmospheric boundary conditions (described below) with the only difference being the land cover as specified in LEAF-2. I assigned the historical and present-day land cover to grid 3 only, so this grid also represented the full spatial extent of my 1880 census data. For all runs, the NLCD-based land cover was used on grids 1 and 2. In this way, I attempt to isolate the sensitivity of these simulations to land cover changes within and adjacent to NJ. Ideally, I would have preferred to use the census data as the surface boundary on grid 2 in the historical simulations, but given the coarse 40 km effective resolution and limited thematic detail of the reconstructed census land cover, my primary consideration was to take maximum advantage of the unique high-resolution 2-km 1880 land cover data for NJ.

On all grids, I specified a maximum of six surface types per grid cell (including water) to represent subgrid-scale land cover detail in LEAF-2. The use of this 2-km grid cell size (and its subgrid-scale patches) for my finest grid distinguishes this study relative to other LULCC studies that employ coarser-resolution models. In addition, I also specified a soil type of silt clay loam everywhere.[4]

Initial atmospheric conditions for both sets of simulations were specified using 6-hourly, 2.5° longitude x 2.5° latitude National Centers for Environmental Prediction (NCEP)/National Center for Atmospheric Research (NCAR) reanalysis data [*Kalnay et al.*, 1996]. The first reanalysis data time was used for initializing the entire domain, and subsequent data times were then used for specifying the lateral boundary conditions for the parent grid (grid 1). For each simulation, RAMS was run for two months, June-July 1999. This time period coincided with an intense regional drought in the northeastern U.S., with record or near-record high temperatures and heat wave impacts at many locations during July. New Jersey experienced the second driest four-month period (April to July 1999) in the state's 105-year historical record [*Morehart et al.*, 1999]. Rainfall deficits were severe enough that, by mid-August, the U.S. Department of Agriculture declared nine states, including NJ, NY, and PA, as agricultural drought disaster areas [*Heim*, 1999]. The choice of this time period allows me to examine the sensitivity of the regional climate system to land surface properties under extreme conditions and to explore ways in which changes to the landscape over a period of time might affect the severity of prolonged seasonal droughts. I chose to use this anomalously dry summer as background conditions in my study for two reasons. First, the land surface response is usually stronger during a warm season (July) than a cold season

[4] Silt clay loam is not the predominant soil type in NJ. Initial trial simulations using the predominant soil type (sandy loam) showed that soil moisture in the model rapidly drained to deeper soil layers. Silt clay loam helped retain moisture in the upper soil layers, yielding simulated surface temperatures and dewpoints that were more consistent with observed values in the region.

(January). Second, in general, the interactions between the surface and the atmosphere are typically more pronounced during a dry period than a rainy period. In this broad context, the use of 1999 NCEP reanalysis data over historical land cover allows RAMS to simulate what the climate of the summer of 1999 would have looked like if the land surface resembled that of the 1880s rather than the present-day.

2.6. Land surface initialization and experimental design

To accurately reflect the persistent drought conditions of June-July 1999, I initialized the land surface state of my RAMS model configuration, and its soil moisture, using a spinup. The month of June was used as the spinup period and the month of July as the analysis period. I accomplished this spinup by running RAMS for one full month (12:00UTC 1 June to 12:00UTC 1 July, or 8:00am 1 June to 8:00am 1 July) using grids 1 and 2 only, forcing RAMS more strongly with the reanalysis boundary conditions (i.e., by using stronger nudging) to ensure that the soil spinup would be as consistent as possible with the actual atmospheric conditions leading up to the start of my analysis period. For soil moisture at the start of the spinup period, 1 June, I used a horizontally homogeneous but vertically varying profile on both grids, with 50 percent saturation at the surface to 70 percent in the deepest soil layer. This profile is loosely based upon observed soil moisture estimates for NJ and the immediate region during the first week of June 1999 [*USDA*, 1999]. I disaggregated the 12:00UTC 1 July soil temperature and soil moisture values resulting from the spinup at each horizontal cell and vertical layer from grid 2, horizontally smoothed these disaggregated fields, and applied them as initial conditions to grid 3 for all sets of my simulations (historical and present-day).

My spinup strategy is very similar to the approach used successfully in *Weaver* [2004a, 2004b]. This approach allows for the development of more realistic, heterogeneous, fine-scale soil moisture and soil temperature features by the start of the analysis period that are consistent with the land and atmospheric components of the particular model used (in my case, RAMS). The spinup was designed carefully to ensure a good match of the July simulations with observations, particularly critical since July 1999 was an anomalous drought period. Therefore, I performed a number of test runs where I varied the soil moisture at the start of the spinup from these initial 50/70 percent values and compared modeled and observed trends in near-surface air temperature and dewpoint into the first few days in July[5], eventually settling on these values as providing the best overall agreement. I also tested the impact of a longer spinup on my results and found little systematic difference between a one-month and two-month (May-June) spinup period.

A key feature of my experimental design is the use of ensembles of simulations for both the historical and present-day land covers. This was designed to allow me to average over the effects of internal atmospheric variability and increase the robustness of my findings. Because the simulations were so computationally expensive, especially when considering the number of grid cells on the finest grid, I was limited to only three members for each ensemble. I performed a set of three simulations using my reconstructed 1880s-era land cover data and a separate set of three simulations using the NLCD-derived land cover data for the same region. The three simulations for a given land cover dataset were each initialized using slightly different model atmospheres that reflected 29 June, 1 July, and 3 July initial conditions. Each simulation is thus started at a

[5] In these test runs, the soil type across the domain was also varied to determine this sensitivity as well.

different initial time with all three of the simulations overlapping. Specifically, after each spinup ended (i.e., at 12:00UTC on 29 June, 1 July, and 3 July, respectively), I added the third grid with its specified land cover dataset, initialized the land surface state on grid 3 according to the above spinup procedure, and restarted the simulation, running the model until 04:00UTC 1 August (i.e., 12:00am local time on 1 August). To obtain ensemble means, I averaged the three simulations over the same model times on grid 3. *Arritt et al.* [2004] discuss this lagged-average ensemble method (with lags between ensemble members on the order of a day or so) as an accepted technique for generating ensembles over monthly-to-seasonal timescales in nested regional climate simulations. As described above, all six model runs used the same spun-up 1 July soil moisture and soil temperature, allowing me to isolate the atmospheric response to its land cover specification.

Since the analysis period of the 29 June ensemble member was 96 h longer than that of the 3 July ensemble member, due to a shorter spinup, I distributed the ensemble member weights equally by examining only the period where all three simulations for each ensemble overlap in time – from 12:00UTC 3 July to 04:00UTC 1 August. In the next two chapters, I mostly present my results as the difference between the ensembles (i.e., the ensemble with present-day land cover minus the ensemble with historical land cover) for each grid cell or vertical layer on grid 3, or a composite of grid cells, during this period.

2.7. Chapter summary

New Jersey is one of the few states in the nation to have a series of spatially-accurate late 19th-century topographical maps that describe a relatively rural and predominantly agrarian landscape during the 1880s era. I found the Cook map series to be a reliable data source that allowed me to create a high-resolution and thematically-detailed digital reconstruction of 1880s-era NJ land cover that was an important component of my simulations. I meshed this historical dataset for NJ with county-level 1880 U.S. Census data for the surrounding states, creating a continuous 19th-century landscape reconstruction for the entire region. Likewise, my present-day dataset was derived from 1992 Landsat TM satellite imagery of the same multi-state region. These historical and present-day datasets were then reconciled with each other and subsequently re-mapped to a common set of eight land cover classes, which helped me isolate the land cover changes from the late 19th century to the late 20th century.

I used these land cover reconstructions in a set of experiments with a mesoscale numerical model, RAMS, coupled to a land surface model, LEAF-2, a set-up that has provided me with a framework to evaluate the response of the warm-season climate to historical land use changes within the region. Each of these simulations used identical NCEP reanalysis data that reproduced the anomalously dry summertime period of June-July 1999. As soil moisture was initialized homogeneously across the RAMS domain, the first month (i.e., June) was used as a spinup period to promote the development of realistic, heterogeneous soil moisture and soil temperature features by the start of the July analysis period. Furthermore, to obtain more robust results for each land cover reconstruction, I applied a lagged-average ensemble technique by slightly varying the length of the June spinup periods in each set of simulations to create a three-member ensemble for both the historical and present-day land covers.

Before I present my results in Chapters 4 and 5, I first compare these land cover reconstructions in the next chapter and describe the documented land cover changes in this region that have resulted from socioeconomic developments and technological advances since the late 19th century. By gathering and interpreting a variety of data sources to establish what we believe to be a reasonably accurate representation of local land use shifts in NJ and the region between the late 19th and late 20th centuries, I consider Chapter 3 to be one of the highlights of my study.

References

Anderson, J. R., E. E. Hardy, J. T. Roach, and R. E. Witmer (1976), A land use and land cover classification system for use with remote sensor data, *U.S. Geological Survey Professional Paper No. 964*, 28 pp., USGS, Washington, D.C.

Arritt, R. W., C. J. Anderson, E. S.Takle, Z. Pan, W. J. Gutowski, Jr., F. O. Otieno, R. da Silva, D. Caya, J. H. Christensen, D. Lüthi, M.A. Gaertner, C. Gallardo, S.-Y. Hong, C. Jones, H.-M. H. Juang, J. J. Katzfey, W. M. Lapenta, R. Laprise, J. W. Larson, G. E. Liston, J. L. McGregor, R.A. Pielke, Sr., J.O. Roads and J.A. Taylor (2004), Ensemble methods for seasonal limited area forecasts, paper presented at the *20th Conf. on Weather Analysis and Forecasting / 16th Conf. on Numerical Weather Prediction*, Am. Meteorol. Soc., Seattle, Washington, 12-16 January.

Cotton, W. R., R. A. Pielke Sr., R.L. Walko, G. E. Liston, C. J. Tremback, H. Jiang, R. L. McAnelly, J. Y. Harrington, M. E. Nicholls, G. G. Carrio, and J. P. McFadden (2003), RAMS 2001: Current status and future directions, *Meteorol. Atmos. Phys.*, *82*, 5-29, DOI 10.1007/s00703-001-0584-9.

Dickinson, R. E., A. Henderson-Sellers, and P. J. Kennedy (1993), Biosphere-Atmosphere Transfer Scheme (BATS) version 1e as coupled to the NCAR Community Climate Model, 72 pp., NCAR Tech. Note NCAR/TN-387+STR.

Harrington, J. Y. (1997), The effects of radiative and microphysical processes on simulated warm and transition-season Arctic stratus. Ph.D. dissertation, 270 pp., Dept. of Atmos. Sci., Colorado State Univ., Fort Collins, CO.

Heim, R. (1999), Climate of 1999: July drought in the U.S., *National Climatic Data Center (NCDC) Climate Services Division*, *13 August 1999*, NCDC, Ashville, North Carolina.

Kain, J. S., and J. M. Fritsch (1992), The role of the convective trigger functions in numerical forecasts of mesoscale convective systems, *Meteorol. Atmos. Phys.*, *49*, 93-106.

Kalnay, E., M. Kanamitsu, R. Kistler, W. Collins, D. Deaven, L. Gandin, M. Iredell, S. Saha, G. White, J. Woollen, Y. Zhu, A. Leetmaa, B. Reynolds, M. Celliah, W. Ebisuzaki, W. Higgins, J. Janowiak, K.C. Mo, C. Ropelewski, J. Wang, R. Jenne, and D. Joseph (1996), The NCEP/NCAR 40-Year Reanalysis Project, *Bull. Am. Meteorol. Soc.*, *77*, 437-472.

Lee, T. J. (1992), The impact of vegetation on the atmospheric boundary layer and convective storms, Ph.D Dissertation, 137 pp., Dept. of Atmos. Sci., Colorado State Univ., Fort Collins, CO.

Letts, T. (1905), New maps, in *Bulletin of the American Geographical Society of New York*, vol. 37, pp. 497-502, The American Geographical Society of New York, New York.

Mellor, G. L. and T. Yamada (1982), Development of a turbulence closure model for geophysical fluid problems, *Rev. Geophys. Space Phys.*, *20*, 851-875.

Morehart, M, N. Gollehon, R. Dismukes, V. Breneman, and R. Heimlich (1999), Economic assessment of the 1999 drought: Agricultural impacts are severe locally, but limited nationally, *Agriculture Information Bulletin No. 755*, 20 pp., U.S. Department of Agriculture, Washington, D.C.

Schott, C. (1882), A comparison of the relative value of the polyconic projection used on the Coast and Geodetic Survey, with some other projections, in *Report of the Superintendent of the U.S. Coast and Geodetic Survey for the fiscal year ending June 30, 1880*, pp. 287-296, U.S. Government Printing Office, Washington, D.C.

Sidar, J. W. (1976), *George Hammell Cook: a life in agriculture and geology*, 282 pp., Rutgers University Press, New Brunswick, New Jersey.

Steyaert, L. T. and R. A. Pielke (2002), Using Landsat-derived land cover, reconstructed vegetation, and atmospheric mesoscale modeling in environmental and global change research: Abstracts, *53rd International Astronautical Congress*, 12 pp., World Space Congress, Houston, Texas, October 10-19.

U.S. Department of Agriculture (USDA) (1999), National Agricultural Statistics Service (NASS), Vol. 60(10), *New Jersey Weekly Crop Progress Report – June 7, 1999*.

Vermeule, C. C. (1889), Topographical Atlas Sheets 1-17, *Atlas of New Jersey, Geological Survey of New Jersey*, 62 x 88 cm, 1883-1889, Julius Bien and Company, New York, NY, Special Collections and University Archives, Rutgers University Libraries.

Vogelmann, J. E., S. M. Howard, L. M. Yang, C. R. Larson, B. K. Wylie, and N. Van Driel (2001), Completion of the 1990s National Land Cover Dataset for the Conterminous United States from Landsat Thematic Mapper Data and Ancillary Data Sources, *Photogrammetric Engineering and Remote Sensing*, *67*, 650-662.

Walko, R. L., and C. J. Tremback (2000), Regional Atmospheric Modeling System Users Guide: Version 4.2MRC, ASTeR internal report, ASTeR Div., Mission Research Corporation, Fort Collins, Colorado.

Walko, R. L, W. R. Cotton, J .L. Harrington, and M. P. Meyers (1995), New RAMS cloud microphysics parameterization. Part I: The single-moment scheme, *Atmos. Res.*, *38*, 29-62.

Walko, R. L., L. E. Band, J. Baron, T. G. F. Kittel, R. Lammers, T. J. Lee, D. Ojima, R. A. Pielke, C. Taylor, C. Tague, C. J. Tremback, and P. L. Vidale (2000), Coupled atmosphere-biophysics-hydrology models for environmental modeling, *J. Appl. Meteorol.*, *39*, 931-944.

Weaver, C. P. (2004a), Coupling between large-scale atmospheric processes and mesoscale land-atmosphere interactions in the U.S. Southern Great Plains during summer: Part I. Mesoscale case studies, *J. Hydrometeorol.*, *5*, 1223-1246.

Weaver, C. P. (2004b), Coupling between large-scale atmospheric processes and mesoscale land-atmosphere interactions in the U.S. Southern Great Plains during summer: Part II. Large-scale-mean impacts of the mesoscale, *J. Hydrometeorol.*, *5*, 1247-1258

Wichansky, P. S., C. P. Weaver, L. T. Steyaert, and R. L. Walko (2006), Evaluating the effects of historical land cover change on summertime weather and climate in New Jersey, p. 128-163, in *New Jersey's Environments: Past, Present, and Future*, edited by Neil M. Maher, Rutgers University Press, New Brunswick, New Jersey.

CHAPTER 3 – Documented Land Cover Changes between 1880s-1992

3.1 Introduction

Significant differences between the 1880s-era and present-day landscapes are apparent from the reconstruction datasets, and these differences agree reasonably well with our understanding of the historical transformation of land cover that has occurred within and around New Jersey (NJ) during the last century. This includes an extensive regional expansion of impervious surfaces resulting from dramatic urban and suburban growth, a progressive and accompanying loss of agricultural land, both decreases and increases in forest cover (depending on location), and isolated changes in the coverage and extent of wetlands. The result today is a significantly more heterogeneous and fragmented landscape. I summarize these changes in Figure 3.

3.2. Shifts in agricultural and pasture land

In the 1880s, central and northern NJ, along with adjacent eastern Pennsylvania (PA) and southern New York (NY), was an area of extensive agricultural land. In the lowlands of eastern PA, for example, mixed agriculture was by far the dominant land cover type during this period [*U.S. Bureau of the Census*, 1960]. Over the ensuing century, however, much of the agricultural land in these regions was lost (Figure 3(a)) – either abandoned and reverted to forest, or developed to create the modern urban and exurban sprawl. Given the intensity of mixed agriculture that once characterized areas like southeastern PA, and the minimal forest cover as described in the 1880 U.S. Census, I believe that the relative lack of spatial heterogeneity of the 19th-century agrarian landscape in this region is likely real and that it also contrasts realistically with the significantly enhanced heterogeneity evident in my present-day land cover dataset, due to these land use processes.

Agriculture was the predominant land cover type in 19th-century NJ. Of all states, NJ was, at that time, first in farm income per acre; the state's economy was historically based upon agricultural exports such as peaches and tomatoes, but began to witness an early 20th-century shift to professionally managed industrial and commercial enterprises [*Cunningham*, 1981]. The geographic location of NJ between the major markets of New York City and Philadelphia helped to foster urban and suburban growth at the expense of agricultural land resources. As a result, the total acreage of NJ farmland sharply declined from 2.9 million acres in 1880 to 848,000 acres by 1992, a decrease of about 70 percent [*Schmidt*, 1973; *USDA*, 1992]. Higher land values also meant that agricultural production per unit land area could no longer be as profitable as potential suburban land uses such as residential developments or industry [*Stansfield*, 1998]. Other factors have also been involved. For example, mechanization and advances in plant science have dramatically increased the efficiency of the remaining farms, providing a significant economic advantage to farmers [*Hart*, 1991]. Intensive farming practices that raised agricultural productivity have, unfortunately, also accelerated soil erosion and general land degradation [see *Boardman and Favis-Mortlock*, 2001]. All these factors, including the higher taxes placed upon farmland, technological advances, and shifting socioeconomic drivers, have continued to play a role in transforming the late 19th-century agrarian landscape of NJ [*Agthe*, 1964].

Apart from this general decrease, some increases in agricultural land use have occurred, notably within the inner coastal plain of southern NJ. Over time, truck farming became a significant boon for the state, as the growing 20th-century transportation network opened up large industrial and consumer markets for NJ farmers. The increasing demand for locally-grown produce such as blueberries and spinach made it necessary to form cooperative produce auctions [*Fabian and Burns*, 1966] where fruits and vegetables could be priced competitively and exported to urban markets via railroad and trucks.

3.3. Shifts in forest cover

The land cover change since the 1880s-era in NJ and the surrounding region is also characterized by patterns of reforestation and deforestation (Figure 3(b)). Extensive forest regrowth occurred in the northern highlands of NJ and eastern PA following farmland abandonment. In contrast, forest regrowth and deforestation patterns are more localized and heterogeneous in the lowland areas of NJ (see Figure 3(b)). In addition to farmland abandonment, the present-day forest regrowth also regenerated on burned-over lands that resulted from extensive wildfires during the early 1900s prior to fire-suppression programs [*Little*, 1979]. Deciduous broadleaf (DBL) trees are dominant in the present-day NJ forest in terms of total area [*Vogelmann et al.*, 2001] and total tree volume [*Widmann*, 2002]. Comparison of my reconstructed forest cover data for 1880 and the present-day forest cover based on the NLCD classification further suggests increased deciduousness of the forest. For example, red maple has become a common tree in NJ [*Alderman et al.*, 2005]. In addition, landscape fragmentation has probably contributed to increased deciduousness within the present-day land cover due to grasses, shrub, and small DBL tree regeneration following disturbance. The patterns of deforestation, however, are typically associated with residential and urban development such as in central NJ (e.g., Ocean County), near the Atlantic City metro area in the southeastern part of the state (e.g., Atlantic County), and on Long Island (LI).

Refer to section 3.6 for a more detailed description of the potential changes in forest composition that have likely occurred in this region.

3.4. Increases in urban and suburban land cover

The rapid expansion of urbanization since the late 19th century is strikingly illustrated in Figure 3(c). This growth has centered around, and extended outwards from, the densely populated cities of Philadelphia and New York, consuming both agricultural and forested lands, as discussed above. Expansive metropolitan areas of residential and commercial suburbs now almost completely cover several counties in NJ [*Lathrop and Hasse*, 2006] and its bordering states. Figure 3(c) also implies an extensive regional expansion of dry impervious surfaces.

3.5. Shifts in wetlands

Finally, Figure 3(d) shows the patterns of wetlands change based on differences between the reconstructed 1880 and the present-day land cover datasets. Because there is much uncertainty in these patterns due to the difficulties in the characterization and inventory of wetlands under any circumstances, these results are supplemented by historical studies. For example, the tidal and freshwater wetlands that originally covered parts of northeastern NJ have been radically altered by various land-reclamation projects, with approximately 108 km^2 of wetlands – as calculated by *Vermeule* [1897] in an 1896 U.S. Geographical Survey (USGS) study – reduced to 33 km^2 by the late 20th century [*Marshall*, 2004]. Many of these conversions of wetlands to drylands suitable for agricultural, commercial, and industrial uses occurred prior to shifts in public attitudes towards environmental conservation in the 1960s and 1970s, and the subsequent state and federal legislation. For example, within southern coastal NJ, the wetlands patterns for the 19th and 20th centuries are quite similar, primarily as a result of legislation such as the New Jersey Coastal Wetlands Act of 1970. However, the implied wetland increases in Delaware (DE) are an artifact because the 1880 census data did not include a wetlands category. In addition to difficulties and accuracy issues associated with the mapping of small, highly localized wetland areas, the differences in grid resolution and map projections between the Cook map series and 1992 National Land Cover Dataset (NLCD), combined with the manual digitization procedure I used to reconstruct the historical land cover for the state, probably introduced some biases into the observed changes compared to those for the other land cover types. Together, these can yield additional spatial uncertainties in my documented wetlands change within NJ.

3.6. Shifts in forest composition

For a given grid cell, the land use changes that I have described above can significantly alter the properties of the surface, but a change in forest type can also modify components of the land surface energy budget (particularly albedo) and thus deserves special mention in this chapter. The panels of Figure 4 illustrate the changes in forest composition according to my reconstructed land cover datasets. Figure 4(a), for example, suggests a large and particularly fragmented increase in DBL coverage in the region during this time period. In general, these DBL forest increases are consistent with the broad reforestation pattern shown in Figure 3(b). Aside from the reforestation of many areas of eastern PA and northwestern NJ, the DBL forest increases over the present-day landscape are accompanied by local increases in evergreen needleleaf forest (ENL, Figure 4(b)) in the Pine Barrens region of southern and south-central NJ. Furthermore, the mixed forest that was once dominant in these areas during the late 19th century (Figure 4(c)) has likely trended towards an increased deciduousness component (Figure 4(a)). As surface albedo is highly dependent on forest type, any change in forest composition within a given area (e.g., a conversion from mixed to DBL which has likely occurred in south-central NJ) can have important effects on surface albedo and other components of the land surface energy budget. These effects are described in Chapter 4.

3.7. Changes in surface spatial heterogeneity and dominant land cover

The land cover changes shown in Figures 3(a)-(d), in addition to the forest composition changes in Figures 4(a)-(c), are accompanied by a remarkable transition from a relatively homogeneous 19th-century land surface to one that has become heterogeneous and fragmented. Specifically, the present-day landscape of NJ is characterized by a heterogeneous mosaic of DBL, ENL, and mixed forests interspersed among fields, farms, wetlands, towns, adjacent suburbs, and large urban areas. Natural vegetation responses to these manmade disturbances also have likely contributed to the general transformation. For example, in coastal and south-central NJ, there has probably been an overall increase in the deciduousness of the tree cover due to changes in forest composition (i.e., as suggested in the panels of Figure 4), regenerating vegetation associated with disturbance, isolated patches of increased agricultural and pasture land, and forested wetlands change. The combination of these semi-natural vegetation patterns have increasingly fragmented the late 19th-century land surface, and together with some urban development and encroachment onto formerly agricultural or forested land, have significantly enhanced its spatial heterogeneity. These changes can have important effects on the land surface energy budget.

Figure 5 summarizes the principal trends illustrated in Figure 3 with three main themes that reflect the 19th-to-20th century shift in NJ and environs from a region dominated by agriculture to a heterogeneous mosaic of cities and suburbs, forests, fields, and farms: urbanization (Figure 5(a)), reforestation (Figure 5(b)), and localized deforestation patches (Figure 5(c)). Here I show only those grid cells where the dominant land cover shifted from one type to another between the historical and present-day reconstructions. For example, Figure 5(a) shows those cells for which forest and agriculture had at least 50 percent fractional coverage in the historical reconstruction but more than 50 percent urban fractional coverage in the present-day reconstruction. Similarly, Figure 5(b) shows those grid cells that converted from dominant agriculture to dominant forest[1], and Figure 5(c) shows a localized conversion from forest to any non-forest land cover type. I return to these three themes later in the thesis as a way to highlight general ideas about the impact of different land conversions on interactions between the land surface and the atmosphere, specifically by compositing various climatological variables over these different sets of grid cells. According to these

[1] By this definition, the present-day forest composition is ignored. Hence, reforestation as defined here represents any combined conversion from historical agricultural and pasture land to DBL, ENL, and mixed forest types.

themes, so-defined, 17 percent of all land surfaces in the region have been affected by urbanization, 22 percent by reforestation, and 8 percent by deforestation. However, it is important to recognize that urbanization and deforestation are not mutually exclusive land use trends, as some of these grid cells overlap (i.e., compare Figures 5(b) with 5(c)). Using my criterion, for example, 47 percent of the land that has been deforested has also accounted for 24 percent of the total acreage of land that has become urbanized.

I have used a threshold of 50 percent (applied to both the historical and present-day datasets) to identify grid cells with one of these conversions. Such a threshold can be considered to be somewhat arbitrary, as different criteria would include or exclude different percentages. Applying different threshold values, however, would not qualitatively affect my conclusions.

3.8. Chapter summary

A comparison of these historical and present-day land cover reconstructions clearly reveals a dramatic decline in prime agricultural land across NJ and the region and a simultaneous expansion of urban land surfaces, especially in central and northeastern NJ, and in far southeastern PA and NY, during this time period. Reforestation has occurred within a broad region of eastern PA into northern NJ, with some patches of deforestation in central and southern NJ and on LI. These datasets have shown that 17 percent of all land surfaces in the region have been affected by urbanization, 22 percent by reforestation, and 8 percent by deforestation. These land use shifts, in effect, have transformed a homogeneous and predominantly agrarian landscape into a heterogeneous mosaic of forests, farms, fields, and urban areas over a roughly century-long time period.

References

Agthe, D. E. (1964), A study of the effect of urbanization on agriculture in New Jersey, M.S. thesis, 59 pp., Rutgers, the State University of New Jersey, New Brunswick.

Alderman, D. R., Jr., M. S. Bumgardner, and J. E. Baumgras (2005), An assessment of the red maple resource in the northeastern United States, *Northern J. Appl. Forestry*, *22*, 181-189.

Boardman, J., and D. T. Favis-Mortlock (2001), How will future climate change and land-use change affect rates of erosion on agricultural land?, paper presented at the *Soil Erosion Research for the 21st Century, Proc. Int. Symp.*, Honolulu, Hawaii, 3-5 January.

Cunningham, J. T. (1981), New Jersey's rich harvest: a brief history of agriculture in New Jersey, paper published in commemoration of the 200th anniversary of the New Jersey Agricultural Society, 29 pp., The New Jersey Agricultural Society, Trenton, New Jersey.

Fabian, M. S., and D. J. Burns (1966), The role of farmer-owned fruit and vegetable marketing organizations in New Jersey: Part I: Present status, 57 pp., New Jersey Agricultural Experiment Station, Department of Agricultural Economics and Marketing (A.E. 315), Rutgers, the State University of New Jersey, New Brunswick, New Jersey.

Hart, J. F. (1991), The perimetropolitan bow wave, *Geogr. Rev.*, *81*, 35-51.

Lathrop, R., and J. Hasse (2006), Tracking New Jersey's changing landscape, in *New Jersey's Environments: Past, Present, and Future*, edited by Neil M. Maher, pp. 111-127, Rutgers University Press, New Brunswick, New Jersey.

Little, S. (1979), Fire and plant succession in the New Jersey Pine Barrens, in *Pine Barrens: Ecosystem and Landscape*, edited by R. T. T. Forman, pp. 297-314, New York Academic Press, New York City, New York.

Marshall, S. (2004), The Meadowlands before the commission: Three centuries of human use and alteration of the Newark and Hackensack Meadows, *Urban Habitats*, *2*, 4-27.

Schmidt, H. G. (1973), *Agriculture in New Jersey: A three-hundred year history*, 335 pp., Rutgers University Press, New Brunswick, New Jersey.

Stansfield, C. A. (1998), *A geography of New Jersey: A city in the garden*, 304 pp., Rutgers University Press, New Brunswick, New Jersey.

U.S. Department of Agriculture (USDA) (1992), National Agricultural Statistics Service (NASS), Vol. 1(30), Census of Agriculture, *New Jersey State Data, Land Use and Acres Diverted: 1992 and 1987*, p. 17, U.S. Government Printing Office, Washington, D.C.

U.S. House, Bureau of the Census (1960), *Historical statistics of the United States: colonial times to 1957, a statistical abstract supplement*, p. 789, The Social Science Research Council, United States Bureau of the Census, Washington, D.C.

Vermeule, C. C. (1889), Topographical Atlas Sheets 1-17, *Atlas of New Jersey, Geological Survey of New Jersey*, 62 x 88 cm, 1883-1889, Julius Bien and Company, New York, NY, Special Collections and University Archives, Rutgers University Libraries.

Vermeule, C. C. (1897), Drainage of the Hackensack and Newark tide-marshes, Map of Hackensack Meadows, in *Geological Survey of New Jersey, Annual Report of the State Geologist for the year 1896*, pp. 287-318, MacCrellish and Quigley, Trenton, New Jersey.

Vogelmann, J. E., S. M. Howard, L. M. Yang, C. R. Larson, B. K. Wylie, and N. Van Driel (2001), Completion of the 1990s National Land Cover Dataset for the Conterminous United States from Landsat Thematic Mapper Data and Ancillary Data Sources, *Photogrammetric Engineering and Remote Sensing*, *67*, 650-662.

Widmann, R. H. (2002), Trends in New Jersey forests, *Paper NE-INF-148-02*, USDA Forest Service, Northeastern Research Station.

CHAPTER 4 – Surface Meteorological and Energy Budget Changes

4.1. Introduction

In the previous chapter, I described the pronounced land use shifts that have occurred in New Jersey (NJ) and the surrounding states during a roughly century-long period of time. For instance, the increase in 20th-century urban land cover (with a concomitant loss of 19th-century vegetation) may be reflected in significant changes to the land surface parameters (LSPs), including surface albedo, net roughness, and fractional vegetative cover. In effect, vegetated land surfaces have in many areas been largely replaced by impervious urban surfaces with very different physical properties. Combined with the trends of reforestation and isolated deforestation that have also occurred in the region, these land cover changes have created a modified set of surface boundary conditions for the lower atmosphere, altering the radiative, energy, and soil moisture budgets that help modulate land-atmosphere exchanges and thus influence weather and climate [*Giorgi and Avissar*, 1997; *Pielke*, 2001].

As numerical studies have shown that the surface climate can be sensitive to these land use trends, the initialization of the Regional Atmospheric Modeling System (RAMS) model with my land cover reconstructions, together with the specification of identical background weather conditions, have provided me with a strategy to quantify the mean warm-season climate response to the land cover changes. In this chapter, I first evaluate the present-day ensemble of RAMS runs with the corresponding observations at weather stations across the region. This procedure helps me understand model performance better, identifying systematic errors and sources of bias. I then describe the mean monthly changes in near-surface air and dewpoint temperatures, monthly rainfall, soil moisture, and other meteorological variables that result from the simulated land use and land cover change (LULCC). Finally, I show how land use trends in this region modify the components of the land surface energy budget, including the turbulent heat and radiative exchanges between the surface and lowest atmosphere.

4.2. Model Evaluation

I evaluated my model configuration by comparing temperatures and dewpoints, as simulated in the present-day ensemble of RAMS runs (hereafter referred to as the control run ensemble), with observations from 15 surface weather stations within the region. These stations, as shown in Figure 6(a), are located within grid cells that have a variety of present-day land cover types (Figure 6(b)). Some of these locations have a large fraction of urban cover, while other locations are characterized by patches of forested land, surface water, or other vegetation types with varying fractional coverage.

Mean observed and model-simulated air and dewpoint temperatures for July 1999, listed in Table 4 for each station, indicate that observed temperatures (both air and dewpoints) are generally warmer than those of the control run ensemble. Over all 15 stations, observed surface air and dewpoint temperatures averaged 1.5°C and 1.8°C higher, respectively, than those of the control run ensemble, implying that the model underestimates air and dewpoint temperatures. Although this cool bias suggests that initial soil moisture values were still too high during the spinup, considering the prolonged drought used as background conditions, the soil moisture and soil temperature values I used to initialize the spinup (as I described earlier in section 2.6) resulted in the closest match between model values and surface observations across the region. Figure 7(a) and 7(b) show the monthly time-series of observed and simulated air and dewpoint temperatures, respectively, regionally averaged over these 15 stations. Compared to observations, the model is clearly moister during some periods (e.g., 12-16 July) but noticeably cooler and drier during other periods (e.g., 21-24 July). This discrepancy between model-simulated values and observations warranted a closer examination to determine whether or not some stations were largely contributing to the cool model bias.

At least for temperature, the majority of this cool model bias comes from the grid cells containing three stations located closest to the coastline (ACY, NYC, and LGA). Model temperatures at these stations averaged 4.8°C cooler than observed values. The monthly time-series of surface air and dewpoint temperatures that are averaged for these three "coastal" stations, as shown in Figures 7(c) and 7(d), respectively, also indicate that the +/- 1.0 standard deviation can be as large as 2.0°C. It is likely that systematic errors arising from the use of monthly-mean sea surface temperatures (SSTs), and/or the fact that these grid cells in RAMS contained fractional amounts of ocean as well as land, contributed to these larger biases. As these three stations are located within grid cells adjacent to those along the immediate coastline, it is likely that the horizontal diffusion and advection of marine air modified by the monthly-mean SSTs are contributing to the cooling of the grid cells that include these stations, especially during the second half of the analysis period for both air and dewpoint temperatures.

This model-simulated cooling effect is not significant at other stations that have fractional coverage of water within the grid cell, such as PHL (i.e., see Figure 6(b)) or even those in close proximity to surface water or wetlands, such as PNE and ILG. These stations do not show a cool model bias because they are located within grid cells where the areal coverage of surface water or moist soil is not widespread enough to offset the local LULCC-induced warming. In addition, though, the time-series of simulated air temperatures at PHL further suggests that horizontal diffusion and advection of warmer air from the highly urban grid cells adjacent to PHL does not have a significant impact on model air temperatures at PHL. Other stations like NYC are similarly surrounded by highly urban surfaces and yet air temperatures largely respond not to the diffusion/advection processes but to the close proximity of these grid cells to an extensive water body (the ocean). For these reasons, I have removed the 3 "coastal" stations to further evaluate how RAMS would perform regionally, while keeping stations like PHL and PNE in the regionally-averaged time series, described below.

The time series of observed and model-simulated air temperatures and dewpoints, averaged over the remaining twelve "inland" stations and shown in Figures 7(e) and 7(f), suggests that the control run ensemble captures reasonably well the overall day-to-day trends throughout July. The model was generally able to reach daily maximum and minimum temperatures during the full simulation period (Figure 7(e)), with periods of more pronounced cool bias in minimum temperatures during the second half of the month (also visible in the dewpoints, Figure 7(f)). The time-series of the mean standard deviations of these variables (over all twelve stations) for the control run ensemble, also shown in Figures 7(e) and 7(f), are rather small, suggesting that the different model atmospheres are reasonably consistent for temperature and dewpoint during the month. Although the 3 "coastal" stations were removed, the regional time-series still shows a pronounced cool bias during the period of 21-24 July. Persistent low-level clouds (i.e., the lowest 300 m of the model atmosphere) over the entire region, with little or no simulated rainfall, contributed to the cool bias during this period. Varying the soil type and the initial soil moisture and temperature (at the start of the spinup period) did not qualitatively improve these comparisons between model and observations.

Finally, the observed and model-simulated July rainfall totals, averaged over the twelve stations, were 13.2 mm and 13.1 mm, respectively. These are very light monthly amounts that underscore the severity of the regional drought and indicate that, in the broadest terms, it was adequately captured by the model.

4.3. Simulated Differences in Surface Meteorological Variables between the Historical and Present-Day Landscapes

Considering the land use shifts previously described in Chapter 3, I document the sensitivity of simulated surface air and dewpoint temperatures, rainfall, and surface heat and radiative fluxes to the reconstructed late 19th century and satellite-observed late 20th century landscape boundary conditions. Any changes in these meteorological variables, at least for this study, were solely due to the land cover changes between the ensembles and are thus independent of any other anthropogenic forcing.

4.3.1. Air temperatures

Monthly average differences in RAMS air temperatures at the lowest atmospheric level of my model (for the present-day ensemble minus the historical ensemble, for each grid cell, hereafter applied to all variables) are shown in Figure 8. Simulated mean temperatures are 0.3-0.6°C warmer for the present-day landscape over a large portion of the New Jersey (NJ) coastal plain, with additional increases in northeastern NJ, Long Island (LI), and southern Connecticut (CT). Most of this warming is generally consistent with the expansion of urban surfaces in the New York City, LI, northern NJ, and Philadelphia metro areas since the late 19th century (e.g., see Figure 5(a)). The warming that is also evident over the inland coastal plain of southern NJ may be due to some combination of deforestation (Figure 5(c)) and urbanization, in addition to some potential changes in forest composition. For example, the shallower rooting depths that accompany a historical conversion from mixed to evergreen needleleaf (ENL) forest in the Pine Barrens of south-central NJ effectively limits access to deeper soil moisture; the enhanced stomatal resistance contributes to these surface air temperature increases.

In addition, there is a mean cooling of 0.1-0.2°C for the present-day landscape within eastern Pennsylvania (PA) and northwestern NJ. This cooling has generally occurred over locations where there was a conversion from agricultural and pasture land to deciduous broadleaf (DBL) forest. The largest decreases in mean temperature (i.e., the darker blue shaded contours in Figure 8) resemble the locations of reforestation in Figure 5(b).

Since these differences reflect those temperature changes between the ensembles means for my two land cover cases, I also evaluated the variability of the temperature differences between individual ensemble members (Figure 9). The main point is that temperature variation between these different member combinations is, in general (i.e., except for those areas where there are distinct, random spatial differences in localized rainfall, like central NJ in Figure 9(g)), less than the variation between the historical and present-day ensemble means. This gives us additional confidence that the simulated temperature change that accompanies the imposed land cover change in the model is, in fact, robust. The panels of Figure 9 also indicate that the mean monthly temperature change between individual members (for example, the 1 July atmosphere with present-day land cover minus the 3 July atmosphere with historical land cover, as shown in Figure 9(b)) are generally similar to the corresponding temperature changes between old and new land cover.

The variability between the ensemble runs can also be quantified by noting the changes in the standard deviation of mean monthly air temperature $\sigma(T)$, as shown in Figure 10(a). This was calculated by subtracting, at each grid cell, the average monthly $\sigma(T)$ of the historical ensemble members from the respective $\sigma(T)$ of the present-day ensemble members, yielding the net potential change of $\sigma(T)$ between the late 19th and late 20th centuries. The figure further illustrates how the spatial differences in monthly rainfall between the individual ensemble members, and the ensembles themselves, create larger variability in the temperatures at a given location. For example, as will be discussed further in section 4.3.3, an intense convective event that affected the region in the historical ensemble fell on an area of central NJ close to 74.4°W and 40.5°N. Likewise, in the present-day ensemble, intense rainfall from this same convective event affected a different area to the west, close to the PA-NJ state border. The resulting spatial variations in rainfall have increased $\sigma(T)$ by an estimated 0.3-0.4°C at these locations between the ensembles. Finally, Figure 10(b) shows the differences in $\sigma(T)$ between the coolest present-day run and the warmest historical run, hereafter denoted as $\sigma(T_{CW})$. Specifically, at each grid cell, once the temperatures from the warmest run with historical land cover were subtracted from the coolest run with present-day land cover, I calculated the standard deviation with respect to the ensemble mean for each landscape. The figure suggests that the *σ(T)* between the ensemble means is generally smaller in magnitude, and of the opposite sign, compared to $\sigma(T_{CW})$. Since the magnitude of $\sigma(T_{CW})$ is, in general, the opposite sign when the present-day landscape is cooler than the historical landscape, this trend gives us one more measure of confidence that the temperature variation between individual ensemble combinations for a given area or land cover tends to be smaller than the LULCC signal, and my results are therefore robust.

These land cover changes have also influenced the simulated monthly mean daily maximum and minimum temperatures (Figure 11). In general, the patterns match those for the mean temperatures, but with more pronounced changes in the daily maximum temperature. In other words, the present-day landscape seems to be associated with a larger diurnal temperature range (DTR).

This raises an interesting question – because urbanization is a large driver of these simulated temperature changes, why do we not see a decrease in DTR for the more urbanized, present-day landscape? For example, *Collatz et al.* [2000] and *Kalnay and Cai* [2003] suggest that urbanization is consistent with *decreases* in DTR. In a physical sense, the urban heat island (UHI) phenomenon results from the combination of distinct effects of the urban environment on air temperatures. First, the urban landscape, with its darker-colored roof structures and paving materials, can absorb a greater percentage of available incoming shortwave radiation compared to adjacent rural areas [*Taha*, 1997]. Simultaneously, the removal of vegetation shifts the surface energy partitioning into more sensible and less latent heat [*Chagnon*, 1992]. Both of these effects contribute to elevated daytime surface air temperatures, and, as will be discussed shortly, RAMS reproduces this expected behavior.

In addition, however, the built-up areas have increased mass and thus increased heat storage [*Oke*, 1982; *Grimmond and Oke*, 1999]. Other effects, like anthropogenic energy release [*Oke*, 1988] and air stagnation within urban canyons in addition to the urban impact on the boundary layer structure [*Martilli*, 2002], also contribute. Observed nocturnal temperatures within these areas tend to cool much more gradually than they do within the less-developed surroundings, often leading to a relative reduction in the DTR over the city. At this time, the RAMS land-surface scheme does not include these effects, resulting in a likely underestimate of the increase in daily minimum temperature in large urban regions of my model domain. Future versions of the LEAF land surface model will likely address some of these issues, for example, by including urban canopy heating terms as in *Brown and Williams* [1998] and *Voogt and Oke* [1997], and assigning different roughness heights for levels of the urban hierarchy (e.g., town, city, metropolis). In addition, for computational reasons, the vertical grid spacing of the lowest atmospheric layer of my model (i.e., 50 m) is a full order of magnitude higher than what *Pielke et al.* [2007] suggest is needed to properly reproduce observed nighttime temperature trends. Because nocturnal temperatures can be particularly sensitive to boundary-layer variables such as wind speed, surface roughness, and soil heat capacity [*Shi et al.*, 2005], the lack of high vertical grid resolutions on the order of 5 m or less can create additional inaccuracies when modeling near-surface nighttime temperatures [*Pielke et al.*, 2007]. As computing power increases, carrying out simulations with a full urban model coupled to RAMS, and also with a sufficiently high horizontal and vertical grid resolution, is a promising avenue for future study.

Figure 12 shows the monthly mean diurnal cycle of surface air temperature differences for all land surfaces and separately for the grid cells associated with the three land cover change (LCC) themes shown in Figure 5. Over all land surfaces, the peak warming of about 0.2°C lasts from locally late morning to early evening. These temperature differences decrease during the night to a minimum around sunrise. For the grid cells that have experienced urbanization (Figure 5(a)), the pattern is similar but with a much larger signal, e.g., a peak afternoon increase for the present-day landscape by about 0.7°C. Consistent with Figure 8, the reforested grid cells (Figure 5(b)) show slightly cooler temperatures throughout the day. Finally, the deforestation patches (Figure 5(c)) show a similar pattern to the urbanized areas, but with slightly smaller amplitude. The warming in my model over these deforested areas is also generally consistent with the warm-season maximum surface temperature increases [*Narisma and Pitman*, 2003] due to regional deforestation trends in southeastern Australia.

4.3.2. Dewpoint temperatures

Figure 13 shows the differences in mean July 1999 surface dewpoint temperatures T_d between our present-day and historical ensembles. The dewpoint decreases of 0.3-0.6°C within central and southern NJ suggest that the near-surface air over the present-day landscape is less humid. Together with the simulated increase in surface air temperatures, the first atmospheric model layer is warmer and drier for the present-day landscape. By contrast, in the reforested areas of the domain (e.g., in eastern PA), dewpoints are generally greater in the present-day ensemble.

The monthly mean diurnal cycle of dewpoint differences (Figure 14) is consistent with these general trends. Here, the grid cells where localized deforestation has occurred have greater peak dewpoint decreases than the urbanized grid cells (0.6°C compared to 0.4°C), in part because of the compensating effect of the larger temperature increases over present-day urban areas. The peak increase over the reforested grid cells is about 0.3°C during mid-afternoon.

The dewpoint decreases between the individual ensemble members (not shown) are also generally spatially consistent with these changes. For a given land cover dataset, monthly dewpoint values are all within 0.1-0.3°C for individual ensemble members, and like temperature, the standard deviations are slightly larger in magnitude for those grid cells that have been converted to urban land cover, while smaller standard deviations characterize the grid cells that have become reforested. As with temperature, variations in monthly rainfall between the members can produce large spatial differences in dewpoints. For example, for some combinations of ensemble members, there was a persistent (and pronounced) dewpoint decrease in central and southern NJ resulting from the above-mentioned displaced convection. Nevertheless, the broad dewpoint changes are reasonably robust and clearly seem to result from the LULCC.

4.3.3. Rainfall

Figure 15(a) illustrates the mean spatial differences in July rainfall totals for the period from 12:00 UTC 3 July and 04:00 UTC 1 August (i.e., the total rainfall that fell between 8:00 am 3 July and 12:00 am 1 August). The difference pattern is more or less random across the model domain, with patchy decreases and increases adjacent to each other. This suggests slight shifts in the locations of convection rather than systematic changes in the amount and/or character of the rainfall. Consistent with this, the domain-averaged hourly rainfall rates and timing of individual rain events, as shown in Figure 15(b), are similar in both ensembles.

Figure 15(b) also shows that, for a given land cover dataset, the domain-averaged +1.0 standard deviation between the individual ensemble members, added to the respective rainfall rate at each time step, can be quite large during the times of convective events. Thus, the variation of rainfall among the three ensemble members is approximately as large in magnitude as the variation of rainfall between the land cover cases. For instance, during the evening of 17 July, the 29 June present-day land cover ensemble member simulated an intense convective cell in which rainfall rates were 7.0 mm h^{-1} along the NJ/NY state border. At the same time, a weaker (3.5 mm h^{-1}) and smaller convective cell developed in the 1 July ensemble member over the same region, and there was virtually no convection that developed in the 3 July ensemble member around this location, all three runs having the same land cover. The large differences in rainfall rates resulted in significant variations in total rainfall among the ensemble members for a given convective event. This suggests that the changes in monthly rainfall amounts between my land cover cases are random, consistent with the small spatial scale and high degree of non-linearity of summertime convective precipitation in this region. As noted above, temperatures and dewpoint differences between the ensembles can be sensitive to these spatial differences in rainfall, but only in localized areas.

4.3.4. Soil moisture and soil temperature

The relative lack of monthly rainfall over the region has directly impacted soil moisture, which in turn, modulates surface air and dewpoint temperatures. The time series of domain-averaged differences in soil moisture are shown in Figure 16(a). Of the four soil layers shown, the smallest differences in soil moisture have occurred in the topmost layer (5-10 cm) with these differences generally becoming larger with increasing depth.[1] In fact, compared to the other soil layers shown in Figure 16(a), there is a relatively larger increase in present-day soil moisture in the deepest soil layer (80-100 cm) during the start of the July analysis period. This increase may likely be the effect of urbanization, for the following reason.

At the start of the analysis period, all ensemble members were initialized with identical soil moisture values. The present-day landscape, however, has much more coverage of impervious urban surfaces compared to the historical landscape. These impervious surfaces act to significantly limit the availability of soil moisture to the lowest atmosphere, which is an effect that contributes to the enhanced sensible heating and reduced latent heating (besides the lower albedo). An impervious "barrier" is created between the modern landscape and the atmosphere over 17 percent of the region; hence, soil moisture in the upper soil layers that would otherwise evaporate into the atmosphere (i.e., as latent heat flux) drains down to deeper soil layers. This effect in LEAF-2 increases deep-layer soil moisture values at the start of the analysis period. Unlike many other regional models, LEAF-2 does not allow deep-layer soil moisture to drain out the bottom-most soil layer (i.e., the “free-drain” approach) but rather allows incoming soil

[1] This is counter-intuitive, as the soil moisture differences between the ensembles would be expected to be greatest for the soil layers closest to the surface.

moisture from upper soil layers to accumulate there. Figure 16 also suggests that, at least for most upper soil layers, the soil moisture differences for the second half of the month become smaller between the historical and present-day landscapes.

While the conversion to present-day urban land cover has likely increased initial deep-layer soil moisture in LEAF-2, Figure 16(a) also suggests that soil moisture in this layer may also be responding diurnally to the 22 percent of the region that has become reforested. According to Table 3, the rooting depth of any of the present-day forest classes used in LEAF-2 extend deeper into the soil than the historical agricultural and pasture land class. As transpiration strongly depends on LEAF-2 vegetation class [*R. Walko*, 2008, personal communication], an increase in daytime evapotranspiration rates for the grid cells that have become reforested (not shown) suggests that the new forest cover has increased the availability of deep-layer soil moisture to the lowest atmosphere, compared to that of the historical landscape. Since transpiration is the only available mechanism for producing a significant diurnal cycle of deep-layer soil moisture, Figure 16(a) implies that the 80-100 cm soil moisture differences between the landscapes do, in fact, respond to the diurnal cycle of temperatures over the present-day forested landscape.

Domain-averaged soil temperature differences, as shown in Figure 16(b), at least at the 5-10 cm layer, generally follow the diurnal cycle of air temperatures, with the temperature differences becoming larger during the day and smaller at night. Soil temperatures at the deeper depths have reduced diurnal fluctuations, as expected, since these depths are relatively isolated from large surface air temperature variations. Furthermore, at increasing depths, soil temperatures for the present-day landscape generally become slightly cooler than the corresponding historical soil temperatures, especially during the second half of the period. This monthly cooling trend is consistent with the increase in mean soil moisture for the present-day landscape within these layers.

4.3.5. Boundary-layer heights

The mean monthly differences in boundary-layer (BL) heights are shown in Figure 17(a). The spatial pattern of these height differences closely follows the changes in monthly mean near-surface air temperatures that were plotted in Figure 8. The BL heights can generally increase by as much as 150-200m for the present-day compared to the historical landscape where warming of surface and BL temperatures has occurred.

The monthly diurnally-averaged BL height differences for each of our LCCs are shown in Figure 17(b). For those regions that have become urbanized, the daytime BL for the present-day ensemble (at 21:00 UTC or 5:00 pm local time) is higher by about 75 m compared to that for the historical ensemble. For the deforestation LCC, the present-day BL increases in height more rapidly compared to the historical landscape by afternoon, which suggests a faster heating rate in a 3 h period around the time of maximum surface heating. In reforested regions, however, the BL height changes between the historical and present-day landscapes have the opposite trend (to the other LCCs).

4.4 Simulated Differences in the Surface Energy Budget between the Historical and Present-Day Landscapes

4.4.1. Net broadband albedo and heat fluxes

The changes in RAMS-calculated net broadband surface albedo between the present-day and historical ensembles, as shown in Figure 18, are generally consistent with the land cover changes I have described in Chapter 3. Urbanization has produced a strong albedo decrease in the model, which acts as a positive radiative forcing on the surface energy budget. The urban class in LEAF-2 was defined using an estimated broadband surface albedo value of 0.15 which combines the albedos from both residential and traditional urban land cover types into a "harmonized" value representative of a combination of low density residential, high density residential, and urban built-up and commercial surfaces [*Pielke*, 2002; *Offerle et al.*, 2003]. *Jin et al.* [2005] also reported that urban areas have surface albedos that are lower than those of croplands and deciduous forests during summer. As I have documented, the conversion of the predominant 19th-century agricultural and forested landscape to urban areas resulted in decreased albedos in these regions, as well as decreased evapotranspiration (ET) rates due to reduced vegetation and a lower LAI (and the resulting effects on latent heat flux discussed later in this section). The decreased surface albedo and ET rates contributed to the well-defined urban warming in the simulations with present-day land cover and the largest simulated surface air temperature increases in the region.

Within reforested areas, however, there can be two competing influences. First, the increases in albedo in the reforested areas have combined with reduced sensible heating to cool surface air temperatures over the present-day landscape. This surface cooling has occurred primarily over locations where the dominant land use has shifted from 19th-century agricultural and pasture land to 20th-century DBL forest (refer to Figure 5(b)). The other competing influence has occurred in regions like central and south-central NJ where there have been an assortment of land cover changes, including forest regrowth (and increased deciduousness), isolated deforestation, limited agricultural expansion, and urbanization. These are LULCC that have been relatively modest compared to the dominant land use shifts described in Figure 5(b) and 5(c). Despite the albedo increases, these land cover changes have mildly increased sensible heating for the present-day landscape; in effect, they have produced a surface warming that is not quite as pronounced as in the most highly urbanized areas. Furthermore, as these LULCC have occurred within a small area of central and south-central NJ, the accompanying albedo increases are also highly fragmented. This enhanced land surface fragmentation, combined with the repartitioning of energy fluxes towards increased sensible heating, can affect convection initiation and will be examined in greater detail in the next chapter.

While urban surfaces in RAMS have a lower albedo (0.15) compared with many vegetation types I have used in this study, including agriculture and pasture land (0.18) and deciduous forest (0.20), the urban land cover class in LEAF-2 also has a reduced vegetative component that results in a drier surface layer. Sensible heating is thus strong in the daytime, leading to pronounced increases in maximum urban temperatures. These albedos, however, are not relevant during the nighttime hours, and with no representation of anthropogenic heat sources in LEAF-2, modeled nocturnal minimum temperatures are lower than observed values.

The apparent surface albedo increases in central NJ demonstrate that land use practices can alter the radiative energy balance. As I show in the following sections, the removal of the forest canopy shifts the radiative partitioning towards sensible heat flux that warms the overlying air. While the radiative energy balance on local and regional scales can be modified by changes in albedo, it is the changes to the surface thermal and moisture characteristics resulting from LULCC, in this case deforestation, which can alter the partitioning of net shortwave radiation between sensible and latent heat flux.

I consider the energy balance of the surface, defined here to consist of the top layer of soil (5 cm thick in this study), vegetation, and the air within the depth of the vegetation. The net sensible and latent flux leaving this surface is given by:

$$Q_N = Q_H + Q_E + Q_G \tag{1}$$

where Q_H is the turbulent sensible heat flux to the atmosphere, Q_E the turbulent latent heat flux to the atmosphere, and Q_G the sensible heat flux to deeper soil layers. The flux Q_G is a relatively small percentage, generally 10 percent or less, of Q_N when averaged over a diurnal cycle [*Sellers et al.*, 1997], so it is considered negligible in this analysis.

The net radiative flux received at the land surface R_N is defined by:

$$R_N = R_{SW\downarrow} - R_{SW\uparrow} + R_{LW\downarrow} - R_{LW\uparrow} \tag{2}$$

where $R_{SW\downarrow}$ and $R_{LW\downarrow}$ are the downward shortwave and longwave radiative flux components, respectively, that are incident on the land surface; $R_{SW\uparrow}$ is the reflected flux of shortwave radiation; and $R_{LW\uparrow}$ is the upward flux of longwave terrestrial radiation. To further simplify my discussion, I define R_{SW} (note the absence of an arrow in the subscript) as the difference between the incoming and reflected fluxes of solar radiation, and likewise, R_{LW} as the difference between the downward flux of longwave radiation and the terrestrial flux emitted by the surface to the atmosphere. By this definition, and implied by Eq. 2, the net radiative fluxes that are directed toward (away from) the surface are defined as positive (negative). Eq. 2 shows that the sum of R_{SW} and R_{LW} is equivalent to the total net radiation received at the land surface.

I describe the differences in R_{SW} and R_{LW} between the present-day and historical ensembles in the following section on focus here on the turbulent fluxes. Specifically, mean monthly differences in sensible and latent heat fluxes are shown in the panels of Figure 19. Figure 19(a) indicates that Q_H has increased by 10-30 W m^{-2} within the areas where mean temperatures have warmed in my present-day ensemble, and, simultaneously, Q_E has decreased over the present-day landscape in these same regions, as shown in Figure 19(b). The monthly area-averaged trends of these fluxes (not shown) show an overall increase in Q_H with a decrease in Q_E. In fact, between 3 July and 31 July, the mean area-averaged daily Q_H in both ensembles increased by about 65 W m^{-2} (i.e., an estimated 105 percent increase), as the daily area-averaged Q_E sharply declined by 80 W m^{-2} but remained positive at the end of the month (i.e., an estimated 65 percent decrease). These general trends match up reasonably well for those grid cells where urbanization and localized deforestation have occurred. The enhanced Q_H is also consistent with the lack of significant monthly regional rainfall totals simulated by the model.

The mean diurnal cycle of heat flux differences for each of the LCC themes is shown in Figure 20. I supplement this figure with Table 5, which lists the monthly mean percentage change in each of the heat and radiative flux components at 18:00UTC local time (i.e., close to the time of maximum surface heating), together with the respective percentage changes in Q_N and R_N. (These are percentage changes, not absolute changes in W m^{-2}).

Averaged over all present-day land surfaces, there has been minimal change in the intensity of these heat fluxes over the diurnal cycle, aside from a small positive increase in Q_N during the afternoon (3.6 percent). The conversion to urban land cover produces a large change in these heat fluxes. Q_H increases over the present-day urban landscape by an estimated 25 percent during the early afternoon with a reduction of Q_E by 24 percent (see Figures 20(a) and 20(b)). These changes are consistent with the decreases in surface albedo I have described earlier (Figure 18). I also note that *Adegoke and Gallo* [2006] produced similar trends in Q_H and Q_E with their LULCC sensitivity study of the urban Baltimore-Washington D.C. area. Reforestation, however, produces the opposite effect, decreasing Q_H while increasing Q_E. Figure 20(c) shows that upward turbulent energy flux over these reforested areas can increase by 30 W m^{-2} for the present-day landscape. This is very similar to the peak increases over present-day urban regions, but unlike the urbanization LCC, the contribution is due to enhanced latent heating.

For the localized deforestation patches, the peak increase in Q_H during the afternoon is very close in magnitude to the increase over urbanized areas. However, because of the sharper decline in Q_E over these deforested grid cells, the change in Q_N becomes weakly negative during the time of maximum surface heating (Figure 20(c)).

This decrease in Q_N does not necessarily imply that the present-day ensemble atmosphere would be cooler, because horizontal and vertical advective and turbulent heat mixing within the atmosphere, as well as direct radiative heating of the atmosphere, are other pathways that can also warm or cool air temperatures.

4.4.2. Radiative fluxes

Mean monthly differences in R_{SW}, as shown in Figure 21(a), suggest that the present-day landscape has received, in general, about 4-10 W m^{-2} more net shortwave radiative flux compared to the historical landscape. These changes are also positive for nearly the entire state of NJ. The increases in R_{SW} for the present-day landscape imply that more sunlight reaches the surface, especially within urban locations in NY and NJ, which, in turn, suggests less cloudiness in the present-day ensemble. In fact, the month of July 1999 was generally not a cloudy month. The only differences (albeit small) in cloud water mixing ratios between the ensembles generally occurred within the lowest 500m of the present-day urban boundary layer, primarily limited to the morning hours and producing less cloudiness over the present-day urban landscape. Note that these areas have also experienced strong albedo decreases, so the additional R_{SW} contributes to the enhanced surface warming.

There are stronger increases in R_{SW} over some isolated areas of southern NJ in the same locations where my land cover reconstructions suggest a conversion from mixed to ENL forest. In this region centered on 39.7°N and 74.6°W, the resulting forest species change allows 10-16 W m^{-2} more net shortwave radiation to be received by the land surface in my present-day ensemble. There is also an accompanying 0.4-0.8°C warming of present-day soil temperatures within this same region (for the four soil layers above a 30 cm depth), with smaller temperature increases still evident within deeper soil layers.

Conversely, for those areas of eastern PA that have reverted to DBL forest, R_{SW} has decreased by 4-6 W m^{-2} with stronger radiative decreases over some of the more densely reforested areas. The conversion from agricultural and pasture land to DBL forest in these regions has increased the LEAF-2 surface albedo from 0.18 to 0.20 while also enhancing ET rates due to greater rooting depths. This is consistent with the 0.8-1.0°C cooling of the four topmost soil layers in these regions in my present-day ensemble (see Figure 16(b).

The mean monthly differences in R_{LW} between my simulations are shown in Figure 21(b) and in Table 5. The figure reveals little, if any, variation in R_{LW} associated with the urbanized grid cells. The most significant changes in R_{LW} appear to be related to changes in forest cover or composition. If the present-day landscape becomes reforested, which has occurred in the northern and western sections of the domain, R_{LW} has generally increased. However, in central and southern NJ, where the land cover changes have trended towards an increased deciduousness, R_{LW} has declined.

The differences in R_{LW} between my ensembles are induced by a combination of changes to the land surface and the atmosphere, which can, in effect, modulate the upward and downward fluxes of longwave radiation. Though I only illustrate net R_{SW} and net R_{LW} differences in Figure 21 and not the individual up and down components, I provide a general description of the upward and downward longwave radiative trends here. The differences in $R_{LW\uparrow}$ are generally consistent with the changes in surface temperatures between the ensembles and also differences between model emissivity values that can occur due to historical land cover shifts within a grid cell. The differences in $R_{LW\downarrow}$ are, however, due solely to changes in atmospheric conditions, such as differences in cloudiness, air temperature, or air humidity. The modeled decreases in $R_{LW\downarrow}$ are particularly evident near the central NJ coast where daily maximum temperatures over land have warmed by 1.0°C and surface air humidity fractions have also declined by 0.03. In effect, the change in $R_{LW\uparrow}$ is amplified relative to the changes in $R_{LW\downarrow}$, suggesting that the change in surface conditions has a more significant influence on longwave radiative flux than the change in atmospheric conditions that result from land cover change.

The mean diurnally-averaged changes in R_{SW} and R_{LW} for each of the LCC themes are shown in Figures 22(a) and 22(b), respectively, with the trends in total radiative flux R_N summarized in Figure 22(c). While the conversion to urban land cover has produced relatively strong increases in R_{SW} during the morning hours following sunrise, there were little, if any, diurnal changes in R_{LW} in my simulations. As a result, the diurnal increases in R_N (maximizing at 25 W m^{-2}) within urban areas resembled the corresponding trend in R_{SW}. The urbanization and deforestation LCCs also have relatively similar diurnal increases in R_{SW}.

4.5. Chapter summary

Throughout this chapter, I have described the ways in which historical land cover change can modify the properties of the land surface, consequently altering the key components of the surface energy balance that control processes at the land surface-atmospheric boundary. Urbanization has significantly warmed the land surface via strong decreases in albedo and increases in net shortwave radiation, both of which may have enhanced sensible heat flux by as much as 25 percent by early afternoon. However, reforestation (i.e., the conversion of agricultural and pasture land to deciduous forest) has generally increased surface albedo and reduced net incoming shortwave radiation, enhanced ET rates, and cooled surface air temperatures. The surface energy budget has also been strongly influenced by the potential changes in forest composition within central and southern NJ, where an increase in forest deciduousness, combined with isolated increases in agricultural and pasture land, may have enhanced surface albedo and decreased net shortwave and net downward longwave radiative flux. Over deforested regions, the repartitioning towards sensible heat flux with reduced ET rates has likely warmed daytime air temperatures and decreased dewpoints.

Daytime maximum temperatures over the present-day urban landscape also increased considerably more than nighttime minimum temperatures in these simulations, suggesting an enhanced DTR. The warming of nighttime minimum temperatures within these present-day urban areas was likely underestimated in RAMS because the LEAF-2 parameterization does not yet account for the increased thermal and radiative properties of urban surfaces that contribute to anthropogenic energy storage and release. Future versions of LEAF-2 will likely include this effect.

These albedo changes also modify the partitioning of radiative energy into sensible and latent heat fluxes, which can directly affect air temperature increases or decreases. Sensible heat flux has increased where the present-day landscape has warmed. The present-day landscape receives more net shortwave radiation compared to the historical landscape, a trend that is consistent for nearly the entire state of NJ. Over reforested areas, net longwave fluxes have noticeably increased, with the largest increases during the afternoon hours. In addition, my study suggests that a change in land cover type, and the associated change in surface properties, has a more significant influence on net longwave radiative fluxes than does the corresponding change in atmospheric conditions that results from land cover change.

References

Adegoke, J. O., and K. P. Gallo (2006), On the relation between surface spatial heterogeneity and climate prediction: Insights from the integration of fine resolution satellite land information into mesoscale climate models*,* paper presented at 86th Annual Meeting, Am. Meteorol. Soc., Atlanta, GA, 29 Jan-2 Feb.

Brown, M., and M. Williams (1998), An urban canopy parameterization for mesoscale meteorological models, paper presented at the *2nd AMS Urban Env. Symp.*, Albuquerque, New Mexico, 2-6 November.

Changnon, S. A. (1992), Inadvertent weather modification in urban areas: Lessons for global climate change, *Bull. Am. Meteorol. Soc.*, *73*, 619-627.

Collatz, G. J., Bounoua L., Los, S. O., Randall, D. A., Fung, I. Y., and P. J. Sellers (2000), A mechanism for the influence of vegetation on the response of the diurnal temperature range to changing climate, *Geophys. Res. Lett.*, *27*, 3381-3384.

Giorgi, F., and R. Avissar (1997), Representation of heterogeneity effects in earth system modeling: Experience from land surface modeling, *Rev. Geophys.*, *35*, 413-438.

Grimmond, C. S. B., and T. R. Oke (1999), Heat storage in urban areas: Local-scale observations and evaluation of a simple model, *J. Appl. Meteorol.*, *38*, 922-940.

Jin, M., R. E. Dickinson, and D. L. Zhang (2005), The footprint of urban areas on global climate as characterized by MODIS, *J. Clim.*, *18*, 1551-1565.

Kalnay, E., and M. Cai (2003), Impact of urbanization and land-use change on climate, *Nature*, *423*, 528-531.

Martilli, A. (2002), Numerical study of urban impact on boundary layer structure: Sensitivity to wind speed, urban morphology, and rural soil moisture. *J. Appl. Meteorol.*, *41*, 1247-1266.

Narisma, G. T., and A. J. Pitman (2003), The impact of 200 years of land cover change on the Australian near-surface climate, *J. of HydroMeteorol.*, *4*, 424–436.

Offerle, B., C. S. B. Grimmond, and T. R. Oke (2003), Parameterization of net all-wave radiation for urban areas, *J. Appl. Meteorol.*, *42*, 1157-1173.

Oke, T. R. (1982), The energetic basis of the urban heat island, *Q. J. R. Meteorol. Soc.*, *108*, 1-24.

Oke, T. R. (1988), The urban energy balance, *Progress in Physical Geography*, *12*, 471-508.

Pielke, R. A. (2001), Influence of the spatial distribution of vegetation and soils on the prediction of cumulus convective rainfall, *Rev. Geophys.*, *39*, 151-177.

Pielke, R. A., Sr. (2002), *Mesoscale meteorological modeling,* 2nd ed., 676 pp., Academic Press, San Diego, California.

Pielke Sr., R. A., C. Davey, D. Niyogi, S. Fall, J. Steinweg-Woods, K. Hubbard, X. Lin, M. Cai, Y.-K. Lim, H. Li, J. Nielsen-Gammon, K. Gallo, R. Hale, R. Mahmood, R. T. McNider, and P. Blanken (2007), Unresolved issues with the assessment of multi-decadal global land-surface temperature trends. *J. Geophys. Res.*, in press.

Sellers, P. J., Dickinson, R. E., Randall, D. A., Betts, A. K., Hall, F. G., Berry, J. A., Collatz, G. J., Denning, A. S., Mooney, H. A., Nobre, C. A., Sato, N., Field, C. B. and A. Henderson-Sellers (1997), Modeling the exchanges of energy, water, and carbon between continents and the atmosphere, *Science*, *275*, 502-509

Shi, X., R. T. McNider, D. E. England, M. J. Friedman, W. LaPenta, and B. Norris (2005), On the behavior of the stable boundary layer and role of initial conditions, *Pure Appl. Geophys.*, *162*, 1811-1829.

Taha, H. (1997), Urban climates and heat islands: albedo, evapotranspiration, and anthropogenic heat, *Energy and Buildings*, *25*, 99-103.

Voogt, J. A., and T. R. Oke (1997), Complete urban surface temperatures, *J. Appl. Meteorol.*, *36*, 1117-1132.

CHAPTER 5 – Impacts on Lower-Tropospheric Dynamics (Including the Sea Breeze) and Vertical Thermodynamic Profiles

5.1. Introduction

In the previous chapter, I have shown how historical land cover changes in New Jersey (NJ) and the surrounding region result in a relatively warmer and drier simulated surface climate, given identical background conditions. By altering the spatial pattern of the partitioning of turbulent fluxes (including altering the degree of heterogeneity), land use and land cover change (LULCC) can modify horizontal thermal gradients (including the contrast between land and ocean), thereby affecting near-surface wind flows, zones of mesoscale convergence and divergence, and hence the horizontal and vertical advection of atmospheric properties. These changes, combined with the changes in the vertical turbulent transports of heat and moisture, can, in turn, modify the vertical profiles of temperature, water vapor, and other thermodynamic variables in the boundary layer (BL) and lower free troposphere. All these changes have implications for the vertical thermodynamic structure and mesoscale dynamics of the lower atmosphere, including the development of the sea breeze along the NJ coast.

5.2. Simulated Differences in Boundary-layer Dynamics and Thermodynamics between the Historical and Present-Day Landscapes

In this section, I first compare the monthly mean horizontal and vertical wind changes between the landscapes. This allows us to identify the general heights in the BL where changes in the surface energy balance (i.e., turbulent heat fluxes) can enhance or suppress low-level convergence and vertical motion between the ensembles, altering the transport or advection of boundary-layer properties such as temperature and water vapor. I also examine domain-averaged mesoscale dynamics to show how the vertical distribution of atmospheric water vapor can be altered by mesoscale circulations that develop over each landscape.

5.2.1. Monthly mean horizontal and vertical winds

Figure 23 shows the monthly mean wind vector differences at increasing heights within the boundary layer, plotted over the monthly mean sensible heat flux changes between the historical and present-day landscapes. Within interior NJ, the winds close to the surface (200 m, Figure 23(a)) are most affected in areas with the largest increases in surface sensible heating, particularly in a region oriented southwest to northeast across the state. The enhanced sensible heating of the present-day landscape shifts the horizontal low-level wind flow and implies increased low-level convergence where the largest increases in sensible heating can alter the speed and/or direction of the wind vectors between the ensembles. Higher in the BL (800 m, Figure 23(b)), however, the wind differences are smaller across the region, but these differences generally increase again (though with the wind vector differences now more in the opposite direction) towards the upper part of the BL and lower free troposphere (1500 m and 2600 m, Figures 23(c)-(d)). This vertical structure of the change in wind speed reflects the vertical extent of the mesoscale circulation cells set up by the land-surface heterogeneity [*Baidya Roy and Avissar*, 2000; *Baidya Roy et al.*, 2003] and characterized by convergence near the surface and divergence further aloft. Except for the coastal areas in the northern part of NJ and around New York City[1], the mean horizontal winds show the strongest changes averaged over the whole month in the interior of the state, rather than along the coast. The changes in the sea breeze will be examined in more detail in section 5.3.

The changes in near-surface mesoscale convergence and ~2 km divergence can produce significant changes in the vertical winds. Monthly mean differences in vertical velocity *w* at 200 m and 1500 m between the landscapes are shown in Figure 24, generally spatially co-located with the areas of maximum wind speed changes. Figure 24 also illustrates how the differences in *w* between the two ensembles peaks in the middle and upper part of the BL (Figure 24(b)), rather than right near the surface (Figure 24(a)), consistent with our understanding of the dynamics of landscape-heterogeneity-forced mesoscale circulations [e.g., *Weaver*, 2004a].

5.2.2. Vertical heat and moisture transport

These changes in the vertical mesoscale winds described above (in section 5.2.1) influence the vertical transport and distribution of thermodynamic variables. Since inland mesoscale circulations can modify this vertical transport, any domain averages of *w* may be sensitive to large differences in effective resolution between the 1880 census and the U.S. Geological Survey (USGS) 1992 National Land Cover Dataset (NLCD) outside of NJ. Therefore, I longitudinally cropped my grid 3 domain for the analyses in the next two sections (i.e. section 5.2.2 and 5.2.3), removing most of the areas with potentially exaggerated surface heterogeneity increases (e.g., eastern Pennsylvania (PA)). This allowed me to take maximum advantage of the similar resolutions between the Cook map

[1] The location of this metropolis is shown in Figure 6(a), with the station identifier NYC.

series data and the NLCD. I present my results as domain averages on a revised grid 3 (72 x 138 cells), a domain that extends roughly to the far northern, southern, western, and eastern borders of NJ. According to the dominant land cover conversions I have previously defined in Chapter 3 (see section 3.7), 15 percent of this revised domain has been affected by urbanization, 16 percent by reforestation, and 7 percent by deforestation. Later in this chapter, the vertical difference profiles of thermodynamic variables will be categorized using these dominant land use conversions within the revised domain, as noted.

The time-series of mean differences in *w* between the landscapes, domain-averaged on this revised grid, is shown in Figure 25(a). In general, the daytime BL over the present-day landscape has slightly stronger large-scale subsidence (i.e., *w* differences are negative) especially during quiescent weather conditions. For example, during the period of minimal rainfall in this region between 3-12 July, the *w* differences in the lower BL between the ensembles are slightly negative during the afternoon hours. When convection does occur in both ensembles (e.g., during the evening of 17 July and 19 July, as shown in Figure 15(b)), the higher rainfall rates over the historical landscape are usually reflected in decreases of *w* over the present-day landscape (i.e., the darker blue shading in Figure 25(a)) because large-scale uplift is generally stronger in the historical ensemble during these times.

The time series of mean domain-averaged differences in the standard deviation of *w* between the ensembles (Figure 25(b)), hereafter represented by $\sigma(w)$), reveals the distinct signature of landscape-forced mesoscale uplift. The mesoscale circulations developed in both ensembles, generally between 500m and 2500m, but the figure suggests that the differences in *σ(w)* can be enhanced in the historical ensemble. This is in contradiction to the idea that the stronger *σ(w)* should occur in the present-day ensemble, as the significantly enhanced daytime sensible heating combined with the increased surface spatial heterogeneity of the modern landscape would be reflected in enhanced *σ(w)* within the mid BL.

Figure 26(a) shows the time-series of mean domain-averaged differences in the mesoscale vertical flux of θ, hereafter denoted as *tflux*, between the landscapes. In the lower 1500 m of the BL, *tflux* has generally decreased in the present-day ensemble. This suggests that the mesoscale circulations that develop in the present-day ensemble are more effective at reducing the vertical flux of temperature to the mid-BL. In the upper part of the BL (i.e., around 1750 m and higher) and the lower free troposphere, however, *tflux* has increased over the modern landscape. In addition, it is implied in Figure 26(a) that the mesoscale circulations in the present-day ensemble can enhance the entrainment of drier air from above, thus vertically transporting this drier air from the lower free troposphere adiabatically to lower levels and, likewise, increasing *tflux* within the upper BL. I will describe in an upcoming figure that the monthly mean increase in θ within the upper BL does, in fact, support this conclusion.

Figure 26(b) illustrates the time-series of mean domain-averaged differences in the mesoscale vertical flux of moisture *qflux* between the landscapes during this period. This figure suggests that, in general, *qflux* during the late afternoon is generally enhanced over the present-day landscape in a layer extending from near the surface to about 1500m, suggesting that the mesoscale circulations in the present-day ensemble are more effective at redistributing the water vapor in the lowest atmosphere further upwards. At the same time, a reduction in *qflux* above this layer indicates that drier air at even higher levels may be more effectively entrained from above. In effect, the increased *qflux* in the lowest 1500m, with a decrease generally above that level, suggests the formation of stronger mesoscale circulations in the present-day ensemble that enhance the vertical transport of available moisture to higher levels of the boundary layer.

As these mesoscale fluxes transport heat and moisture to different parts of the BL, they also have an effect on the mean quantities themselves. Figure 27(a) shows the time-series of mean domain-averaged differences in θ between the ensemble runs. In general, the increase in θ in the upper BL is consistent with the enhanced *tflux* at these levels. Likewise, the mean differences in the standard deviation of θ, hereafter represented by $\sigma(\theta)$), as shown in Figure 27(b), suggest that the mesoscale perturbations of temperature occur within the BL in two regions. First, the monthly mean increase in $\sigma(\theta)$ within a shallow layer blanketing the present-day landscape may be an effect of the enhanced sensible heating and the vertical advection of warmer surface temperatures away from the surface itself. Second, in a layer from 1500m-2000m above the surface, $\sigma(\theta)$ has increased as well. This is also the height at which mesoscale circulations tend to be most active, so the uplift associated with these circulations may be promoting the mesoscale redistribution of heat within the mid BL.

The domain-averaged changes in water vapor mixing ratio w_{mr} (note that the subscript is used in my thesis to distinguish this variable from vertical velocity w) between the historical and present-day landscapes, as shown in Figure 28(a), can also be a useful proxy for identifying what part of the BL has moistened (i.e., where in the BL the changes in w_{mr} can generally be found). There are two ideas at work here: if mesoscale fluxes transport moisture to one level, it follows that the moisture transport out of the originating level would thereby result in drier air. We clearly see this effect in Figure 28(a): available moisture is more efficiently transported upwards to higher levels of the BL in the present-day ensemble, resulting in a large increase in w_{mr} within a 500m-2000m layer. At the same time, however, the air within the lowest 500m can be drier over the present-day landscape. Though the stronger mesoscale circulations over the present-day landscape may enhance the vertical transport of moisture to higher levels of the BL, the drier lowest atmosphere reduces the moisture content of the air close to the surface.

The mean domain-averaged differences in w_{mr} and its standard deviation, hereafter denoted by $\sigma(w_{mr})$, are shown in the panels of Figure 28. While w_{mr} has increased within a large part of the BL, as suggested in Figure 28(a), the strong afternoon decreases in $\sigma(w_{mr})$ for the present-day landscape, within the lowest 500 m of the BL, further suggest that this shallow layer can be significantly drier (Figure 28(b)). This is also consistent with the near-surface afternoon dewpoint decreases that I have shown in Figure 13 and the enhanced BL *qflux* over the present-day landscape.

5.2.3. Change in vertical thermodynamic profiles

The changes in the mesoscale fluxes can have a significant effect on the principal thermodynamic variables in the boundary layer, including air and dewpoint temperatures. As an example, consider the monthly mean BL temperature differences for each of the land cover change (LCC) themes, domain-averaged on the revised grid, as shown in Figure 29(a). We see that urbanization and deforestation have both warmed mean July temperatures in my model by 0.4°C at the surface with a gradual decrease in warming up to about 550 m. Interestingly, temperatures for the present-day landscape are consistently cooler in a layer from 1000-2200m above the surface regardless of LCC, a trend clearly evident at 18:00 UTC (i.e., 2:00 pm local time, Figure 29(b)) and at 21:00 UTC (i.e., 5:00 pm local time, Figure 29(c)). Apparently, this suggests that the mesoscale circulations in the present-day ensemble may be more effective at cooling the mid-BL by 0.1°C during the afternoon hours, which is generally a consequence of the decrease in *tflux* within the BL. Furthermore, the response of afternoon air temperatures within the lowest BL is consistent with the changes to the surface energy balance that have resulted from these dominant land use shifts (which were defined in section 3.6), even though these surface energy balance changes were examined over a broader multi-state region.

These land cover changes in NJ have also produced sharp differences in BL dewpoints between the ensembles. Monthly mean domain-averaged dewpoints for the present-day landscape can increase in a layer from 400 m to 2000 m, as shown in Figure 30(a), suggesting that available water vapor is lifted to higher levels of the boundary layer. This moistening is even more pronounced at 18:00 UTC and 21:00 UTC (Figures 30(b) and 30(c)) where the increase in dewpoints at the 1500 m level by as much as 0.2-0.4°C is primarily an effect of stronger positive mesoscale vertical moisture flux in the present-day ensemble. Closer to the surface, however, the dewpoints over the present-day landscape are significantly lower than in the historical ensemble, at least for those areas that have become urbanized or deforested. This pronounced drying effect is also consistent with the reduction in surface latent heating that has occurred within a broad region during the afternoon, as shown in Figure 20(b) for NJ and the surrounding states.

These changes in vertical dewpoints, in particular, have been the consequence of changes in the mean vertical profile of specific humidity *q*. Monthly mean domain-averaged differences in *q* between the historical and present-day landscapes are shown in Figure 31(a). Monthly mean *q* values have generally increased by as much as 0.1 g kg^{-1} in a layer that extends from 500 m to 2000 m of the present-day atmosphere, compared to the respective *q* of the historical atmosphere. Not surprisingly, this BL moistening is very consistent with the mid- to late-afternoon dewpoint increases that have occurred in this layer, as shown in the panels of Figure 30. Above 2000 m, however, *q* for the present-day landscape has generally decreased. In particular, the lower dewpoints around this level suggest the enhanced entrainment of drier air from the lower free troposphere into the upper BL that maximizes during the early afternoon (Figure 31(b)) and moderates somewhat by late afternoon (Figure 31(c)). As the boundary layer continues to moisten during the course of the day, the differences in *q* between the NJ landscapes also increase in height. For example, at 18:00 UTC (Figure 31(b)), the largest mean differences in *q* are generally found at a height of 1250 m above the model surface, but three hours later, the largest differences can generally be found at a height of 1500 m.

The warming and drying of the lowest BL, in combination with the cooling and moistening of the mid-BL, can alter the profile of mean equivalent potential temperature θ_e. Monthly mean domain-averaged differences in θ_e between the landscapes are shown in Figure 32(a). Even though the strong decline in dewpoints close to the surface has contributed to a significant drying of the lowest BL, in effect reducing the moisture content of the air over the present-day landscape, the large increase in lowest-BL air temperatures (see Figure 29) offsets any reduction in θ_e close to the surface that would result from drier air alone. As a result, the combined changes in warmer but drier air within the lowest 250m of the BL has neither increased nor reduced atmospheric stability, at least when the full month is considered. However, the significant moistening of a large part of the BL (i.e., from 250 m upwards to 2000 m) has resulted in a pronounced increase in θ_e over the present-day landscape, with the afternoon BL generally becoming more unstable (Figures 32(b) and 32(c)). In effect, the strong increase in mesoscale moisture flux (which, in turn, increases dewpoints) suggests that the mid-BL has become increasingly unstable during the afternoon over the modern landscape.

5.3. Simulated Differences in the Sea Breeze between the Historical and Present-day Landscapes

One of the most common warm-season mesoscale circulations in NJ is the sea breeze that primarily affects coastal regions in the central part of the state. In this analysis, my objective was to try to isolate the impacts of LULCC on the sea breeze (e.g., as distinct from the impacts on the mesoscale dynamics and thermodynamics primarily in the interior of NJ that we have already discussed above). I first isolated a coastal region on grid 3, an area in eastern central NJ where the sea breeze is known to develop and propagate inland during the afternoon. This coastal region is represented in RAMS by a 25x50 grid, covering an estimated 92 km by 142 km area of NJ[2] that has become urbanized near the northern NJ coast (see Figure 3(c)). I created an average "sea breeze" afternoon by compositing six days during my analysis period where well-defined and identifiable sea breezes developed in both the historical and present-day ensembles

[2] The 25x50 coastal domain used for this analysis covers the region shown in Figure 33.

within the region and propagated westward across the coastal domain.[3] The composite represents an average of these six days over each landscape.

5.3.1. Mean horizontal and vertical winds

Figure 33 shows the mean vertical velocity *w* differences at 800m between the historical and present-day landscapes during a composite sea breeze afternoon in this coastal region, supplemented by the mean wind vector differences at 360 m. I chose these two levels because the vertical lift associated with the coastal sea breeze is generally the most pronounced at 800 m above the surface, while examining wind differences at a reasonably lower level in the BL would likely show increased low-level convergence or divergence. At 18:00 UTC (or 2:00 pm local time; Figure 33(a)), the wind vector differences suggest stronger low-level convergence in the present-day ensemble that has increased *w* at 800 m by 8-14 cm s^{-1}, due to an enhanced land-ocean thermal contrast driven by the reduction in surface albedo and increase in sensible heat flux in this region as discussed in section 4.4.1 (see Figures 18 and 19(a)). Enhanced uplift occurs along this front of enhanced convergence. As the composite sea breeze moves inland and matures, the difference in low-level convergence and mid-BL *w* further increases (e.g., at 21:00UTC or 5:00 pm local time, as shown in Figure 33(b)). Not clearly shown in Figure 33 is that, by 21:00 UTC, the sea breeze in the historical composite was roughly 10 km further inland compared to the sea breeze in the present-day composite. These results suggest that the stronger sensible heating of the modern landscape increases uplift of the sea breeze but also slightly slows down its inland

[3] Finding a narrow concentrated band of positive vertical velocity *w* at 800 m during the early afternoon (i.e., at 18:00UTC) along the NJ coast provided a good proxy for identifying a “sea breeze” afternoon.

movement. It is this enhanced uplift in the present-day ensemble that generally reduces the intensity of the horizontal winds associated with the sea breeze, in effect slightly slowing down its inland movement during the afternoon.

5.3.2. Vertical heat and moisture transport

Again, these differences in vertical motion can also modify the BL heat and moisture transport by the sea breeze. Figure 34 illustrates the time evolution of domain-averaged differences in the vertical mesoscale heat and moisture fluxes between the landscapes in this coastal region, plotted using identical units so that the magnitude of these fluxes can be compared. Figure 34(a) suggests that the enhanced uplift of the present-day composite sea breeze has likely resulted in an initial reduction of the mesoscale heat flux *tflux*, in effect producing a mid-afternoon minima centered about 300 m above the surface. This cooling of 4 W m^{-2} eventually is replaced by a stronger positive heat flux by evening, especially within the lowest 1000 m of the present-day BL. Likewise, the changes in the mesoscale vertical flux of moisture *qflux* between the landscapes (Figure 34(b)) suggest a distinct moistening of the lowest 700 m by 18:00 UTC (or 2:00 pm local time). As the afternoon progresses, the enhanced *w* lifts this low-level moisture about 500 m higher in the coastal boundary layer, so that *qflux* becomes sharply higher by 21:00 UTC as a result of the stronger sea breeze over the present-day landscape. By comparison, the mesoscale heat fluxes in the lowest BL are, in general, slightly stronger than the corresponding moisture fluxes during most of the afternoon.

5.3.3. Effects on boundary-layer air and dewpoint temperatures

It is well-known that the sea breeze cools and moistens the lower atmosphere as it sweeps inland during the afternoon. An initial comparison of the sea breeze composites between the historical and present-day ensembles suggests that the sea breeze over the present-day landscape can be stronger in terms of enhanced uplift ahead of the sea breeze front. Should it follow that the stronger sea breeze in the present-day ensemble might be more effective at cooling and moistening the air close to the surface?

The mean air and dewpoint temperature differences between the landscapes, averaged over all times between 18:00 UTC and 00:00 UTC (i.e., between 2:00 pm and 8:00 pm local time) and shown in Figure 35,[4] suggests that this effect is not generally the case. According to this figure, the stronger sea breeze has led to enhanced warming and drying close to the surface, but enhanced cooling and moistening in the middle BL. The lowest boundary layer over the present-day coastal landscape is warmer by 0.6°C at the surface with a gradually decreasing trend to about 1200 m in height. The lower dewpoints, however, suggest that the present-day boundary layer below this level is relatively drier. Such a low-level warming and drying effect suggests that, while the LULCC in this coastal region has resulted in a stronger sea breeze with enhanced uplift, this stronger sea breeze is not intense or long-lived enough to bring complete relief from the LULCC-induced warming (and drying). However, in response to the stronger sea breeze over the present-day landscape, the trends in BL *tflux* and *qflux* has cooled and moistened an estimated 1000m-thick layer centered on 1500 m. At this height (1500 m),

[4] This is a time-averaged vertical difference profile of air and dewpoint temperatures during a composite sea-breeze afternoon. Since the units of air and dewpoint temperature are the same, I have shown the respective differences in a single figure (Figure 35).

the present-day sea breeze has cooled mean afternoon air temperatures by 0.1-0.2°C and increased mean dewpoint temperatures by as much as 0.4°C.

5.4. Chapter summary

The results presented in this chapter have reinforced the idea presented in other studies [*Lyons et al.*, 1996; *Lyons*, 2002; *Weaver*, 2004a,b; *Georgescu et al.*, 2007] that land cover change can modify the dynamic and thermodynamic properties of the boundary layer. I have shown that, within NJ and the surrounding region, the monthly mean horizontal and vertical winds during the afternoon hours respond strongly to the differences in surface sensible heating between the historical and present-day landscapes. The enhanced sensible heating of the present-day landscape has shifted the horizontal low-level wind flow and implies enhanced low-level convergence. These horizontal wind differences are thus strongest close to the surface in the interior portion of the state, diminish into the mid-levels of the boundary layer, and increase again near the top of the boundary layer, suggesting enhanced mesoscale divergence aloft. Though these effects have produced weak uplift and subsidence close to the surface, the vertical motion changes are much more pronounced towards the upper part of the boundary layer where mesoscale circulations tend to be more active. In addition, the monthly mean wind differences between the landscapes were stronger in the interior of the state than they were near coastal areas.

The comparison of mesoscale moisture fluxes has suggested a central conclusion to this chapter: the mesoscale circulations in the present-day ensemble may be more effective at redistributing the available low-level water vapor even higher into the boundary layer, relative to the mesoscale circulations in the historical ensemble. The water vapor mixing ratio has generally increased in the mid-troposphere, which is consistent with the mid- to late-afternoon dewpoint increases that have occurred in this same general layer. Closest to the surface, however, the present-day boundary layer is significantly drier. The drying and moistening of this atmospheric column is supported by the monthly mean increases in afternoon mesoscale moisture flux over the present-day landscape. This effect supports my conclusion that these mesoscale circulations can increase the lift of low-level water vapor to higher levels. At the same time, however, drier air within the upper boundary layer may be more effectively entrained from above. Though the mesoscale circulations enhance the vertical advection of moisture to higher levels, the drier lower atmosphere significantly reduces the moisture content of the air that would be lifted.

The changes in these vertical mesoscale fluxes have modified BL thermal and moisture profiles. I have shown that urbanization and deforestation have both warmed mean monthly temperatures by 0.4°C at the surface with a gradual decrease in warming with increasing altitude, up to the middle troposphere. Above that level, however, the air temperatures within the upper part of the present-day boundary layer are consistently cooler over the region. Within the lower troposphere, in a layer from 400 m to 2000 m above the surface, dewpoints over the present-day landscape increase by as much as 0.4°C. This suggests that the stronger mesoscale circulations in the present-day ensemble may be more effective at cooling the upper boundary layer as they generally moisten a significant part of the lower boundary layer.

While dewpoints increase within a large part of the lower troposphere, the moistening of the lower boundary layer, however, is accompanied by a shallow but pronounced drying of the air close to the surface with a subsequent decrease in near-surface dewpoints. This has an effect of reducing the propensity for surface convection initiation in many parts of central and southern NJ. The strong decline in near-surface dewpoints has produced a significant drying of the present-day atmosphere, and despite an increase in air temperatures, the warming of the lowest boundary layer has not been sufficient to offset the lower moisture content of the air over the present-day landscape.

The sea breeze is another mesoscale circulation which my results have shown may also have been strongly affected by land cover change within coastal regions of NJ. During a composite sea breeze afternoon, a comparison between the landscapes suggests that the extensive urbanization in coastal areas of NJ has locally enhanced surface sensible heating over the present-day landscape. As sea-surface temperatures were held constant between the ensembles, the stronger horizontal thermal gradient at the surface between the warmer present-day landscape and the ocean, in effect, produced increased low-level convergence of the horizontal winds within the lowest boundary layer, thus inducing stronger mid-BL uplift of the sea breeze itself. By late afternoon, while the mesoscale uplift in the present-day ensemble strengthens even further as the sea breeze moves inland, the sea breeze over the present-day landscape has a slightly slower movement inland compared with the faster movement of the sea breeze over the historical landscape.

The increased convergence and uplift of the sea breeze over the present-day landscape has modified the mesoscale transport of heat and moisture within these coastal areas. During the course of a summer afternoon, the initial reduction of mesoscale heat fluxes associated with the present-day sea breeze at low levels has been replaced by a stronger late-afternoon increase, accompanied by a surge of mesoscale heat flux, in a significant part of the BL. This effect can warm BL air temperatures from the surface to about 1200 m, as shown in my ensemble comparison. Simultaneously, despite the reduced latent heating of the present-day landscape in coastal regions, the increased low-level convergence has strengthened the mesoscale moisture flux associated with the sea breeze, lifting moisture from the marine air to even higher levels. Dewpoints over the present-day landscape have consequently increased by as much as 0.4°C in a layer from 400m to 2000m above the surface. In effect, though the increased sensible heating of the present-day coastal landscape has created a warmer and drier lower boundary layer for the sea breeze, the enhanced mesoscale heat and moisture fluxes associated with the present-day sea breeze have slightly cooled but significantly moistened the middle boundary layer. In effect, the stronger composite sea breeze over the present-day landscape is not intense or long-lived enough to bring complete relief from the LULCC-induced warming and drying of the lowest atmosphere.

The historical land cover changes in NJ and the region between the late 19th and late 20th centuries have significantly enhanced the surface sensible heating of the present-day landscape, which impacts the dynamics and thermodynamics of the boundary layer. As I have shown in this chapter, the increased low-level convergence and hence stronger mid-level uplift in my present-day ensemble has occurred over interior areas of NJ that have strong increases in sensible heat flux. While mesoscale circulations have developed in both ensembles, my results have strongly suggested that these circulations in the present-day ensemble are much more effective at lifting available moisture in the lower boundary layer to even higher levels, increasing dewpoints in the middle BL. We have seen this same effect in the present-day ensemble for both inland mesoscale circulations and during an afternoon sea breeze along the NJ coast. In summary, the changes in the surface energy budget, particularly sensible heating, are remarkable at strengthening low-level mesoscale convergence and upper-level divergence that, in turn, can enhance uplift and subsidence in the middle BL.

References

Baidya Roy, S., and R. Avissar (2000), Scales of response of the convective boundary layer to land surface heterogeneity, *Geophys. Res. Lett.*, *27*, 533-536.

Baidya Roy, S., C. P. Weaver, D. S. Nolan, and R. Avissar (2003a), A preferred dynamical scale for landscape-forced mesoscale circulations? *J. Geophys. Res.*, *108*, 8808, doi:10.1029/2002JD003097.

Georgescu, M., G. Miguez-Macho, L. T. Steyaert, and C. P. Weaver (2007), Sensitivity of summer climate to land cover change over the Greater Phoenix, AZ, area. *J. Arid Env.*, submitted.

Lyons, T. J. (2002), Clouds prefer native vegetation. *Meteor. Atmos. Phys.*, *80*, 131–140.

Lyons, T. J., R. C. G. Smith, and X. Huang (1996), The impact of clearing for agriculture on the surface energy balance. *Int. J. Climatol.*, *16*, 551–558.

Weaver, C. P. (2004a), Coupling between large-scale atmospheric processes and mesoscale land-atmosphere interactions in the U.S. Southern Great Plains during summer: Part I. Mesoscale case studies, *J. Hydrometeorol.*, *5*, 1223-1246.

Weaver, C. P. (2004b), Coupling between large-scale atmospheric processes and mesoscale land-atmosphere interactions in the U.S. Southern Great Plains during summer: Part II. Large-scale-mean impacts of the mesoscale, *J. Hydrometeorol.*, *5*, 1247-1258

Weaver, C. P., and R. Avissar (2001), Atmospheric disturbances caused by human modification of the landscape, *Bull. Am. Meteorol. Soc.*, *82*, 269-281.

Yoshikado, H. (1990), Vertical structure of the sea breeze penetrating through a large urban complex, *J. Appl. Meteorol.*, *29*, 878–891.

Yoshikado, H. (1992), Numerical study of the daytime urban effect and its interaction with the sea breeze, *J. Appl. Meteorol.*, *31*, 1146-1164.

CHAPTER 6 – Summary of the Impacts of LULCC in NJ and Future Research Avenues

6.1. Introduction

I have performed a sensitivity experiment which complements recent LULCC studies such as those by *Pielke et al.* [1999], *Mölders* [2000], *Marshall et al.* [2004a, 2004b], and *Schneider et al.* [2004]. Each of these studies used mesoscale models and sensitivity analysis to quantify the potential effects of land use change on regional weather and climate. In this study, I reconstructed the late 19th-century landscape of New Jersey (NJ) and the surrounding states, which was compared with late 20th-century satellite-observed land cover for the same region. These two land cover datasets were each initialized by a mesoscale numerical model, the Regional Atmospheric Modeling System (RAMS), in a series of experiments designed to quantify the impacts of historical land cover change on regional weather and climate. Unlike other land use and land cover change (LULCC) studies, however, this project was unique in that the grid scale used in RAMS was 2 km, which is a higher resolution that enabled me to reasonably resolve smaller-scale atmospheric features (such as convection) that respond most closely to the surface forcing.

The direct modification and conversion of the landscape has resulted in a dramatic modification of its biophysical properties, particularly during the last three centuries at the global scale [*Ramankutty and Foley*, 1999]. The effects of anthropogenic land use and land cover change (LULCC), as a result of socioeconomic drivers, still remains an unanswered question in the often-controversial policy considerations that some believe may minimize global climate change. Various land use practices such as overgrazing [*Balling*, 1988], agriculture [*Segal et al.*, 1989; *Pielke and Avissar*, 1990], and urbanization [*Karl et. al.*, 1993; *Gallo et al*., 1996] have demonstrated that changes to the existing land cover can further modify mean temperatures, wind speed, humidity, cloudiness, and precipitation. Such studies have shown that historical changes to the land cover itself may already be having pronounced effects that could potentially alter climate on a variety of scales, possibly even accelerating global climate change [*Bonan*, 1997].

6.2. Summary of historical land use change in the state

The land cover changes in this region were categorized according to three principal LULCC trends since the late 19th century: urbanization, reforestation, and isolated deforestation. Urbanization has occurred in many areas of central and northeastern NJ, Long Island (LI), and in far southeastern Pennsylvania (PA) and New York (NY), and has been generally associated with the loss of prime agricultural land and an expansion of impervious surfaces. Further to the north and west, from southeastern PA into northern NJ, the abandonment of 19th-century agricultural land use practices, combined with selective timber harvesting, has led to a broad reforestation of this region. In addition, local deforestation has also occurred in southern NJ and LI. Although 17 percent of all land surfaces have been significantly affected by urbanization, 22 percent by reforestation, and 8 percent by deforestation, some of these LULCC trends, particularly urbanization and deforestation, are not mutually exclusive. During this time, the regional landscape has become increasingly fragmented and spatially heterogeneous.

As each of these land cover changes has modified surface properties that have, in turn, altered the partitioning of the turbulent fluxes of heat and moisture in different ways, the identification of the principal land use trends has allowed me to differentiate the impacts of different land conversions on interactions between the land surface and the atmosphere. Once I categorized the land cover change as urbanization, reforestation, deforestation, or "all land grid cells" in the region, using an arbitrary threshold value to determine changes in dominant land use patterns, various climatological variables were then composited over these different sets of grid cells. This strategy allowed me to examine, for example, the surface and boundary-layer response to urbanization as well as separate the urbanization impacts from those of deforestation.

6.3. Primary impacts of LULCC on regional weather and climate

The historical and present-day landscape reconstructions that document these land use trends were used in the RAMS model, at a grid cell size of 2 km, to evaluate the sensitivity of changes in land cover on its weather and climate for July 1999 drought conditions. Ensembles of three simulations each were carried out for both the historical and present-day land cover conditions. For the present-day landscape, many regions that have experienced urbanization or deforestation have higher surface air temperatures combined with lower dewpoints in the model, suggesting warmer and drier near-surface air. Potential shifts in forest composition and rainfall differences may also have contributed to the dewpoint declines. The diurnal cycle of surface air temperature and dewpoint differences between my present-day and historical simulations are consistent with these trends. Differences between the individual ensemble members are, in general, similar to those between the ensemble means, though the use of ensembles helps to smooth the variability associated with convective rainfall that can have pronounced effects on surface temperature, dewpoint, and surface heat and radiative fluxes.

Daytime maximum temperatures over the present-day urban landscape also increased considerably more than nighttime minimum temperatures in our simulations, suggesting an enhanced diurnal temperature range (DTR). The warming of nighttime minimum temperatures within these present-day urban areas was likely underestimated in RAMS because the LEAF-2 parameterization does not yet account for the increased thermal and radiative properties of urban surfaces that contribute to anthropogenic energy storage and release. Future versions of LEAF-2 will likely include this effect.

The responses of air and dewpoint temperatures suggest that land cover type can significantly modulate surface albedo and other key components of the land surface energy budget. Surface albedos have significantly declined in present-day urban regions. However, within central and southern NJ, the large patchy increases and decreases in surface albedo are due primarily to an overall increased deciduousness of its land cover in combination with local changes in forest composition, the regeneration of vegetation associated with disturbance, isolated patches of increased agricultural and pasture land, and forested wetlands change. Together, these conversions within a small region have increasingly fragmented the 19th-century landscape and imply that the present-day surface energy budget is more heterogeneous.

These albedo changes also modify the partitioning of radiative energy into sensible and latent heat fluxes, which can directly affect air temperature increases or decreases. Sensible heat flux has increased where the present-day landscape has warmed.

The present-day landscape receives more net shortwave radiation compared to the historical landscape, a trend that is consistent for nearly the entire state of NJ. Over reforested areas, net longwave fluxes have noticeably increased, with the largest increases during the afternoon hours. In addition, my study suggests that a change in land cover type, and the associated change in surface properties, has a more significant influence on net longwave radiative fluxes than does the corresponding change in atmospheric conditions that results from land cover change.

Land cover change can also modify the dynamics and thermodynamics in the BL. I have shown that the repartitioning towards sensible heating has shifted the horizontal low-level wind vectors and implies enhanced convergence (and likewise, enhanced divergence further aloft) over the present-day landscape. There is also a vertical signature to these horizontal wind differences: they are strongest close to the surface in the interior portion of the state, weaken in the mid-BL, and increase near the top of the boundary layer and the lower free atmosphere. This effect does not strengthen the vertical velocity close to the surface, but rather within the mid-BL where mesoscale circulations tend to dominate during the afternoon. The mesoscale circulations that have developed over the present-day landscape in my model, in effect, are more effective at vertically transporting available moisture to higher levels of the BL. However, this has generally reduced the actual moisture content of the lowest 500m of the BL, and the mesoscale vertical fluxes of heat and moisture support this hypothesis. These effects have slightly cooled but significantly moistened the mid-BL, generally decreasing atmospheric stability in the mid levels while having little or no effect on the warmer but significantly drier lowest BL.

The sea breeze is another mesoscale circulation that has been affected by land cover change in coastal NJ. The enhanced sensible heating within coastal areas has intensified the horizontal thermal contrast between land and ocean, given that sea surface temperatures were held constant in my model. This had the effect of increasing low-level convergence and uplift in the mid-BL, clearly strengthening the vertical motion of the sea breeze. As this vertical motion over the present-day landscape can become even stronger as the sea breeze moves inland, this apparent strengthening is also accompanied by a slightly slower inland movement of the sea breeze itself. In effect, the present-day landscape warms and dries the air closest to the surface, but it is the enhanced mesoscale fluxes associated with the sea breeze as well as inland landscape-forced circulations that help to significantly moisten the middle levels of the present-day lower atmosphere. For the reasons described here, and the results presented in this study, I have demonstrated that historical land cover change can modify surface climate and the properties of the daytime boundary layer.

6.4. Future research avenues

Most regional LULCC studies have alternatively assumed land cover conditions of different time periods in a mesoscale atmospheric model initialized with relatively wet or dry background conditions to examine the impact of landscape change on surface weather and climate [e.g., *Georgescu et al.*, 2007]. However, the background conditions in my study were quite extreme, as a significant drought period, combined with record high temperatures and heat wave impacts, resulted in major agricultural losses in several northeastern U.S. states, including NJ, NY, and PA [*Heim*, 1999]. While the sensitivity of the regional climate system to landscape change was explored under these extreme conditions, the landscape change itself was also extreme in a sense too: from a relatively homogeneous and predominantly agricultural landscape to one with a fragmented, highly urban character during a roughly century-long time period. If one of these extremes is varied (i.e., the background weather conditions), we can investigate how this pronounced land use change can impact weather and climate under different climatological scenarios.

One of these climatological scenarios could be a typical summer climate. The drought period that I used for background conditions in this study has significantly reduced vegetative transpiration, and with crop death prevalent [*Morehart et al.*, 1999] throughout the entire region, the effects of the predominantly agricultural and pasture landscape of 19th-century NJ cannot be fully appreciated. Moreover, the use of a typical summer weather regime has value for evaluating the effects of climatologically-normal evapotranspiration rates and latent heat flux, for instance, which may be a particularly strong factor in inducing clouds and moderating temperatures more than what my results show in the historical ensemble. Since more vegetation (i.e., agricultural and pasture land) covered the region in the late 19th century, we would expect less available radiative energy to be received by the historical surface. This would likely have stronger influences on other variables in the climate system, including convective rainfall and soil moisture. In addition, as historical LULCC datasets are digitized and enhanced [*Steyaert and Knox*, 2008], the use of refined historical land cover reconstructions during different time periods is a promising area for future study.

While the LEAF-2 module within RAMS also provides a detailed representation of heat and moisture exchanges between the lower atmosphere, the surface and its land cover, and the subsurface soil layers, it is, however, limited by the absence of any anthropogenic heat storage terms associated with its single present-day urban land cover type. These heat storage terms would significantly influence the nighttime thermal profile which contributes to the overall UHI, likely producing a more pronounced increase in the daily minimum temperatures within present-day urban areas. In addition, I propose that future studies can add land surface classes that describe increasing levels of the urban hierarchy (i.e., town, city, metropolis), each with different surface albedos that would be related to both population size and the density of the urban area. I believe that all of these enhancements would yield stronger land cover influences upon the present-day urban atmosphere, beyond what was simulated between the ensembles.

I have also shown in Chapter 3 that the close proximity of NJ to the major urban centers of Philadelphia and New York City has likely contributed to the dramatic loss of prime agricultural land and a simultaneous expansion of urban land surfaces. Since population growth is expected to continue in this region, it may be useful to theoretically "urbanize" all land surfaces within the entire state in a mesoscale model, thus removing all traces of vegetation. This strategy, although physically unrealistic in the real world due to the intense environmental resistance in the community that would precede it, would allow us to numerically determine an upper bound on surface air and dewpoint temperatures in the region, convective rainfall, subsurface soil moisture unavailable to the lower atmosphere, and the sharply drier boundary layer that would result. Since there is no vegetation in this hypothetical scenario, we would not need to worry about the dramatic vegetation changes that would otherwise result. This could potentially become a future research avenue similar to the natural vs. potential vegetation scenarios that some numerical studies have investigated [e.g., *Bonan*, 1997].

6.5. Chapter summary

The landscape change that we have observed over historical time is expected to continue and even accelerate into the future, driven primarily by the effects of a rapidly growing world population and the anthropogenic pressures exerted on natural environmental and ecological systems. The northeastern U.S., in particular, was a very rapidly growing region of the world during the time period of this study (i.e., 20th century), and we have documented the extensive shifts from a predominantly agricultural landscape to a highly urban one within a relatively short time period. This climate sensitivity analysis, even with the lack of an interactive urban model (which likely make my results a conservative estimate of the effects of LULCC on climate in this region), suggests that historical LULCC has the potential to modify surface properties with pronounced impacts on weather and climate, perhaps similar in magnitude regionally to those associated with increasing greenhouse gas concentrations [*IPCC*, 2007]. These findings are consistent with recent suggestions that assessing the full anthropogenic impact on the climate system will require expanded definitions of what constitutes "climate forcing" [*NRC*, 2005].

Based upon an extrapolation of the land cover trends identified in our study, what are some of the changes that we could anticipate in this region, perhaps one hundred years from now? As a broad estimate, I expect urbanization to continue to expand outwards from the two large metropolitan areas, consuming even more agricultural and pasture land within NJ and its adjacent states. Reforestation rates may drop, as any abandoned agricultural land is more likely in the future to be converted to urban and commercial use. Deforestation rates and wetlands losses may also decline, due to the continued enforcement of strict environmental laws and wetlands preservation. In light of these possible changes and the results of my simulations, we can anticipate that the future landscape will likely be warmer and drier than today.

References

Balling, R. C., Jr. (1988), The climatic impact of a Sonoran vegetation discontinuity, *Clim. Change*, *13*, 99-109.

Bonan, G. B. (1997), Effects of land use on the climate of the United States, *Clim. Change*, *37*, 449-486.

Gallo, K. P., D. R. Easterling, and T. C. Peterson (1996), Notes and correspondence: The influence of land use/land cover on climatological values of the diurnal temperature range, *J. Clim.*, *9*, 2941-2944.

Georgescu, M., G. Miguez-Macho, L. T. Steyaert, and C. P. Weaver (2007), Sensitivity of summer climate to land cover change over the Greater Phoenix, AZ, area. *J. Arid Env.*, submitted.

Heim, R. (1999), Climate of 1999: July drought in the U.S., *National Climatic Data Center (NCDC) Climate Services Division*, *13 August 1999*, NCDC, Ashville, North Carolina.

IPCC (Intergovernmental Panel on Climate Change) (2007), *Climate Change 2007: The Physical Science Basis. Contribution of Working Group I to the Fourth Assessment Report of the Intergovernmental Panel on Climate Change* [Solomon, S., D. Qin, M. Manning, Z. Chen, M. Marquis, K. B. Averyt, M. Tignor and H. L. Miller (Eds.)], 996 pp., Cambridge University Press, Cambridge, United Kingdom and New York, NY, USA.

Karl, T. R., P. D. Jones, R. W. Knight, G. Kukla, N. Plummer, V. Razuvayev, K. P. Gallo, J. Lindseay, R. J. Charlson, and T. C. Peterson (1993), A new perspective on recent global warming: Asymmetric trends of daily maximum and minimum temperature, *Bull. Am. Meteorol. Soc.*, *74*, 1007-1023.

Marshall, C. H., Jr., R. A. Pielke, L. T. Steyaert, and D. A. Willard (2004a), The impact of anthropogenic land-cover change on the Florida peninsula sea breezes and warm season sensible weather, *Mon. Weather Rev.*, *132*, 28-52.

Marshall, C. H., Jr., R. A. Pielke Sr., and L. T. Steyaert (2004b), Has the conversion of natural wetlands to agricultural land increased the incidence and severity of damaging freezes in South Florida?, *Mon. Weather Rev.*, *132*, 2243-2258.

Mölders, N. (2000), Similarity of microclimate as simulated in response to landscapes of the 1930s and the 1980s, *J. Hydrometeorol.*, 1, 330-352.

Morehart, M, N. Gollehon, R. Dismukes, V. Breneman, and R. Heimlich (1999), Economic assessment of the 1999 drought: Agricultural impacts are severe locally, but limited nationally, *Agriculture Information Bulletin No. 755*, 20 pp., U.S. Department of Agriculture, Washington, D.C.

NRC (National Research Council) (2005), *Radiative Forcing of Climate Change: Expanding the Concept and Addressing Uncertainties* [Jacob, D.J., R. Avissar, G. C. Bond, S. Gaffin, J. T. Kiehl, J. L. Lean, U. Lohmann, M. E. Mann, R. A. Pielke, Sr., V. Ramanathan, and L. M. Russell (Eds.)], 207 pp, The National Academies Press, Washington, DC.

Pielke, R. A., and R. Avissar (1990), Influence of landscape structure on local and regional climate, *Landscape Ecology*, *4*, 133-155.

Pielke, R. A., R. L. Walko, L. T. Steyaert, P. L. Vidale, G. E. Liston, W. A. Lyons, and T. N. Chase (1999), The influence of anthropogenic landscape changes on weather in south Florida, *Mon. Weather Rev.*, *127*, 1663-1673.

Ramankutty, N., and J. A. Foley (1999), Estimating historical changes in global land cover: Croplands from 1700 to 1992, *Global Biochem. Cycl.*, *13*, 997-1027.

Schneider, N., W. Eugster, and B. Schichler (2004), The impact of historical land-use changes on the near-surface atmospheric conditions on the Swiss Plateau, *Earth Interactions*, *8*, 1-27.

Steyaert, L. T., and R. G. Knox (2008), Reconstructed historical land cover and biophysical parameters for studies of land-atmosphere interactions within the eastern United States, *J. Geophys. Res.*, 113, D02101, doi:10.1029/2006JD008277

FIGURES

Figure 1

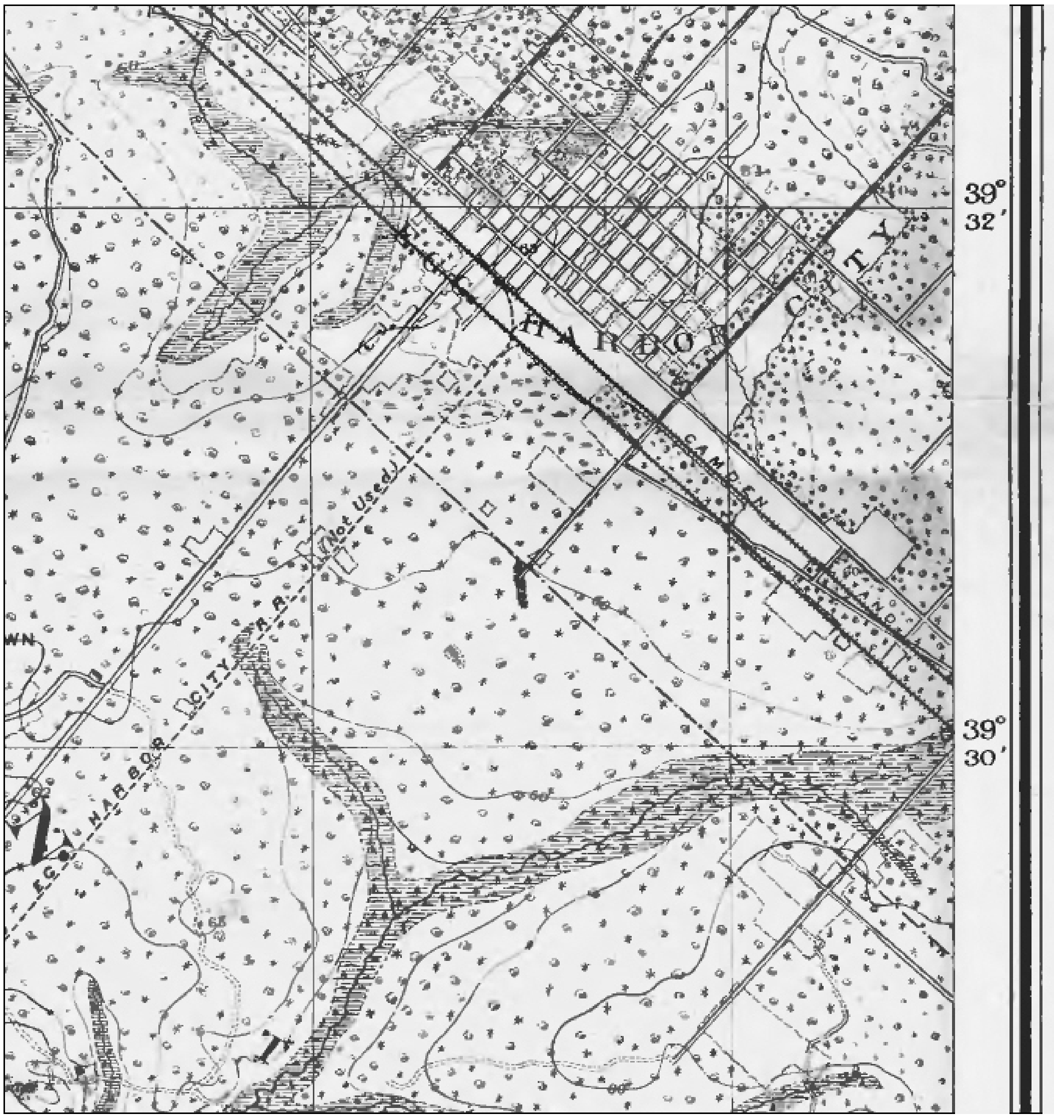

Figure 1. A sample portion of the Cook map series, showing the land cover of the Atlantic County area of NJ as it appeared in the late 19th century. The city of Egg Harbor is near the top of the image. Note the mixed forest to the south of Egg Harbor City, while the forested wetlands are represented by finely-spaced horizontal lines that imply saturated soil conditions.

Figure 2

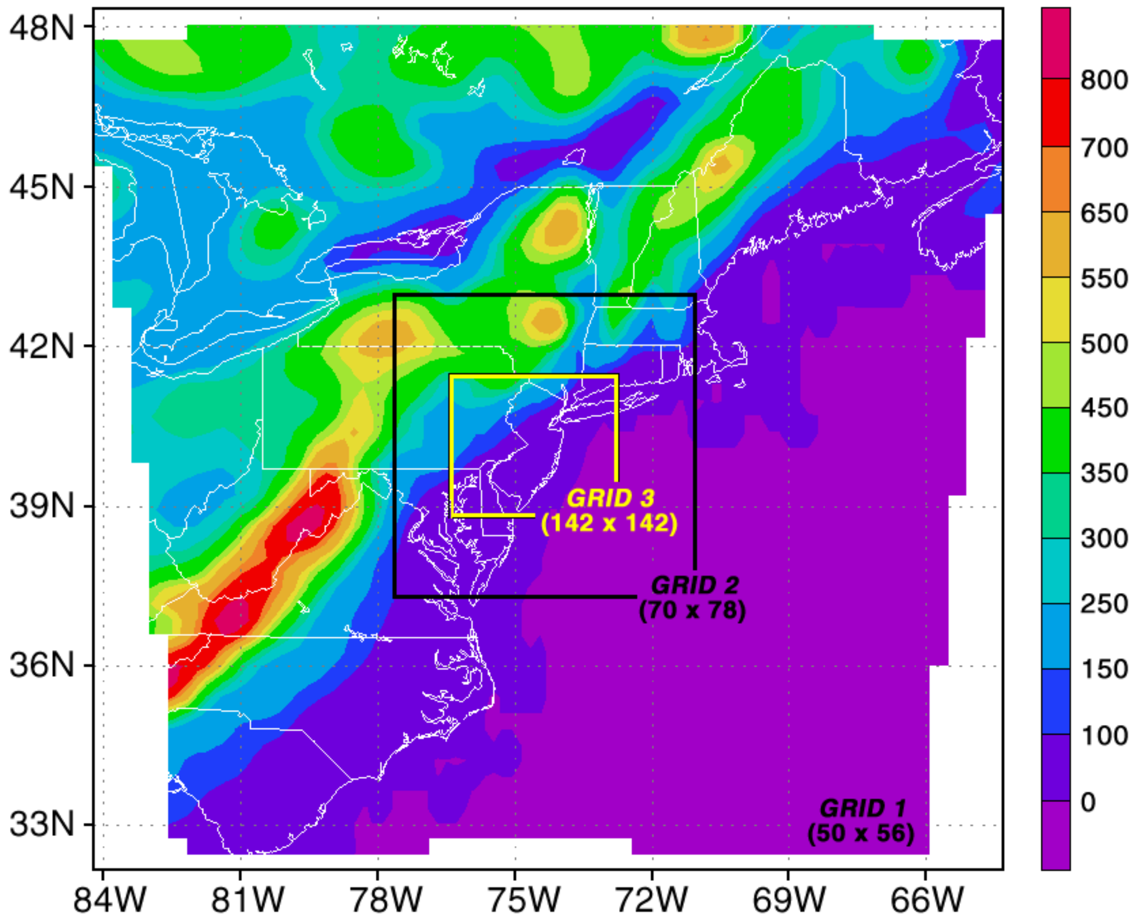

Figure 2. Geographical configuration of the parent grid (grid 1), and the two embedded grids, used in the RAMS ensemble runs with simulated historical and present-day land cover. The contours represent the elevation of the model surface, in m, above mean sea level. The numbers in parentheses indicate the number of horizontal grid cells within the respective domain. The RAMS grids were specified with a grid spacing of 32 km (grid 1), 8 km (grid 2), and 2 km (grid 3).

Figure 3

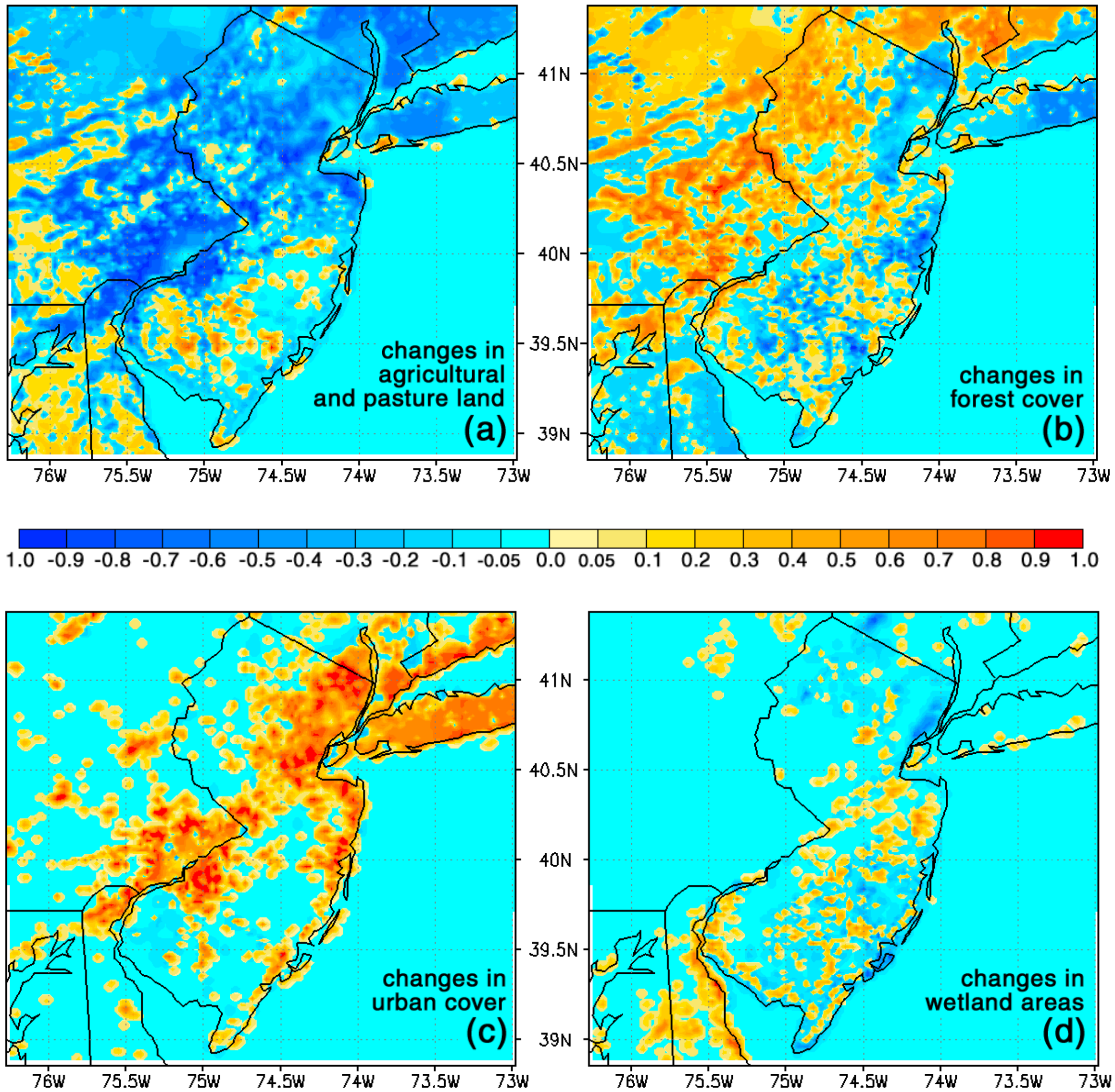

Figure 3. Differences in fractional landcover (present-day fraction of total area minus historical fraction of total area), for grid 3, in (a) agricultural and pasture land, (b) total forested area, (c) urban regions, and (d) nonforested and forested wetlands. The contour interval represents the fractional changes in the respective land cover type.

Figure 4

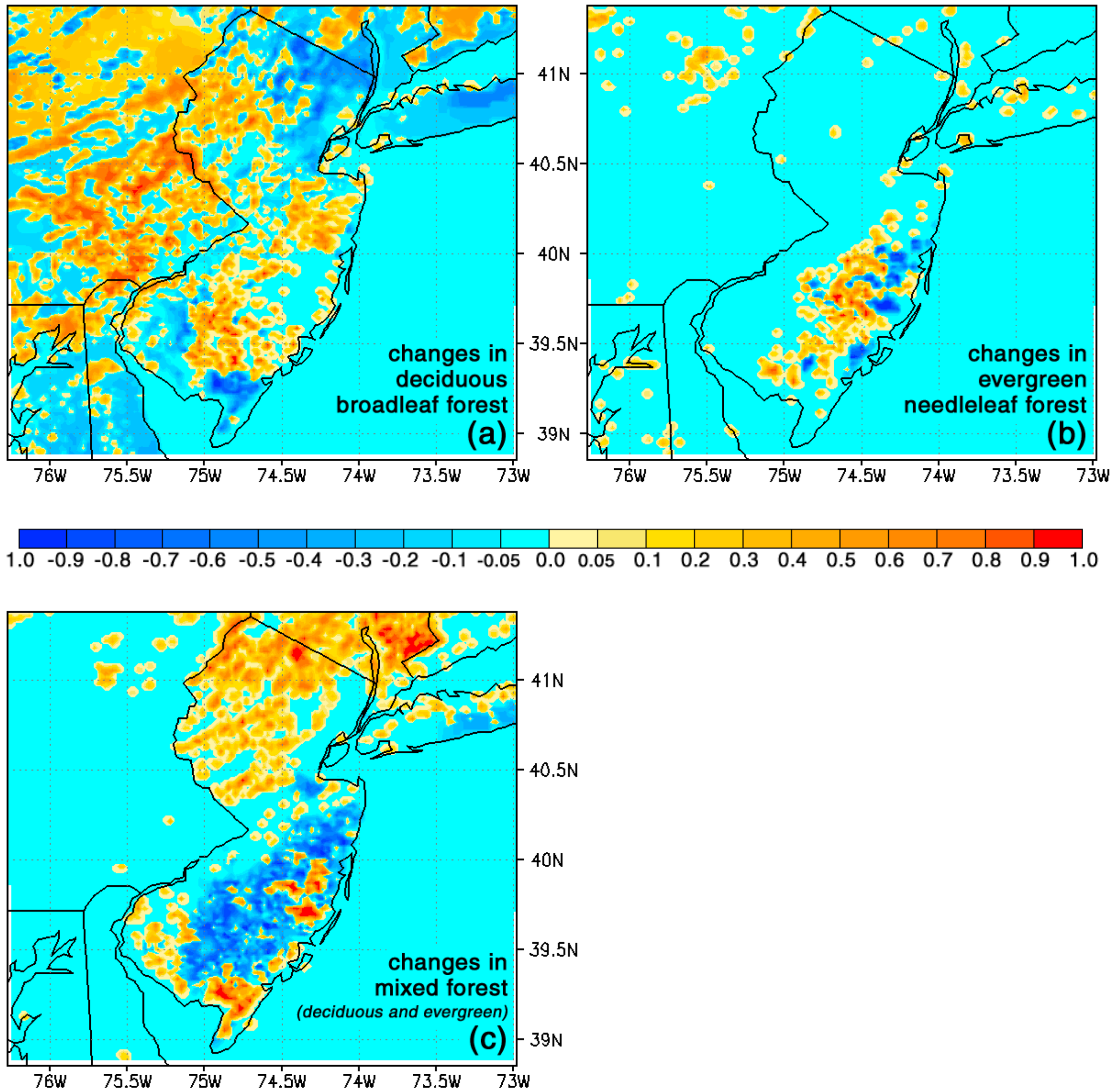

Figure 4. As in Figure 3 except for changes in forest type. These panels show fractional landcover changes in (a) deciduous broadleaf forest, (b) evergreen needleleaf forest, and (c) a mixed forest of deciduous broadleaf and evergreen needleleaf trees.

Figure 5

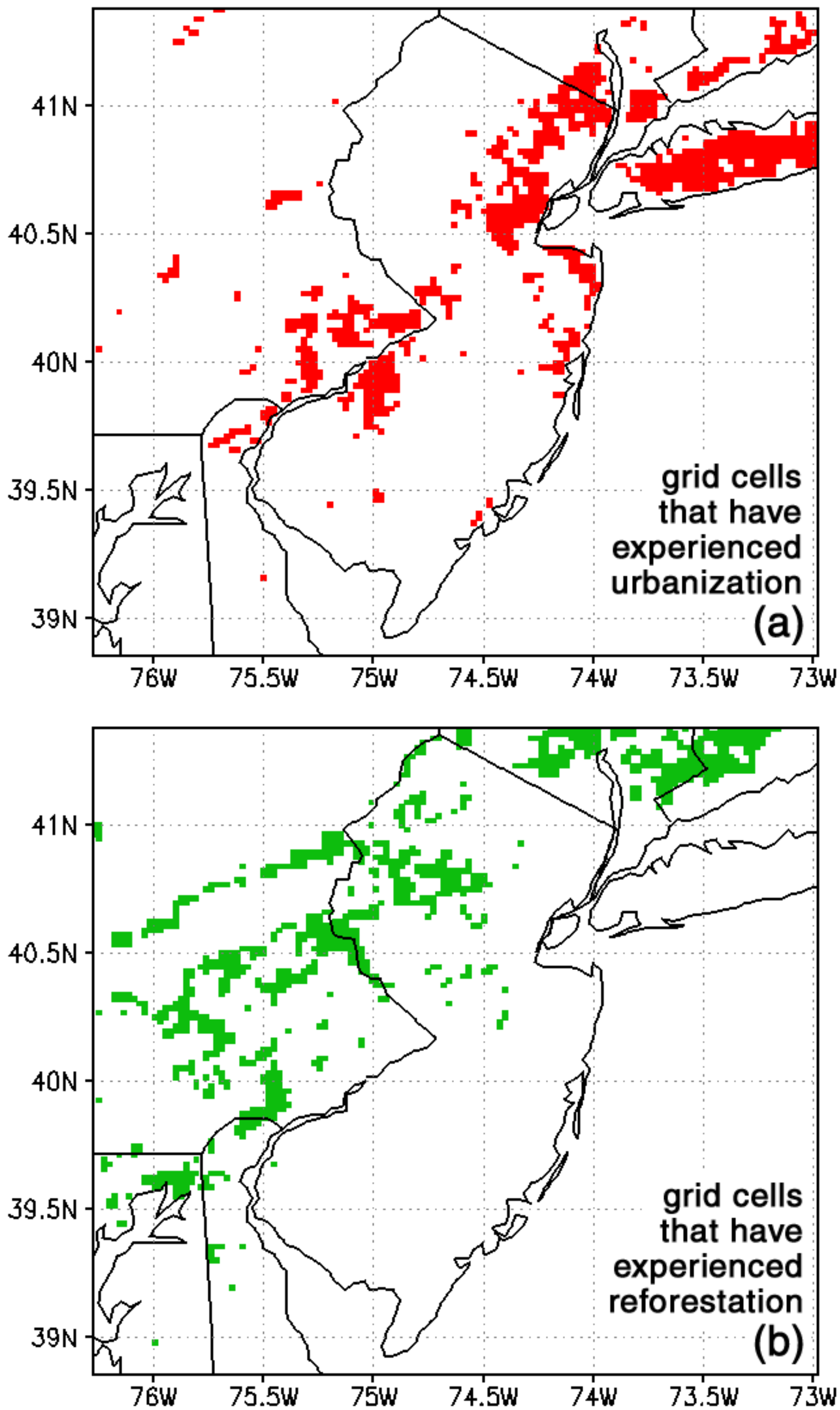
41N
40.5N
40N
39.5N
39N
76W
75.5W
75W
74.5W
74W
73.5W
73W
grid cells that have experienced urbanization
(a)
grid cells that have experienced reforestation
(b)

Figure 5 *(continued from previous page)*

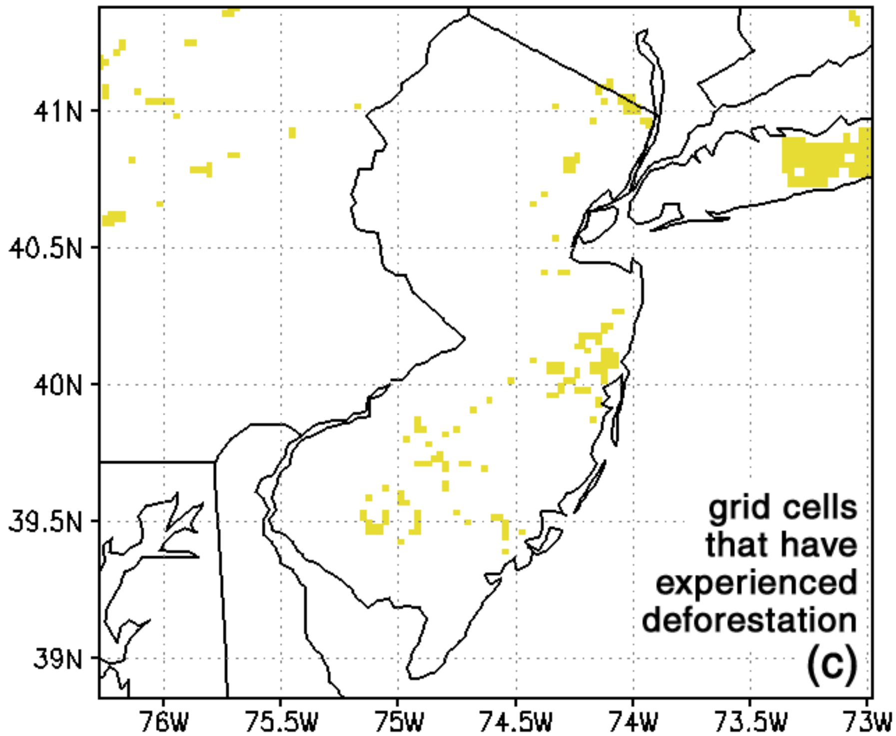

Figure 5. The respective grid cells that have experienced a change in dominant land cover between the historical and present-day datasets. For these grid cells, the dominant land cover changes have resulted from (a) urbanization, shown shaded in red; (b) reforestation, shown shaded in green; and (c) deforestation, shown shaded in yellow. See text for a more precise description of these definitions.

Figure 6

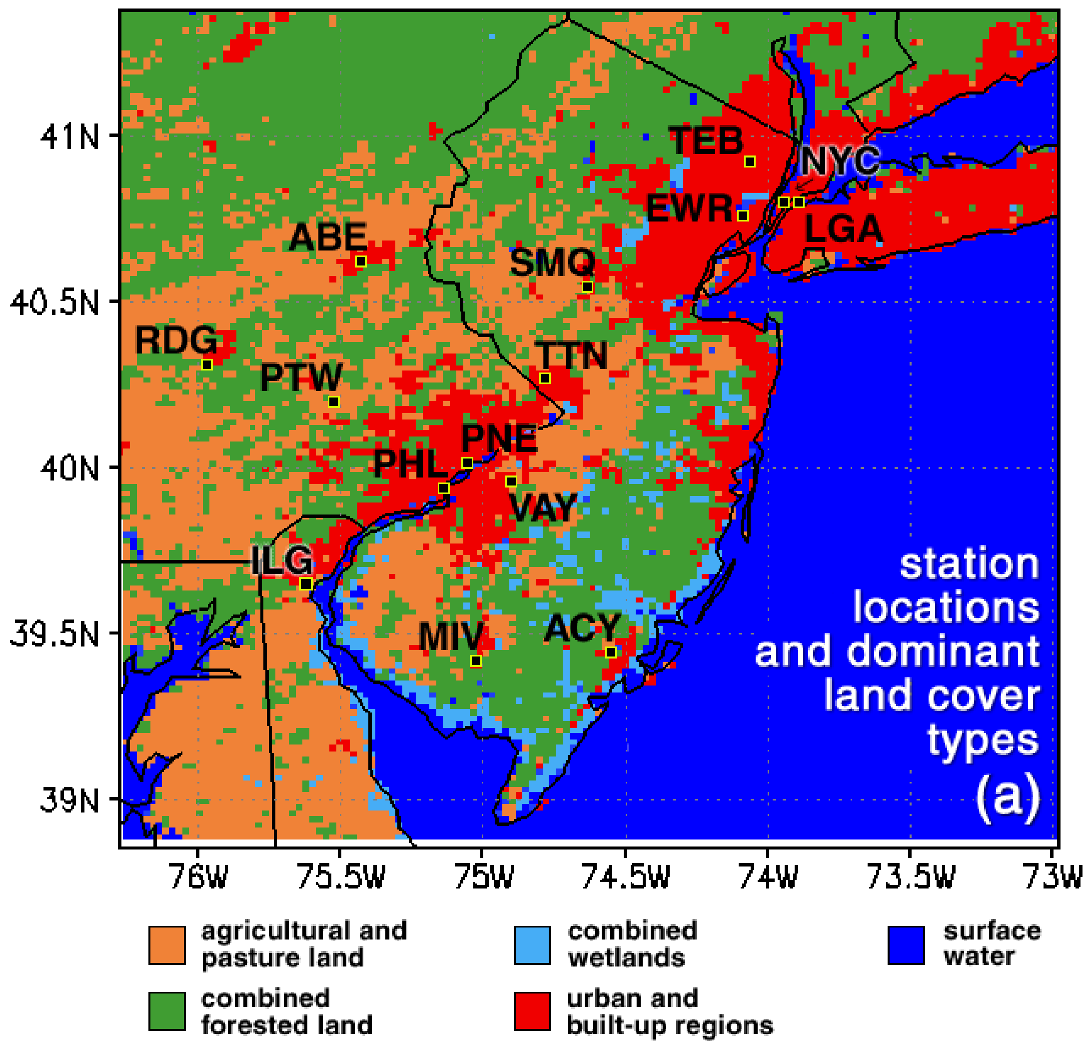
41N
40.5N
40N
39.5N
39N
76W
75.5W
75W
74.5W
74W
73.5W
73W
TEB
NYC
EWR
LGA
ABE
SMQ
RDG
PTW
TTN
PNE
PHL
VAY
ILG
MIV
ACY
station locations and dominant land cover types
(a)
agricultural and pasture land
combined forested land
combined wetlands
urban and built-up regions
surface water

Figure 6 *(continued from previous page)*

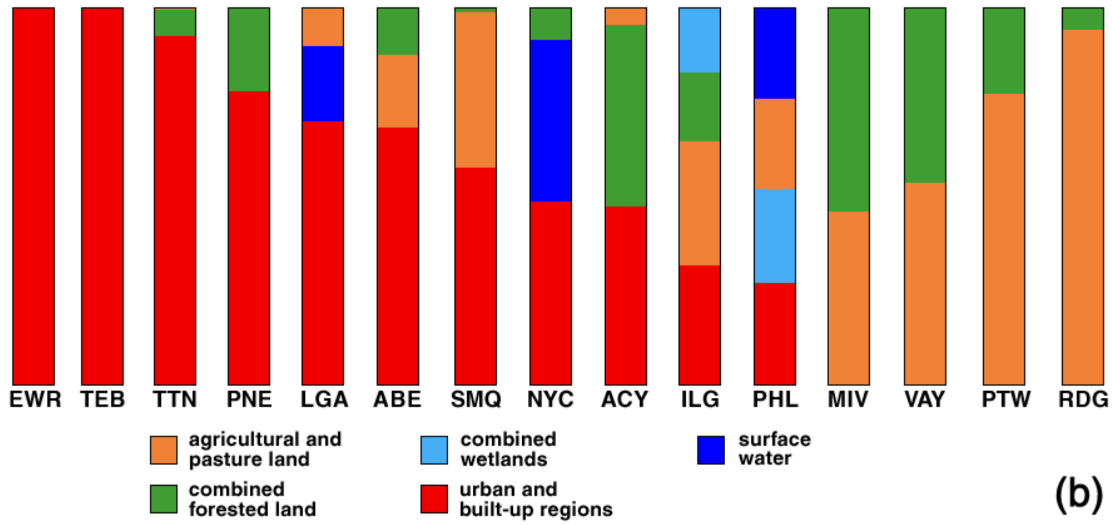

Figure 6. (a) The distribution of present-day land cover types for NJ and its surrounding states, derived from the NLCD dataset, and (b) the relative areal percentages of these land cover types for the fifteen stations identified where hourly temperature and rainfall observations were available for July 1999. The colors represent the dominant land cover type at the nearest grid 3 cell: forested (green), agricultural and pasture land (orange), wetlands (light blue), urban (red), and water (dark blue).

Figure 7

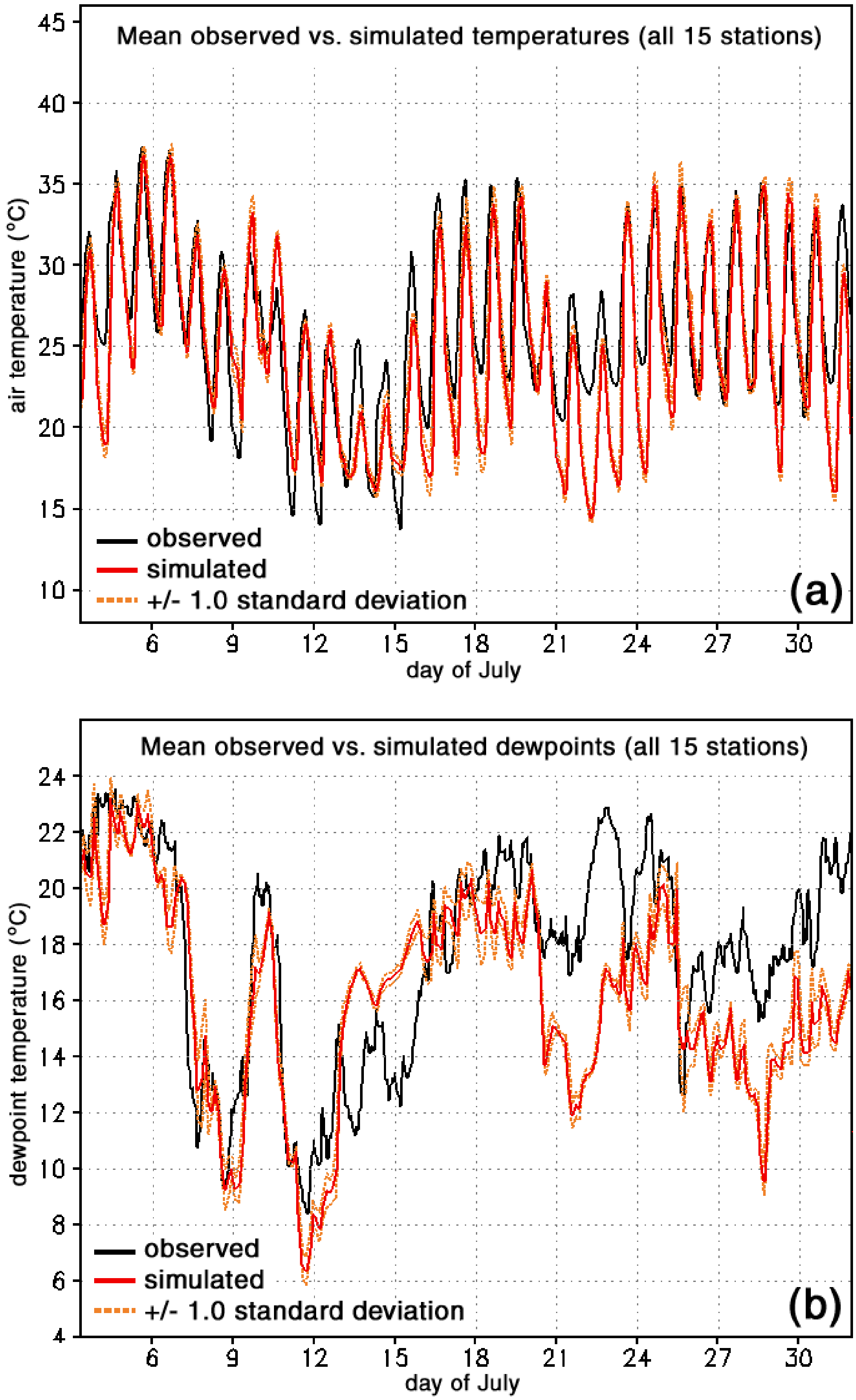
Mean observed vs. simulated temperatures (all 15 stations)
air temperature (°C)
45
40
35
30
25
20
15
10
observed
simulated
+/- 1.0 standard deviation
(a)
6
9
12
15
18
21
24
27
30
day of July
Mean observed vs. simulated dewpoints (all 15 stations)
dewpoint temperature (°C)
24
22
20
18
16
14
12
10
8
6
4
observed
simulated
+/- 1.0 standard deviation
(b)
6
9
12
15
18
21
24
27
30
day of July

Figure 7 *(continued from previous page)*

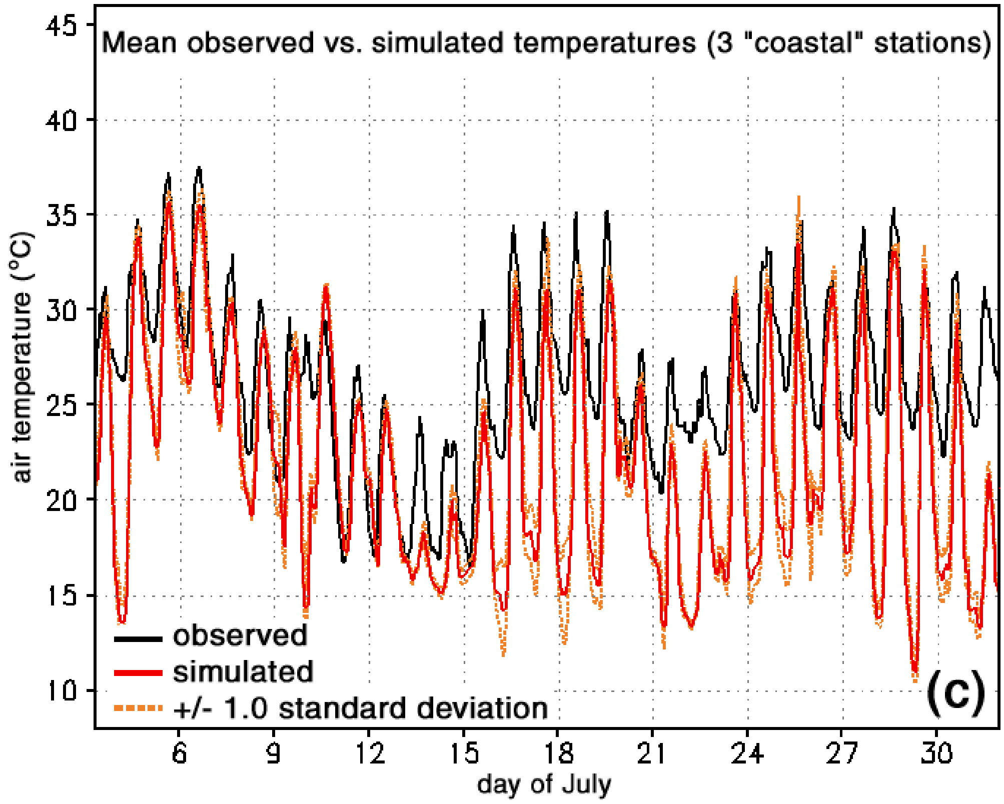

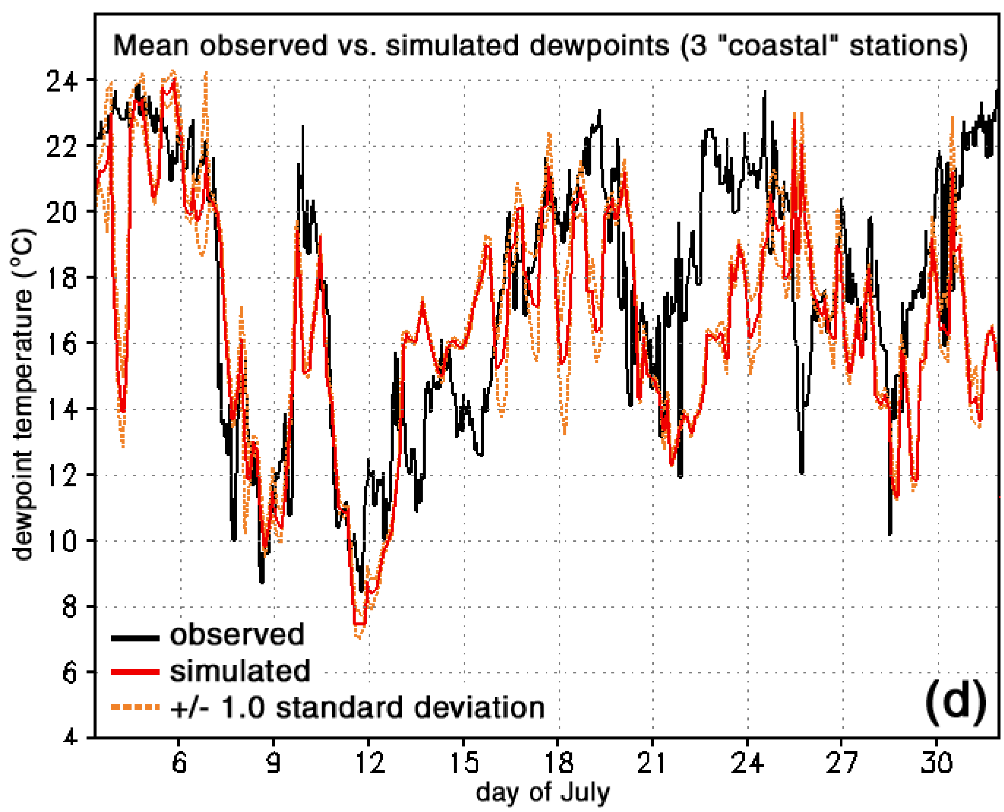

Figure 7 *(continued from previous page)*

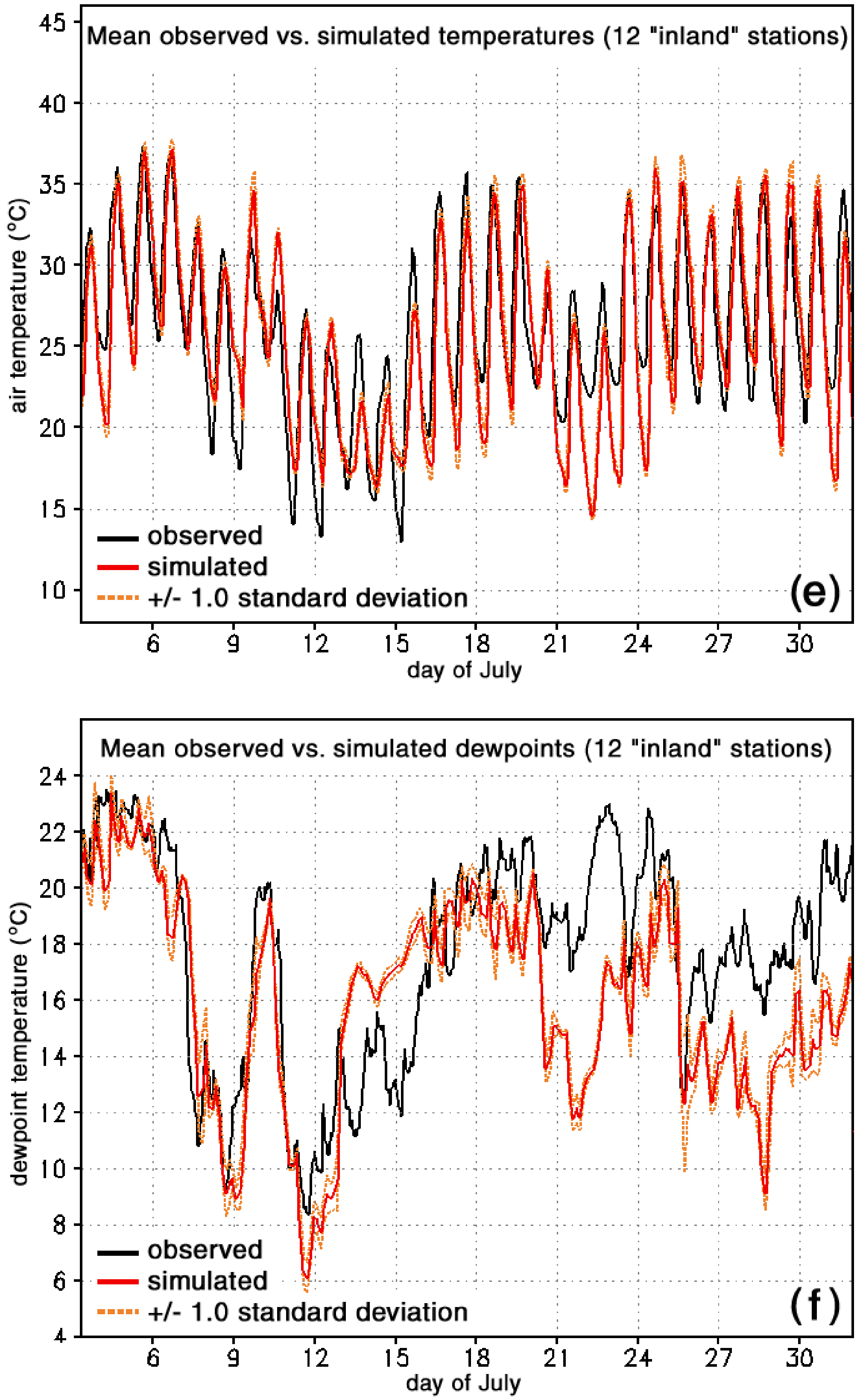

Figure 7 *(continued from previous page)*

Figure 7. The monthly time-series of observed hourly July surface air temperatures (black) and simulated temperatures from the control run ensemble (solid red), in degrees Celsius, averaged over all 15 stations on grid 3 (a); and observed July surface dewpoint temperatures (black) and simulated dewpoint temperatures from the control run ensemble (solid red), in degrees Celsius, averaged over all 15 stations on grid 3 (b). Though this time-series represents a regional average, three stations in coastal areas were determined to have a pronounced cool bias in the model, especially for air temperature. The monthly time-series of observed and simulated temperatures and dewpoints, averaged for these three "coastal" stations, are shown in panels (c) and (d), respectively, and for the remaining 12 "inland" stations in panels (e) and (f). Each plot starts at 8 am local time on 3 July and ends at 11 pm local time on 31 July. For each panel, the +/- 1.0 mean standard deviations of the individual ensemble members, added to the respective simulated values and also in degrees Celsius, are indicated by the red dashed lines.

Figure 8

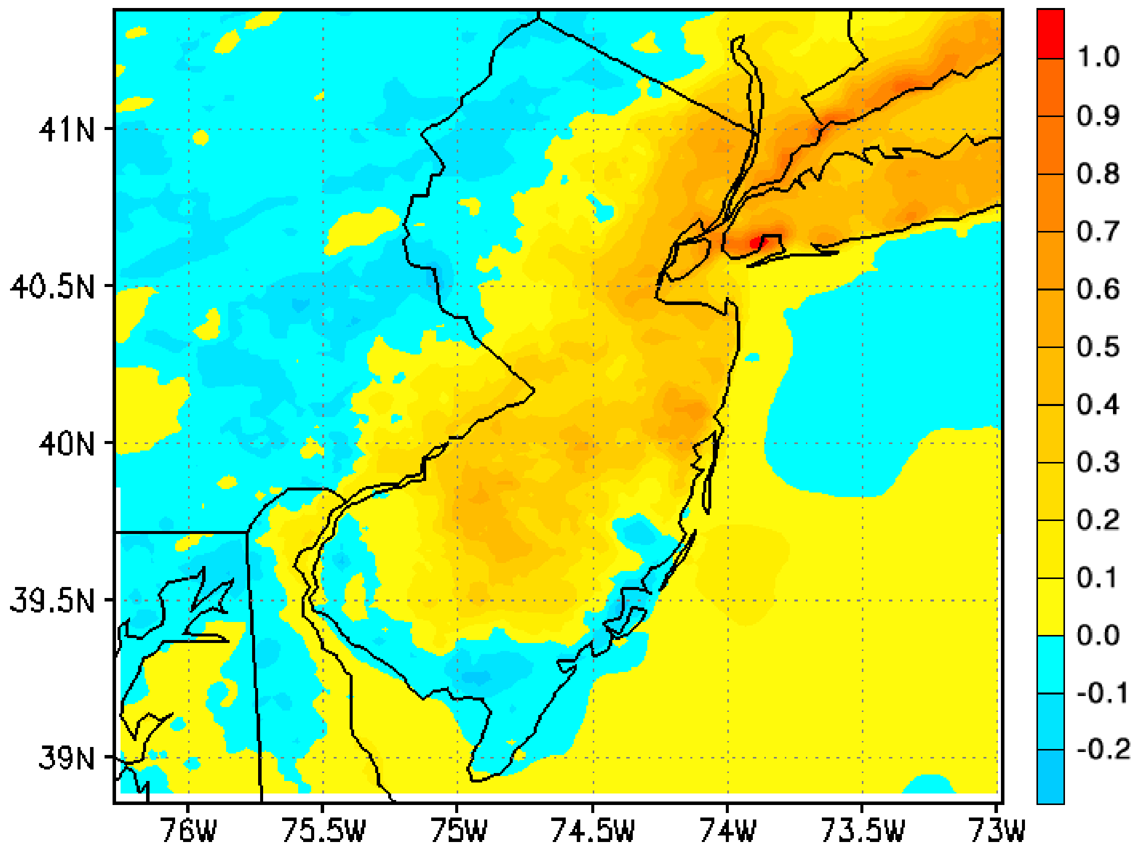

Figure 8. Mean monthly differences (present day minus historical land cover), for July, of hourly RAMS air temperatures between the ensemble run with present-day land cover and the ensemble run with historical land cover. The units are in degrees Celsius.

Figure 9

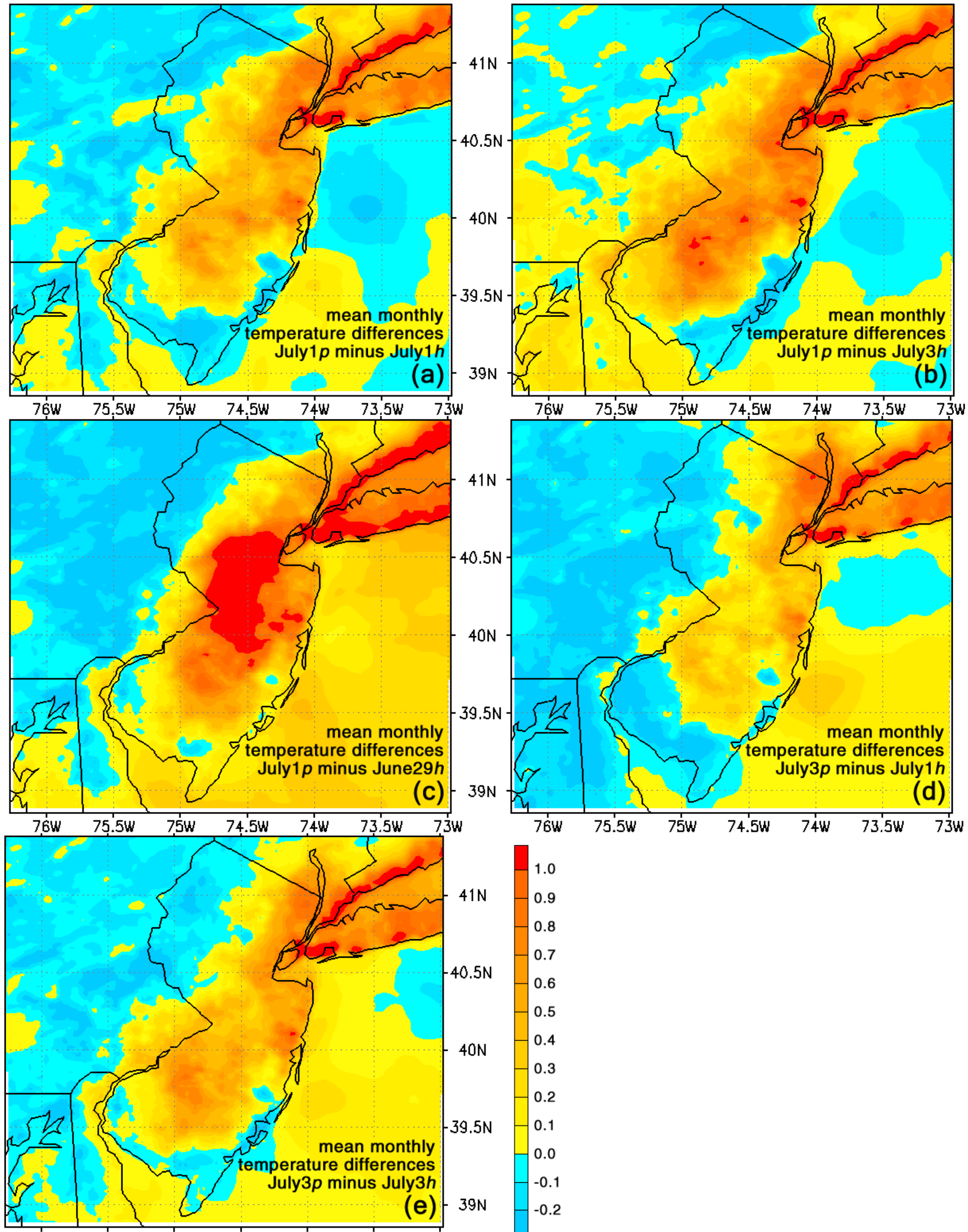
mean monthly
temperature differences
July1p minus July1h
(a)
mean monthly
temperature differences
July1p minus July3h
(b)
mean monthly
temperature differences
July1p minus June29h
(c)
mean monthly
temperature differences
July3p minus July1h
(d)
mean monthly
temperature differences
July3p minus July3h
(e)
41N
40.5N
40N
39.5N
39N
76W
75.5W
75W
74.5W
74W
73.5W
73W
1.0
0.9
0.8
0.7
0.6
0.5
0.4
0.3
0.2
0.1
0.0
-0.1
-0.2

Figure 9 *(continued from previous page)*

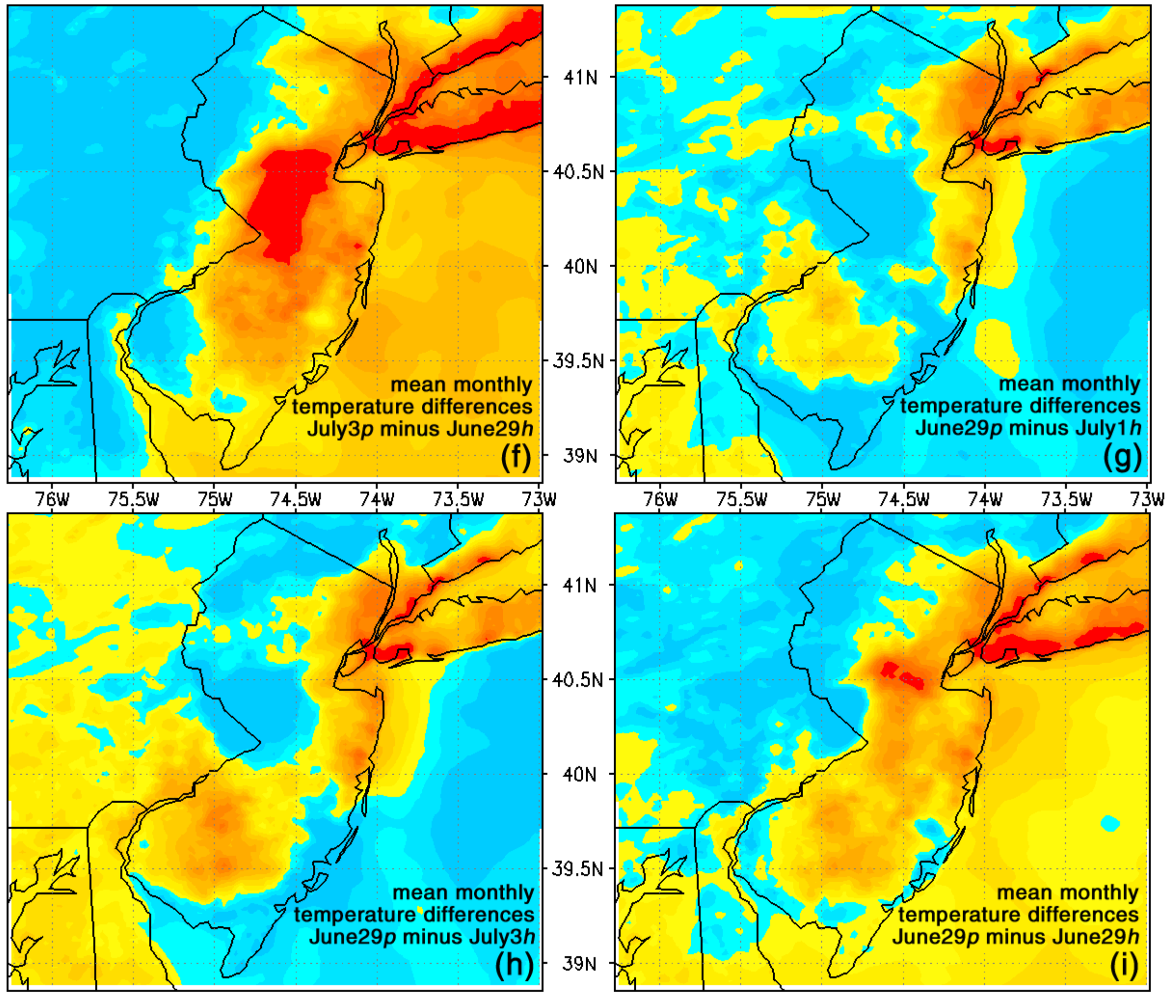

Figure 9. Mean monthly temperature differences, in degrees Celsius, between individual members of the historical and present-day ensembles. Each member is denoted by its initial atmosphere followed by an *h* for the run with historical land cover, and a *p* for the run with present-day land cover: July 1*p* minus July 1*h* (a); July1*p* minus July3*h* (b); July1*p* minus June29*h* (c); July3*p* minus July1*h* (d); July3*p* minus July3*h* (e); July3*p* minus June29*h* (f); June29*p* minus July1*h* (g); June29*p* minus July3*h* (h); and June29*p* minus June29*h* (i).

Figure 10

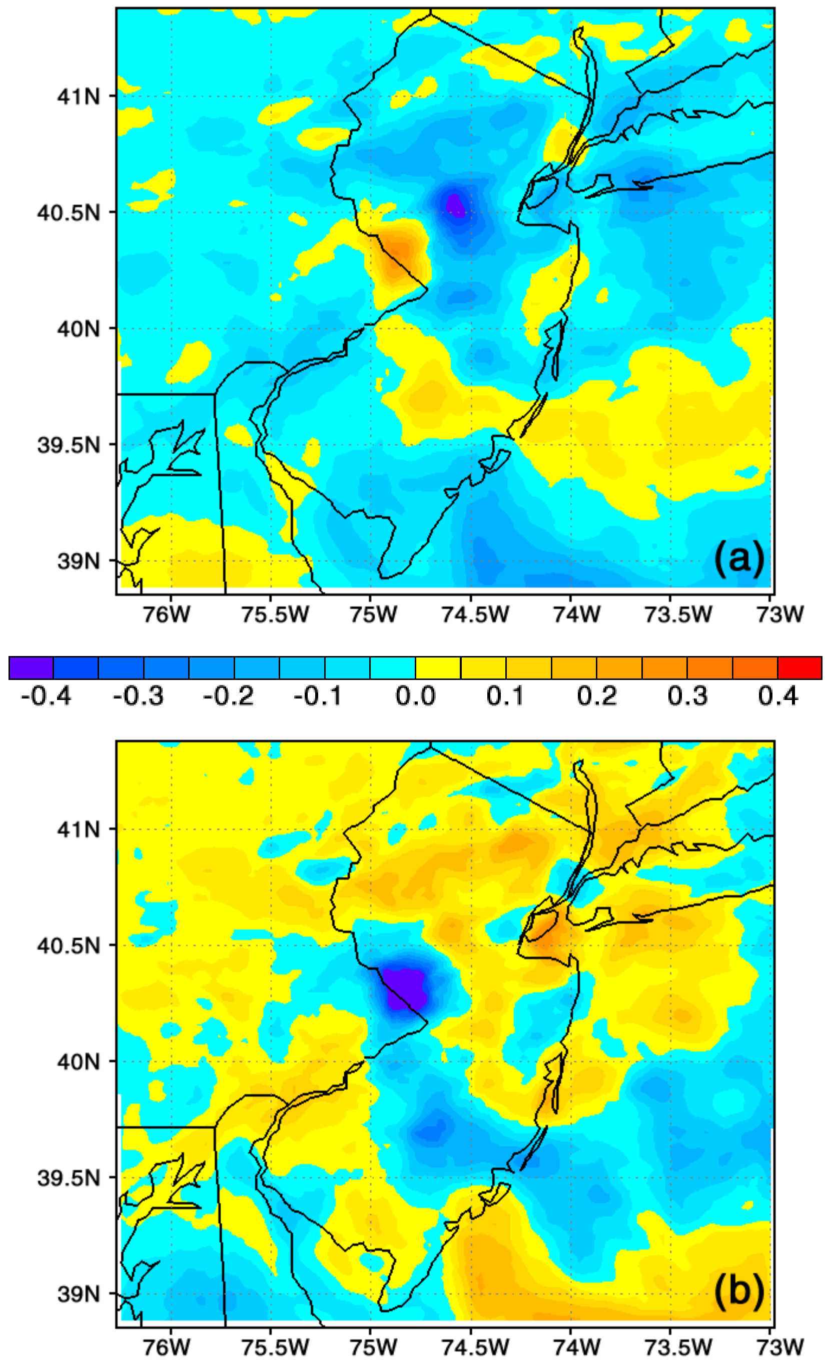

Figure 10. The differences in the standard deviation of mean monthly RAMS temperatures between the historical and present-day ensembles (a), and the corresponding differences in the standard deviation, at each grid cell, between the coolest present-day run and the warmest historical run (b). The units in both panels are in degrees Celsius.

Figure 11

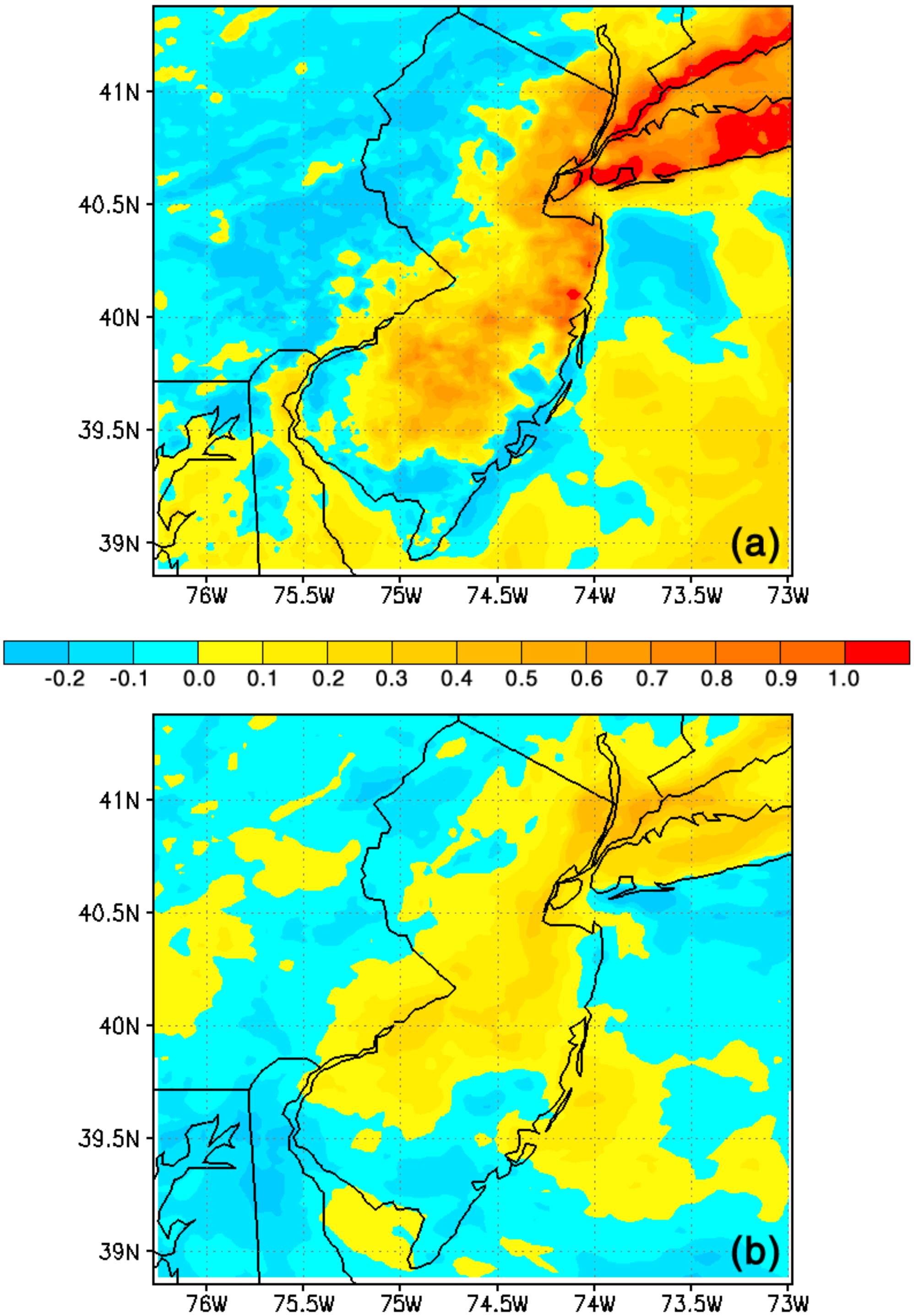

Figure 11. As in Figure 8 except for (a) daily maximum near-surface air temperatures and (b) daily minimum near-surface air temperatures. The units are in degrees Celsius.

Figure 12

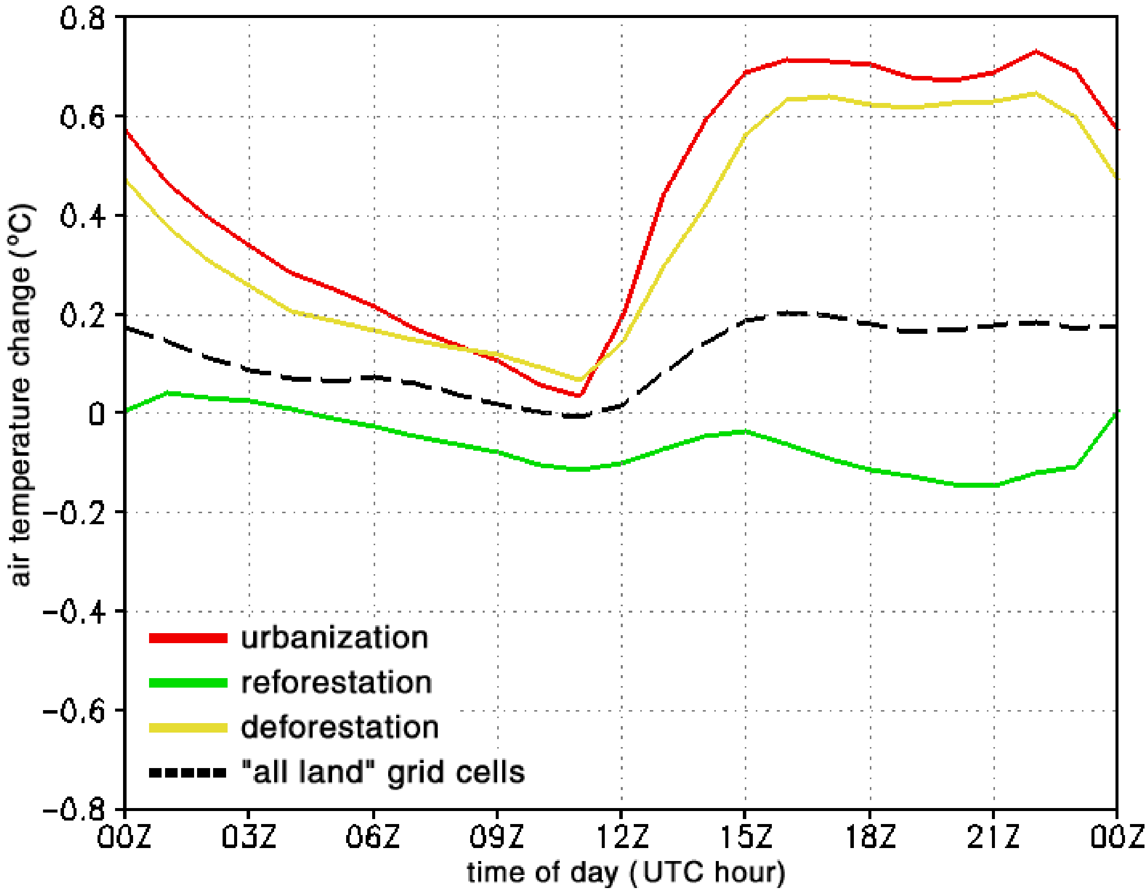

Figure 12. The mean diurnally-averaged monthly time-series of mean July near-surface air temperature differences (present-day minus historical land cover), in degrees Celsius, for those grid cells that have experienced a change in dominant land cover resulting from urbanization (red), reforestation (green), deforestation (yellow), and for all land points on grid 3 (dashed black). The x-axis represents the hour of universal time.

Figure 13

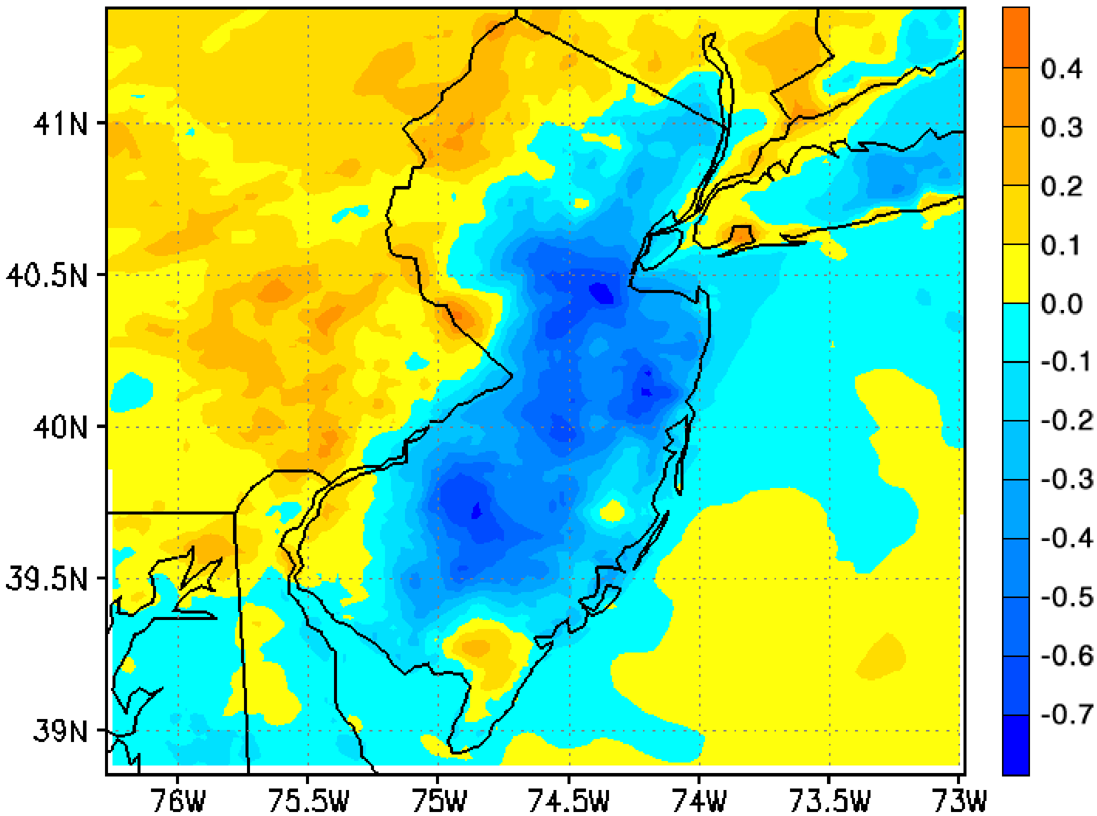

Figure 13. As in Figure 8 except for near-surface dewpoint temperatures. The units are in degrees Celsius. The contour interval for this figure has a different range than those of Figures 8, 9, and 11.

Figure 14

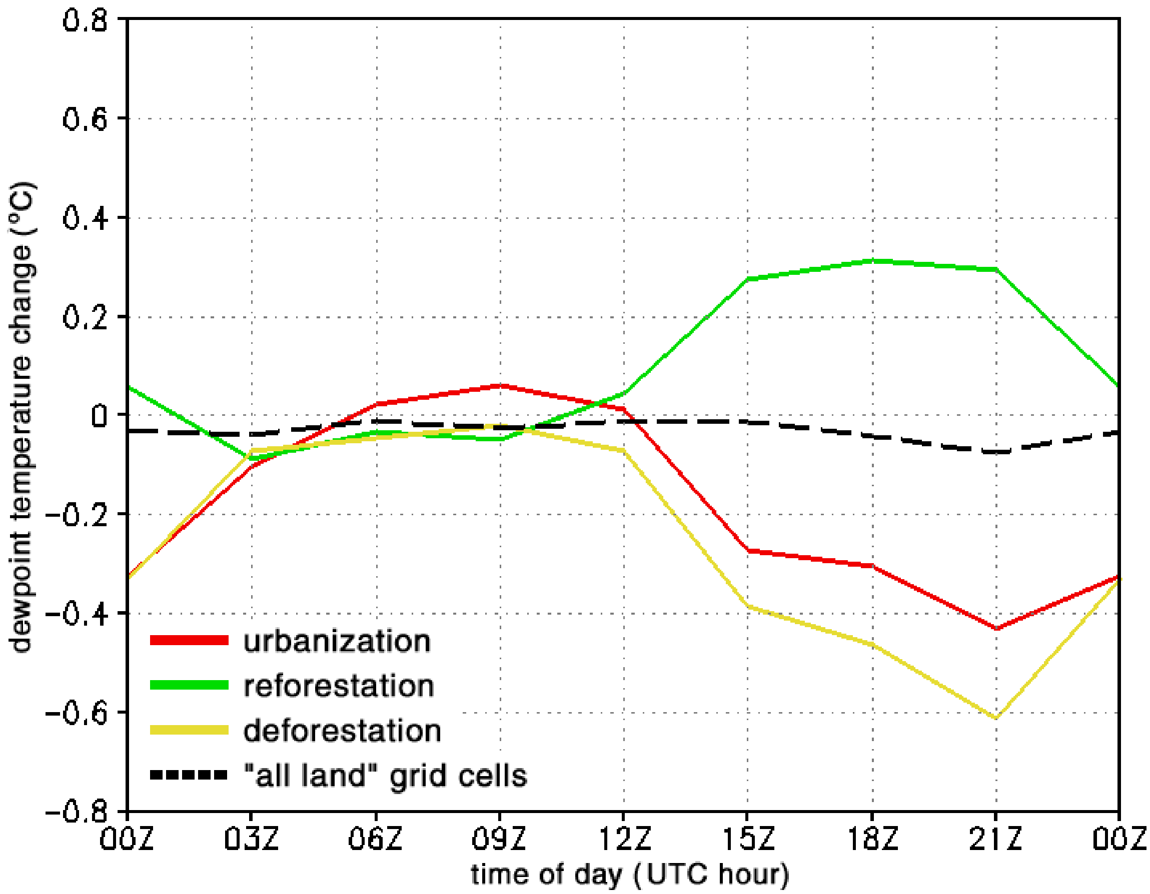

Figure 14. As in Figure 12 except for near-surface dewpoint temperatures.

Figure 15

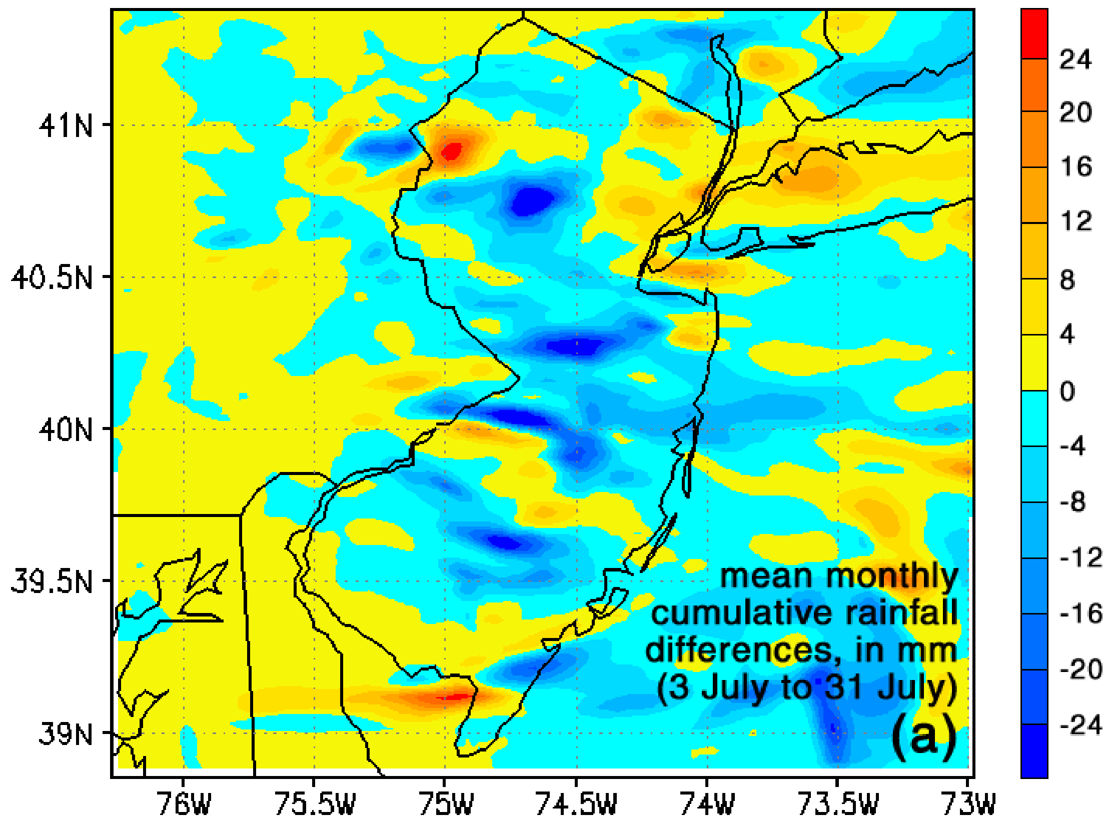
mean monthly
cumulative rainfall
differences, in mm
(3 July to 31 July)
(a)
41N
40.5N
40N
39.5N
39N
76W
75.5W
75W
74.5W
74W
73.5W
73W
24
20
16
12
8
4
0
-4
-8
-12
-16
-20
-24

Figure 15 *(continued from previous page)*

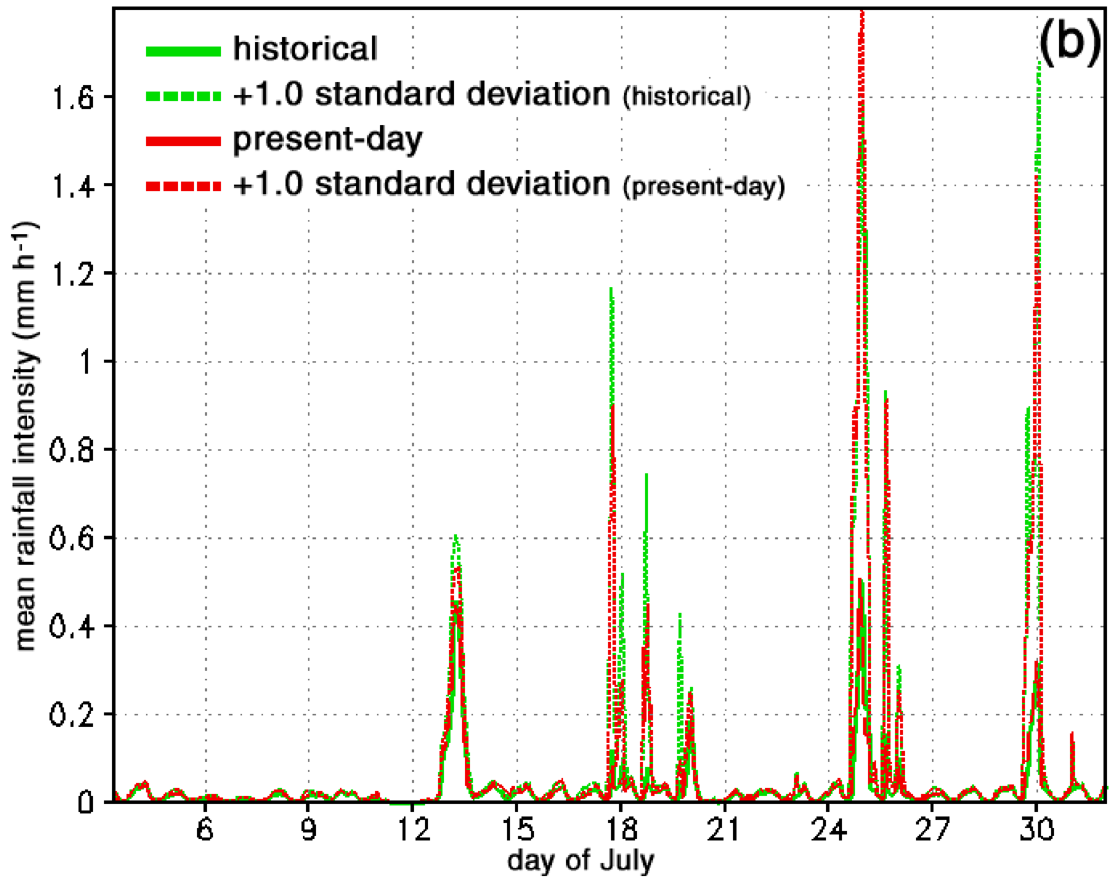

Figure 15. (a) Monthly mean differences (present-day minus historical land cover) in cumulative rainfall totals, in mm, extracted from the final time of the ensembles, at 04:00UTC 1 August, and (b) the domain-averaged monthly time-series of mean rainfall intensity differences, in mm h^{-1}, of the ensemble with historical land cover (solid green) and with present-day land cover (solid red). The time-series of the +1.0 mean standard deviations of hourly rainfall rates, added to the respective mean ensemble values and in mm h^{-1}, are indicated by the dashed lines. The historical standard deviation is represented by the green dashed line and the present-day by the red dashed line.

Figure 16

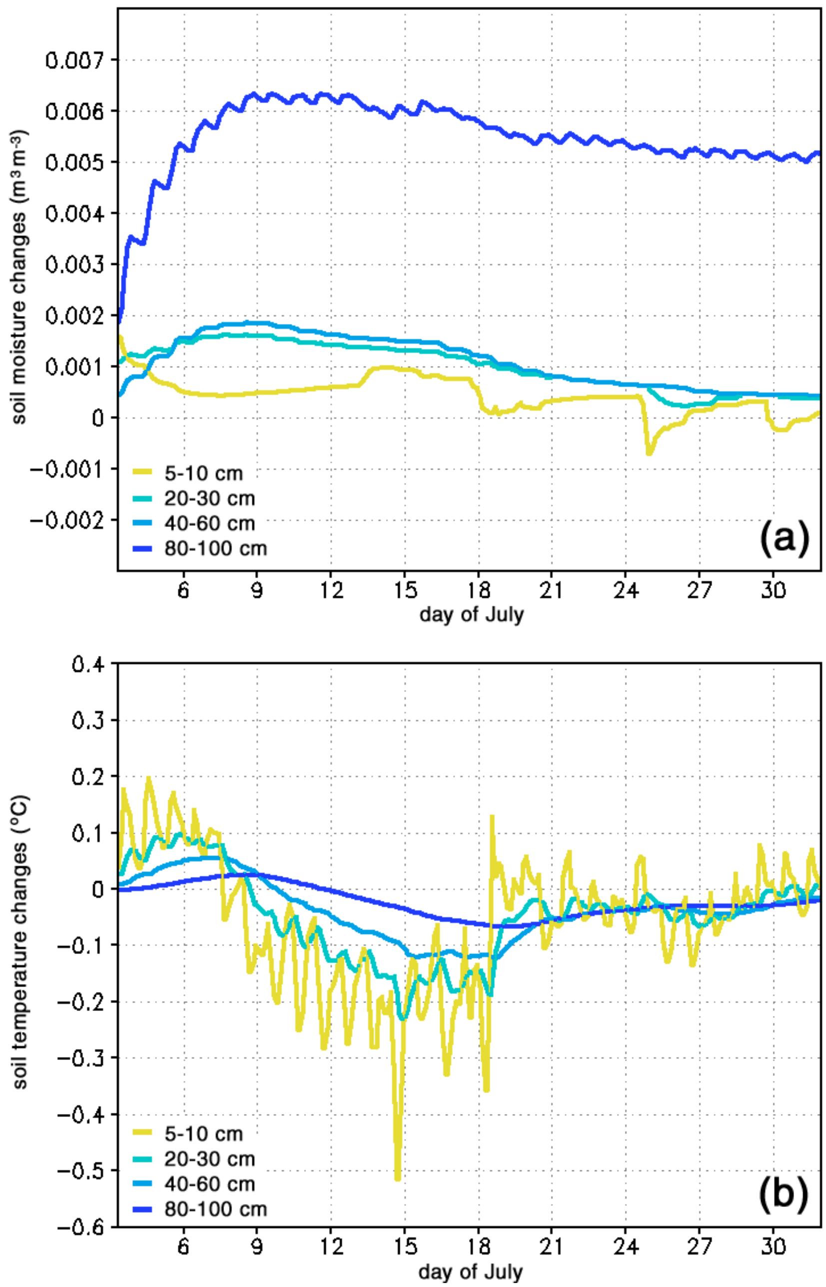

Figure 16. The monthly time-series of mean domain-averaged soil moisture differences, in $m^3\ m^{-3}$, during the analysis period (a), and the corresponding time-series of domain-averaged soil temperature differences, in degrees Celsius (b), between the ensemble runs. The four soil layers shown are 5-10 cm (yellow), 20-30 cm (light blue), 40-60 cm (medium blue), and 80-100 cm (dark blue). The x-axis represents the day of July.

Figure 17

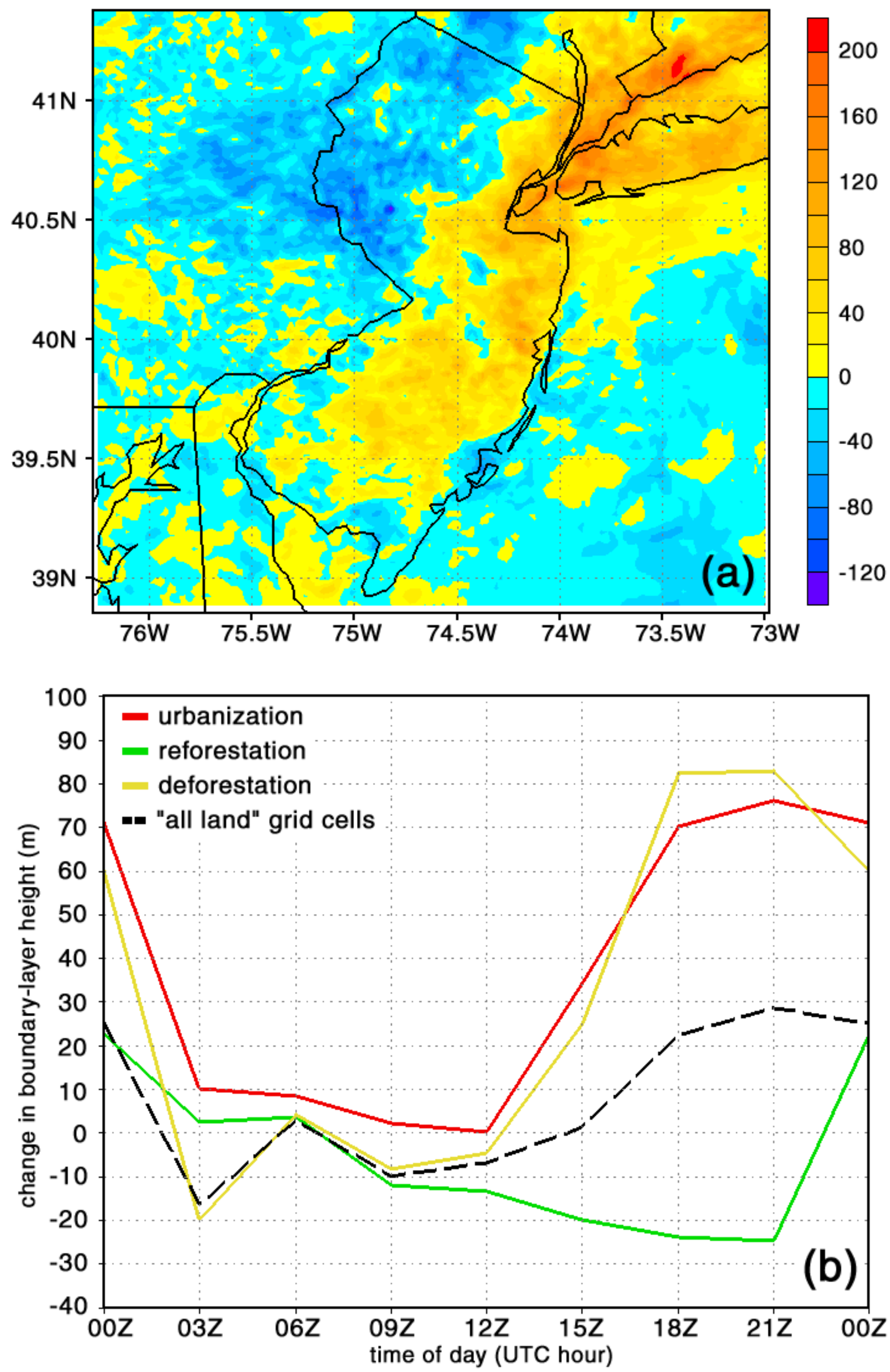

Figure 17. Monthly mean differences (present day minus historical land cover), for July, of boundary-layer heights between the ensemble runs (a); and the time evolution of mean

diurnally-averaged differences in these heights during a full day (b). The colors in (b) represent those grid cells that have experienced a change in dominant land cover resulting from urbanization (red), reforestation (green), deforestation (yellow), and for all land points on grid 3 (dashed black). The units in both panels are in meters.

Figure 18

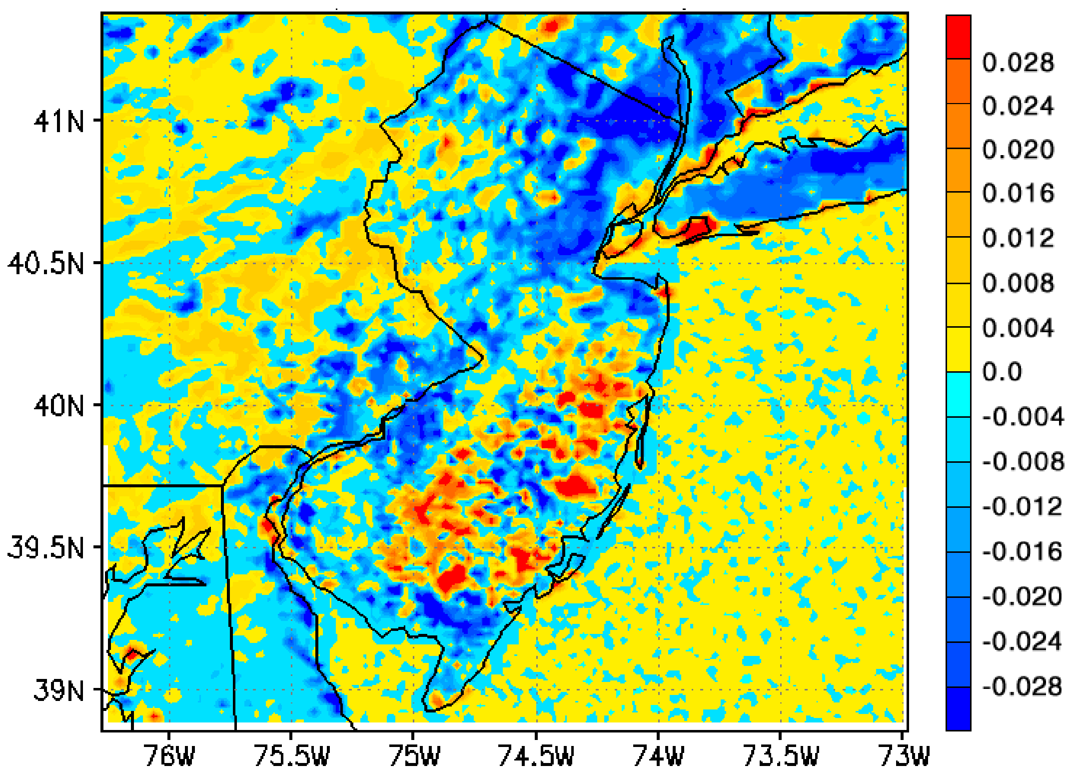

Figure 18. As in Figure 8 except for model-calculated net surface broadband albedo.

Figure 19

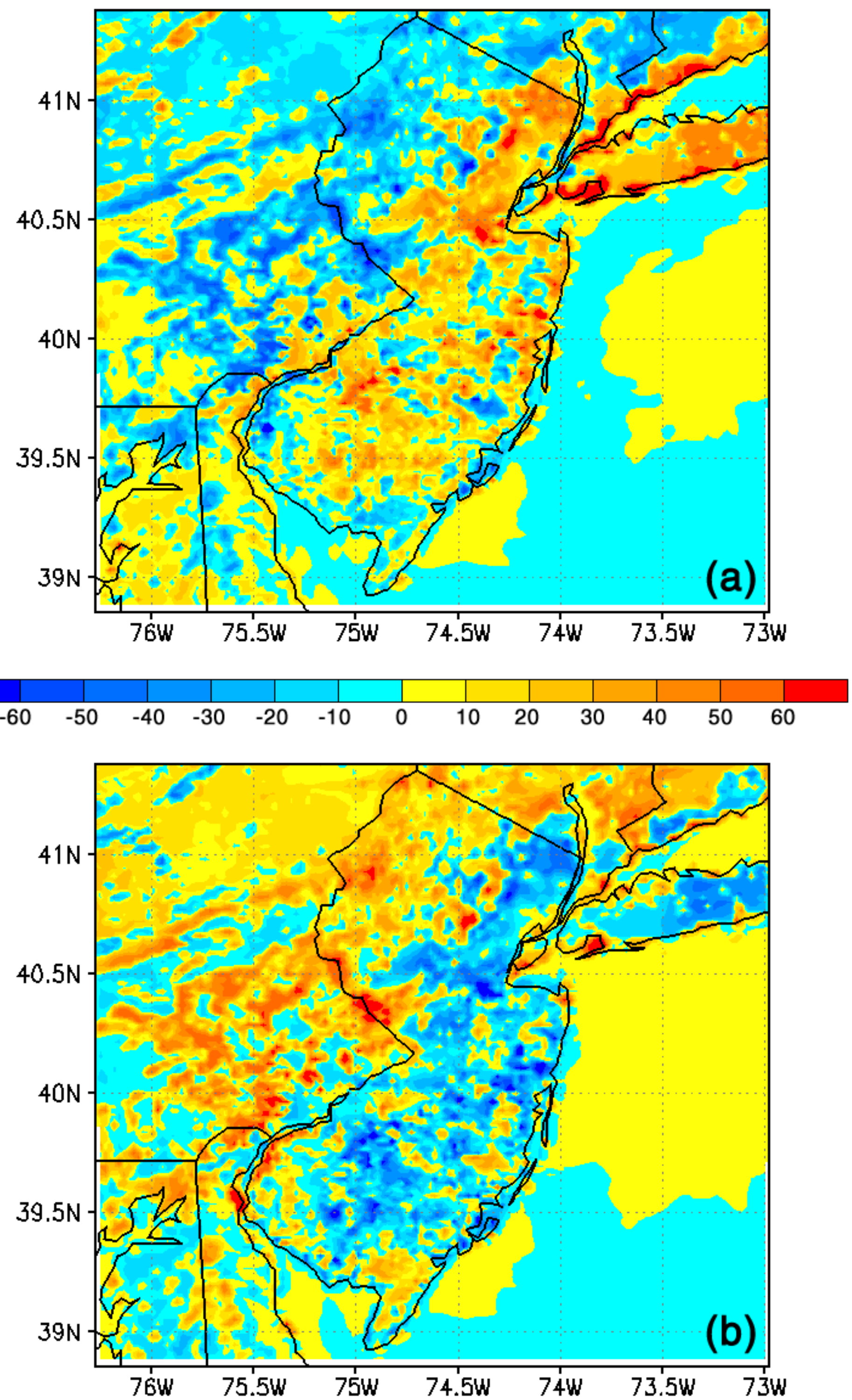

Figure 19. As in Figure 8 except for the differences in (a) surface sensible heat flux and (b) surface latent heat flux. The units are in W m^{-2}.

Figure 20

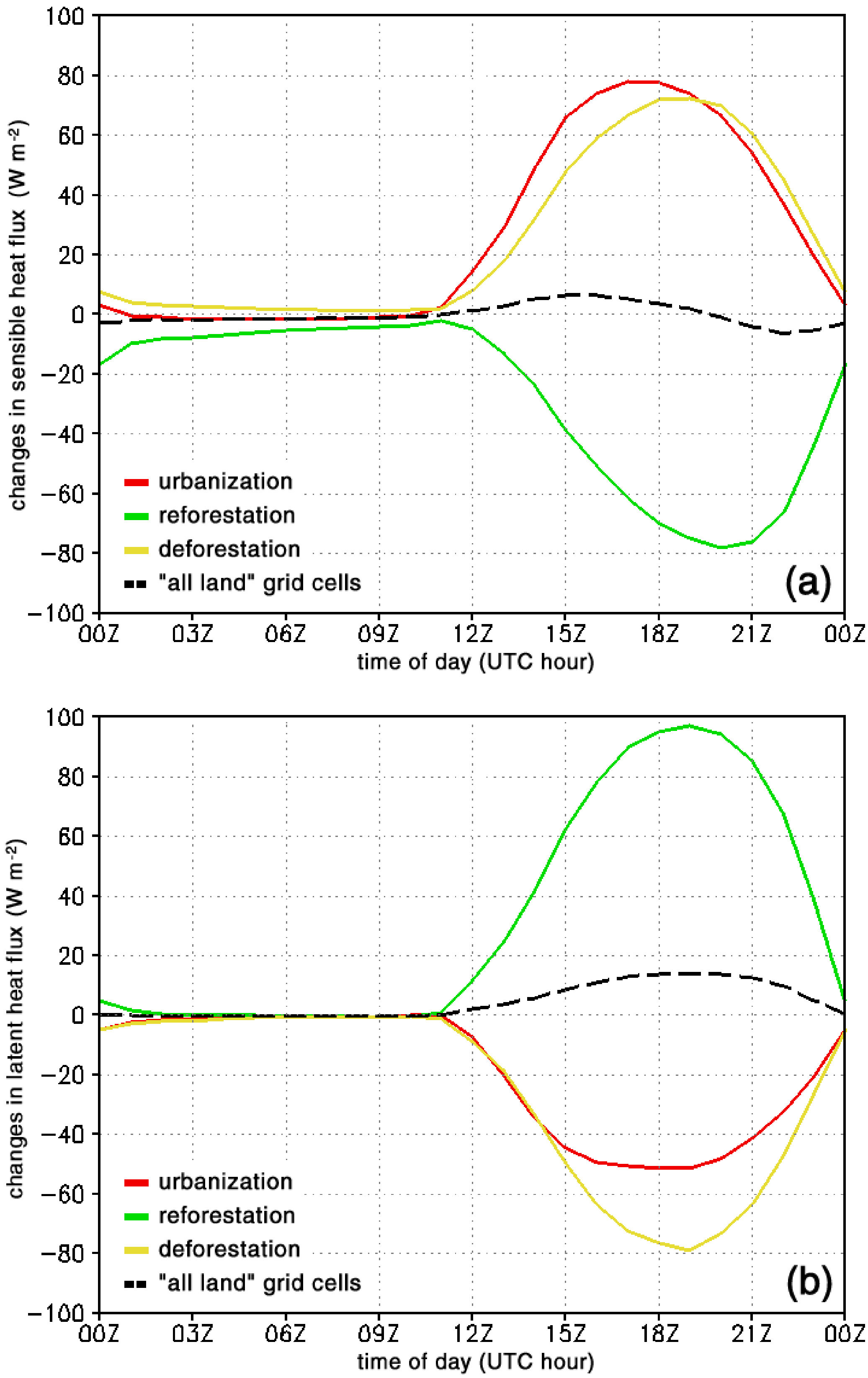
changes in sensible heat flux (W m-2)
urbanization
reforestation
deforestation
"all land" grid cells
(a)
time of day (UTC hour)
changes in latent heat flux (W m-2)
urbanization
reforestation
deforestation
"all land" grid cells
(b)
time of day (UTC hour)

Figure 20 *(continued from previous page)*

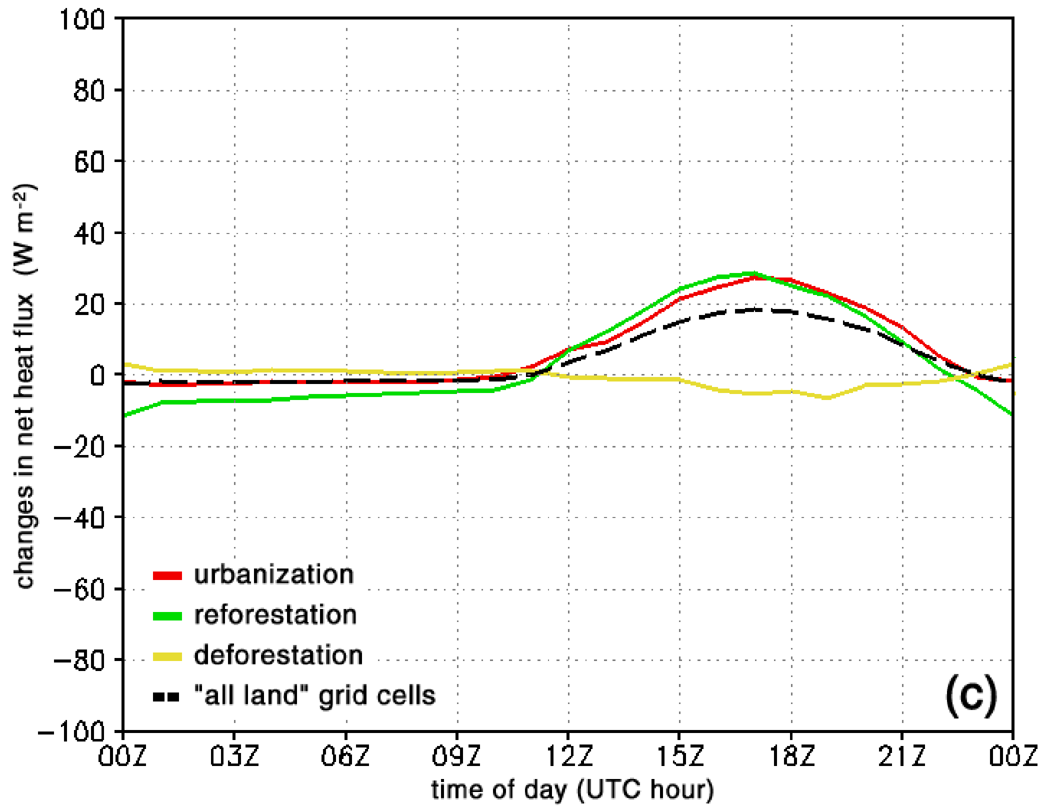

Figure 20. The mean diurnally-averaged monthly time-series of differences (present-day minus historical land cover) in (a) surface sensible heat flux, (b) latent heat flux (b), and (c) net sensible and latent heat flux, for those grid cells that have experienced a change in dominant land cover resulting from urbanization (red), reforestation (green), deforestation (yellow), and for all land points on grid 3 (dashed black). The units in all panels are in W m^{-2}.

Figure 21

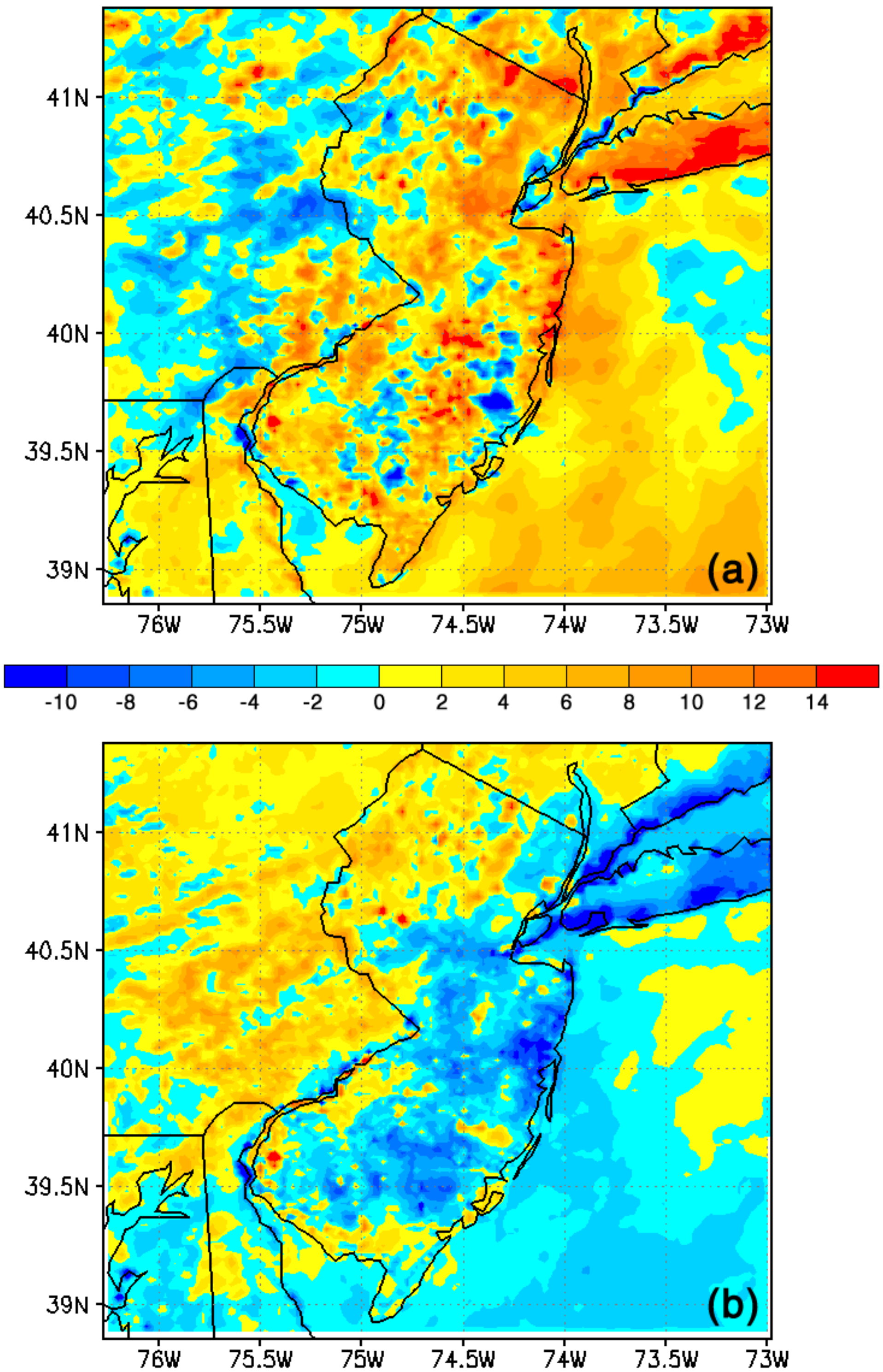

Figure 21. As in Figure 8 except for the differences in (a) net downward shortwave radiative flux and (b) net downward longwave radiative flux. The units are in W m^{-2}.

Figure 22

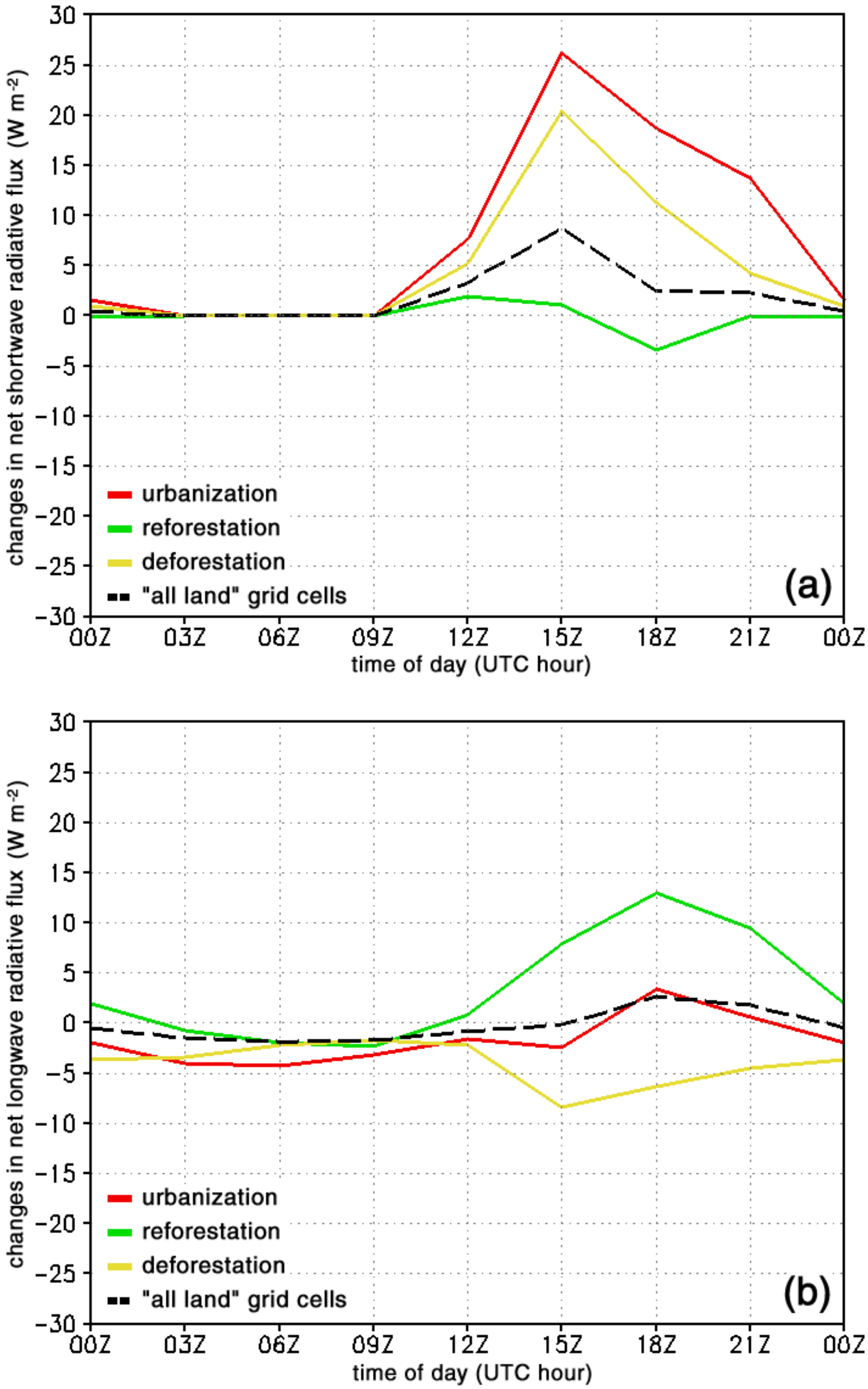
(a)
changes in net shortwave radiative flux (W m-2)
time of day (UTC hour)
urbanization
reforestation
deforestation
"all land" grid cells
30
25
20
15
10
5
0
−5
−10
−15
−20
−25
−30
00Z
03Z
06Z
09Z
12Z
15Z
18Z
21Z
00Z
(b)
changes in net longwave radiative flux (W m-2)
time of day (UTC hour)
urbanization
reforestation
deforestation
"all land" grid cells

Figure 22 *(continued from previous page)*

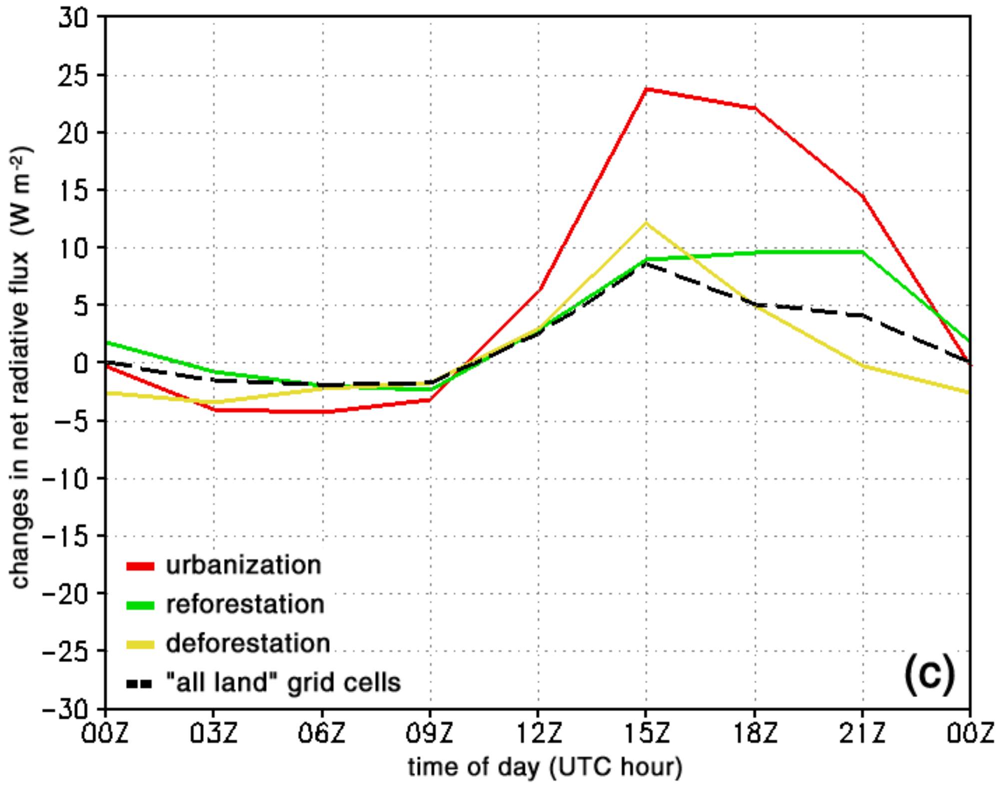

Figure 22. As in Figure 20 except for the differences in (a) net downward shortwave radiative flux, (b) net downward longwave radiative flux, and (c) total net radiative flux received by the surface. The units in all panels are in W m^{-2}.

Figure 23

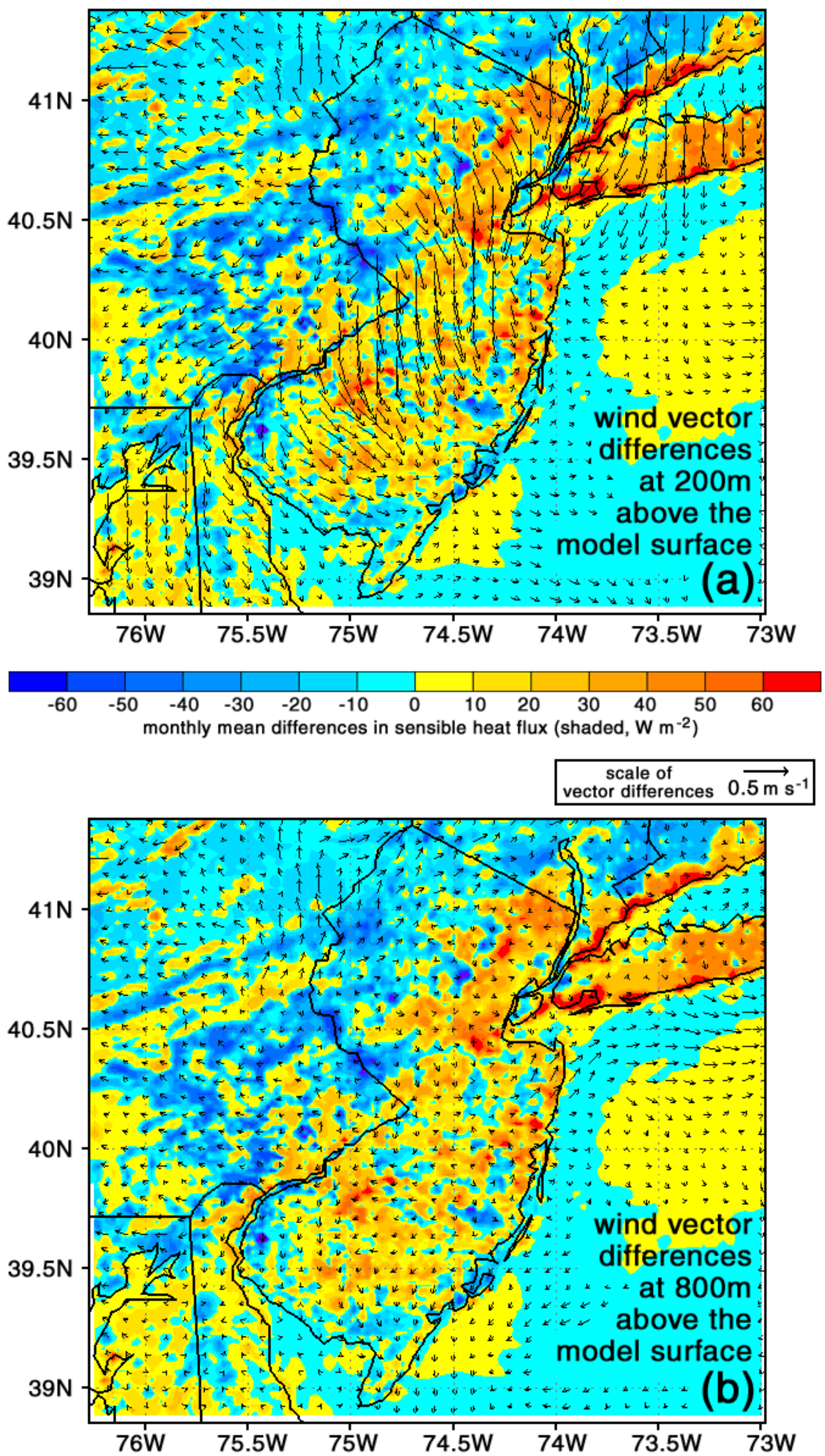

41N
40.5N
40N
39.5N
39N
76W
75.5W
75W
74.5W
74W
73.5W
73W
wind vector differences at 200m above the model surface
(a)
-60 -50 -40 -30 -20 -10 0 10 20 30 40 50 60
monthly mean differences in sensible heat flux (shaded, W m-2)
scale of vector differences
0.5 m s-1
wind vector differences at 800m above the model surface
(b)

Figure 23 *(continued from previous page)*

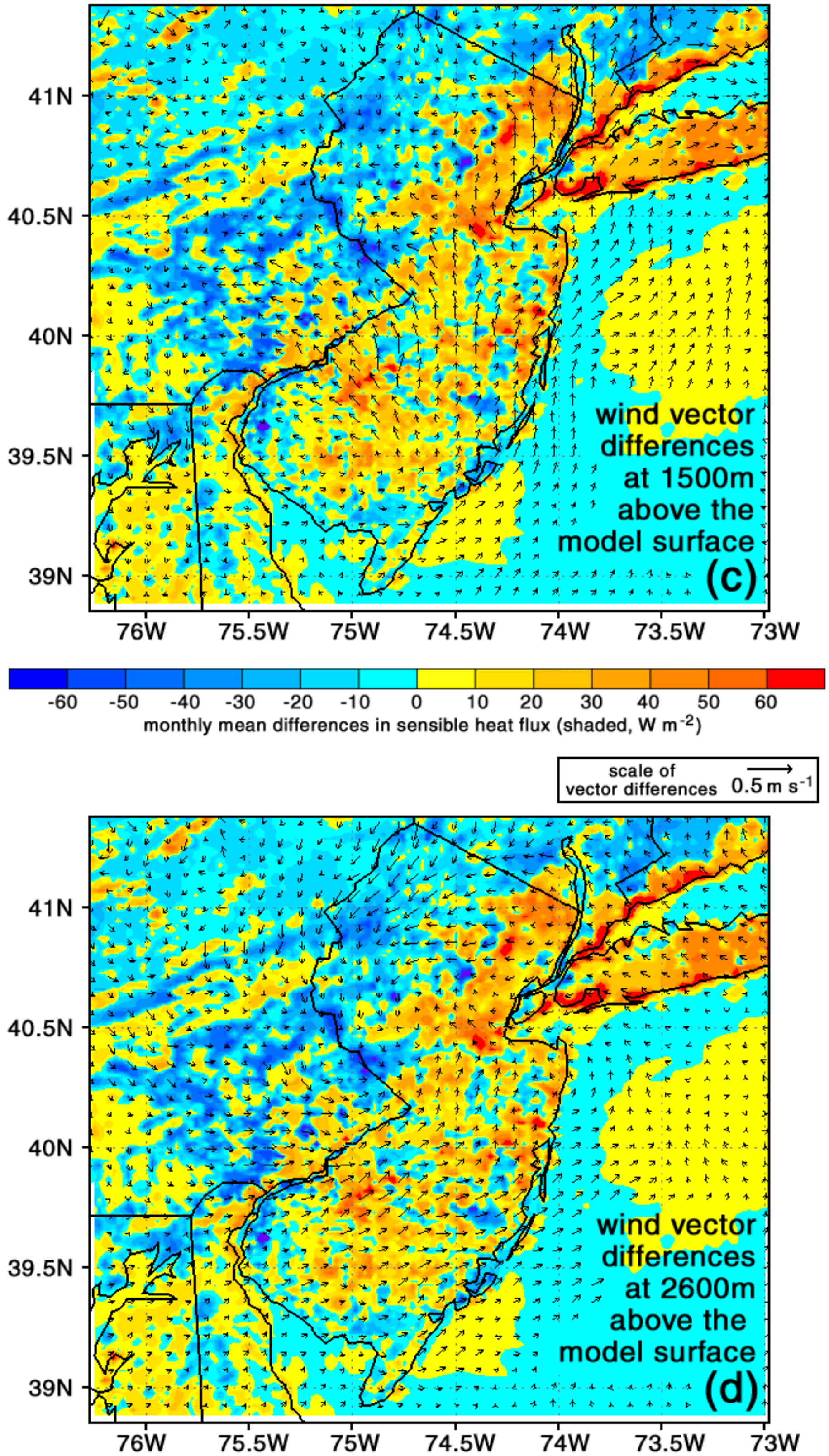

Figure 23 *(continued from previous page)*

Figure 23. Monthly mean horizontal wind vector differences (present-day minus historical land cover) at four heights above the surface: 200m (a); 800m (b); 1500m (c); and 2600m (d). Shaded regions represent monthly mean sensible heat flux differences in W m^{-2}. The wind vector scaling is m s^{-1} with the size of the arrow as shown.

Figure 24

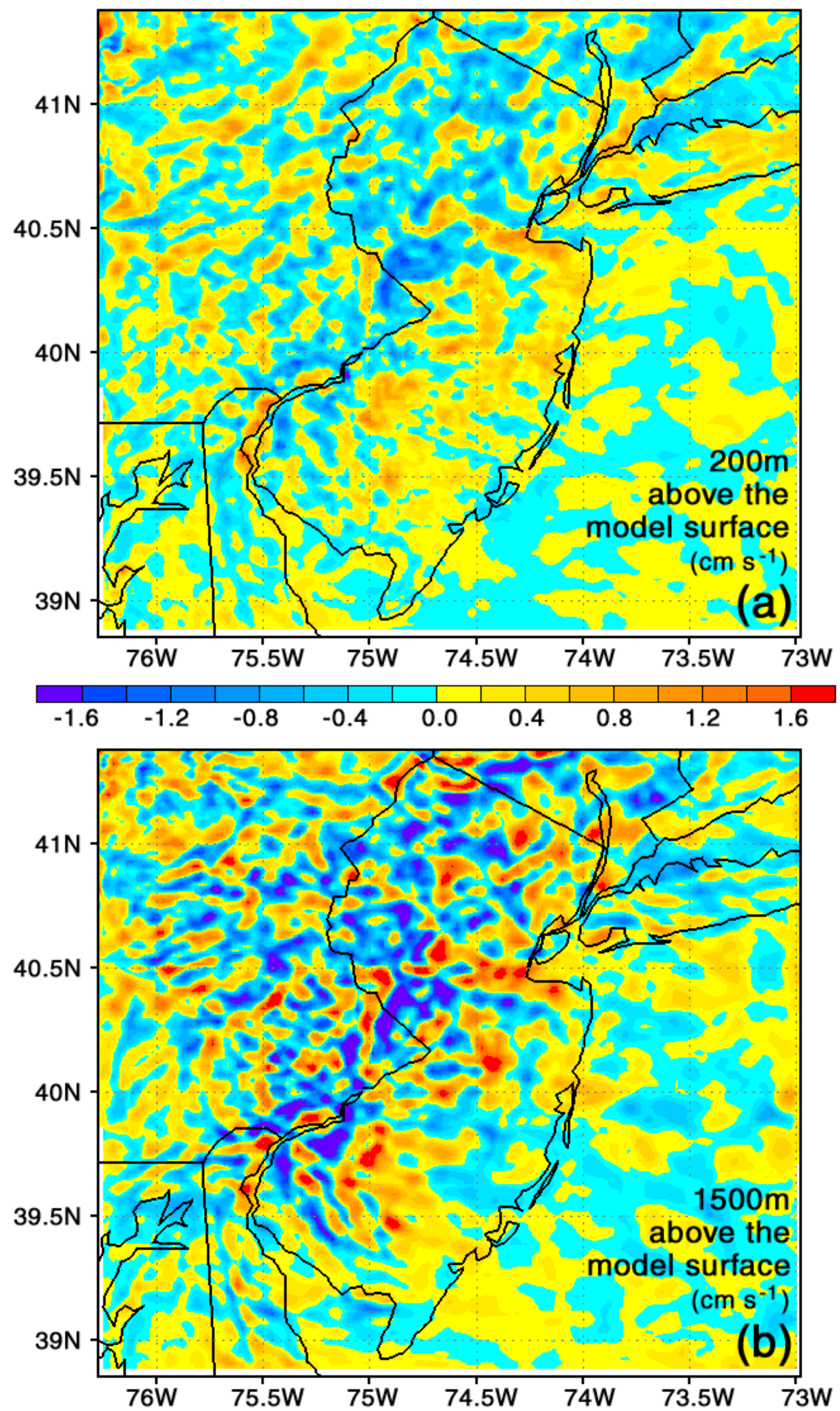

Figure 24. Monthly mean vertical velocity differences (present-day minus historical land cover) at 200m (a) and at 1500m (b). These panels are plotted with units of cm s^{-1}.

Figure 25

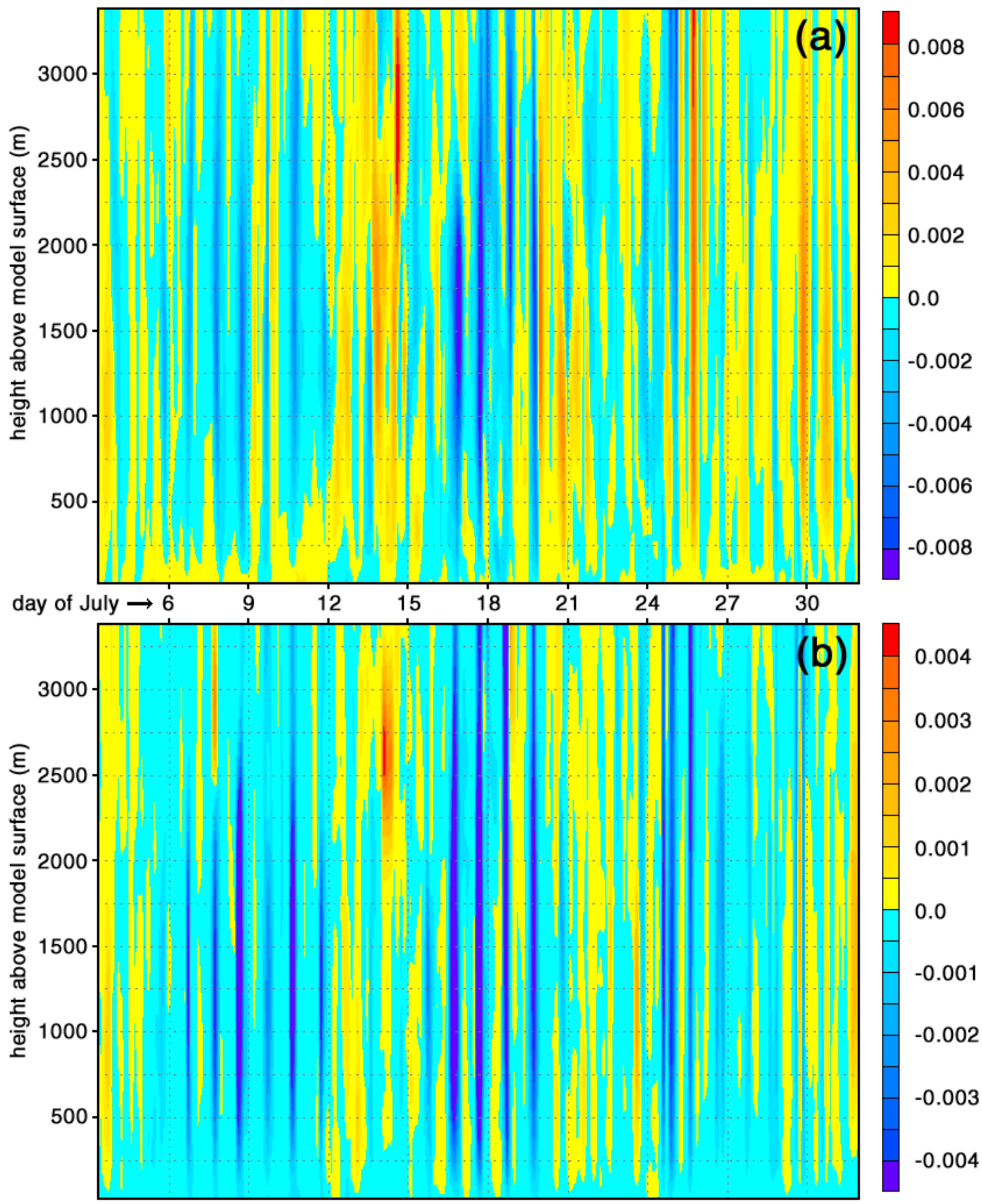

Figure 25. Monthly time-series of mean domain-averaged differences (present-day minus historical land cover) in *w* (a); and the corresponding mean domain-averaged differences in *σ(w)* (b), between the ensemble runs. The units in both panels are in m s^{-1}. The x-axes represent the day of July, and the y-axes the height above the surface, in m.

Figure 26

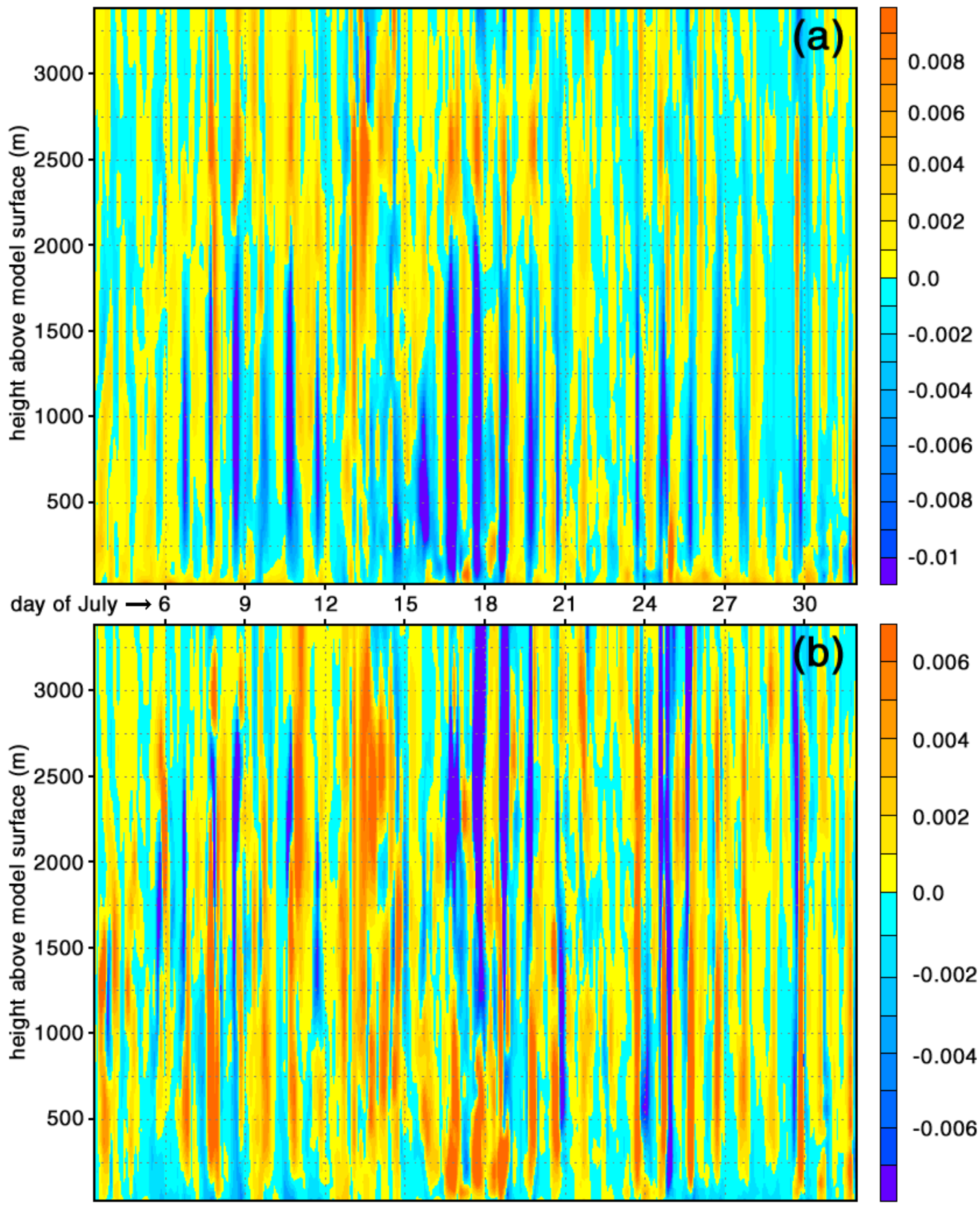

Figure 26. As in Figure 25 except for the differences in the mesoscale vertical flux of theta (*tflux*), shown in K m s^{-1} (a), and in the mesoscale vertical flux of moisture (*qflux*), shown in g kg^{-1} m s^{-1} (b), between the ensemble runs.

Figure 27

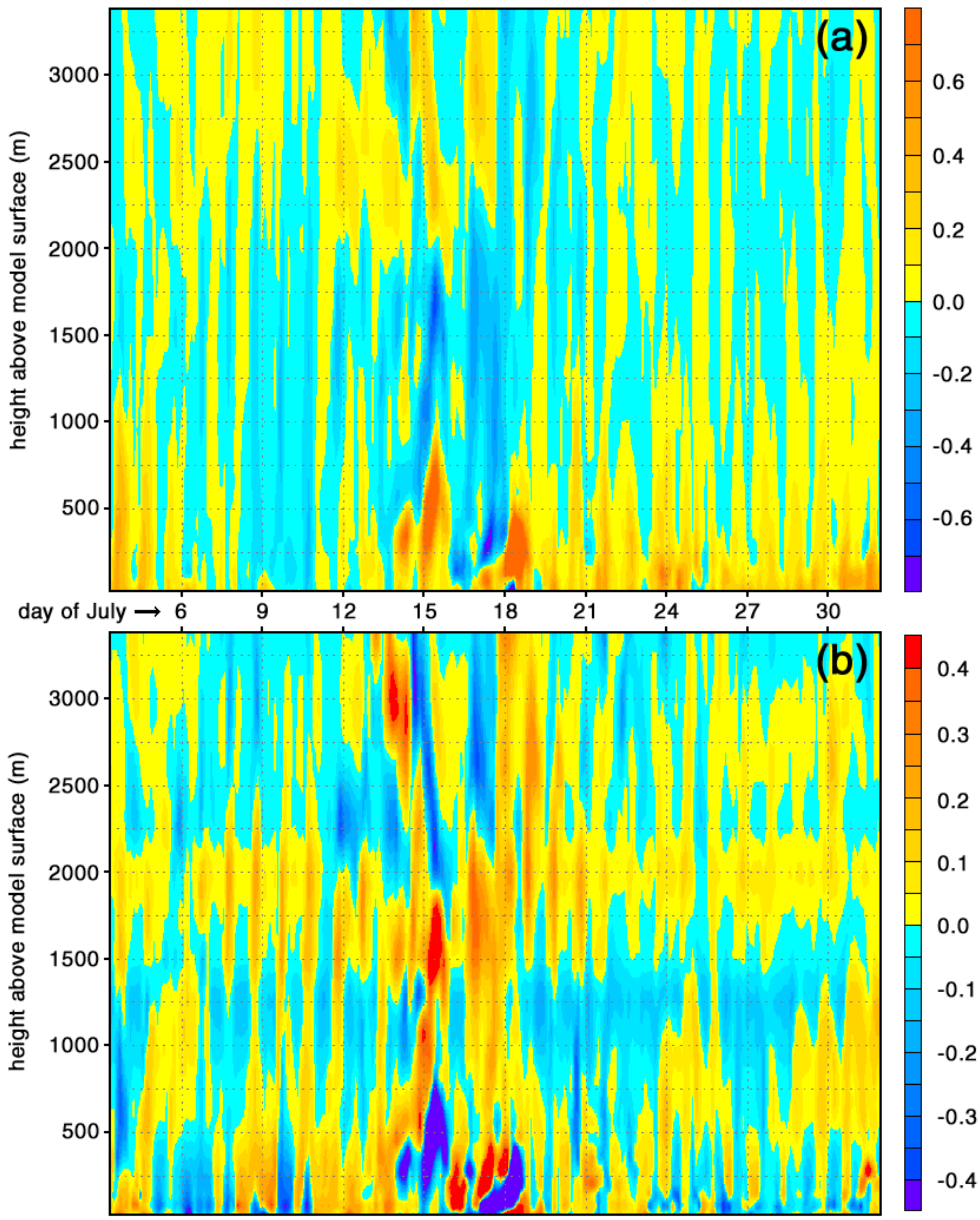

Figure 27. As in Figure 25, except for the differences in θ (a), and the differences in $\sigma(\theta)$ (b), between the ensemble runs. The units in both panels are in K.

Figure 28

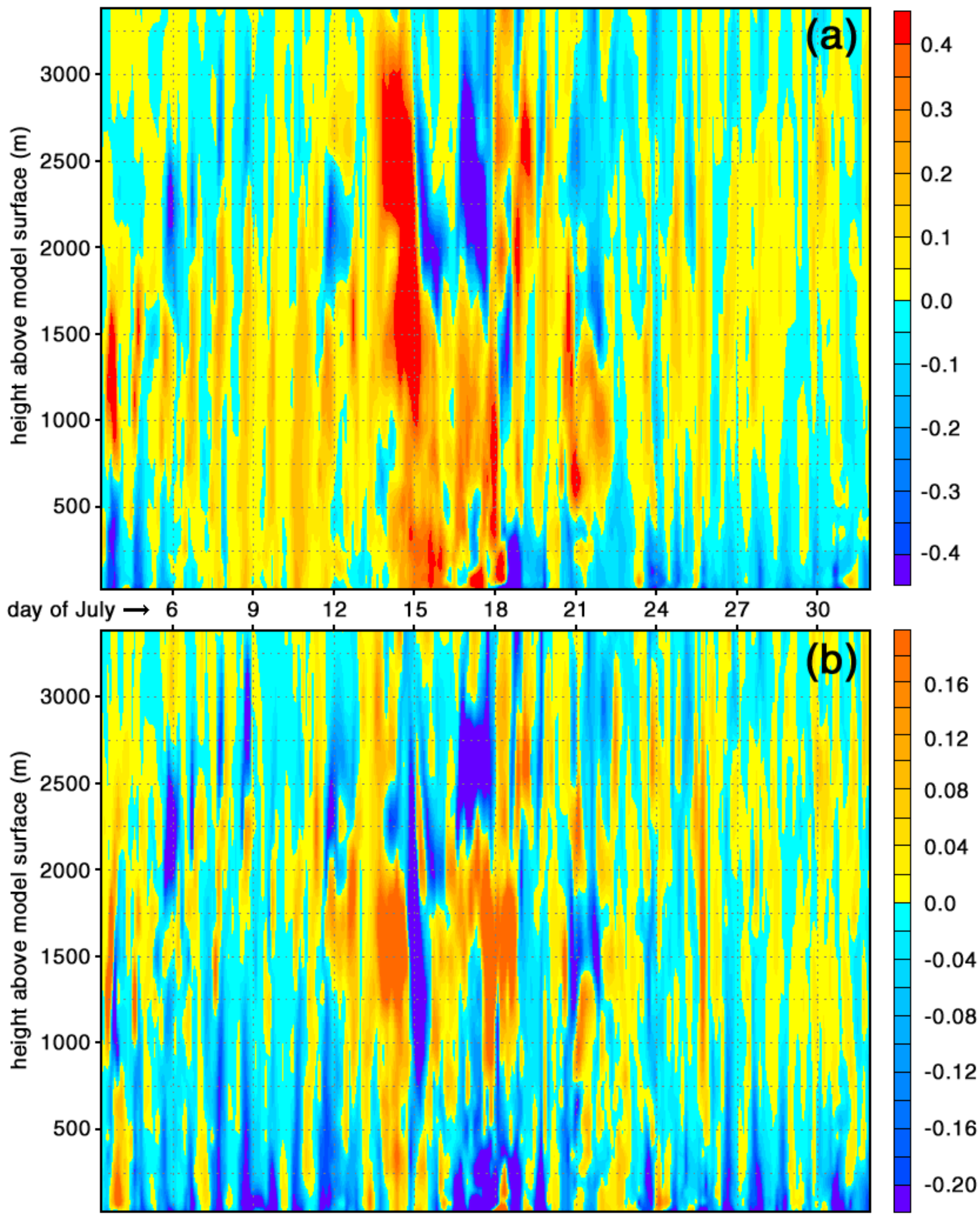

Figure 28. As in Figure 24, except for the differences in water vapor mixing ratio w_{mr} (a), and the differences in $\sigma(w_{mr})$ (b), between the ensemble runs. The units in both panels are in g kg^{-1}.

Figure 29

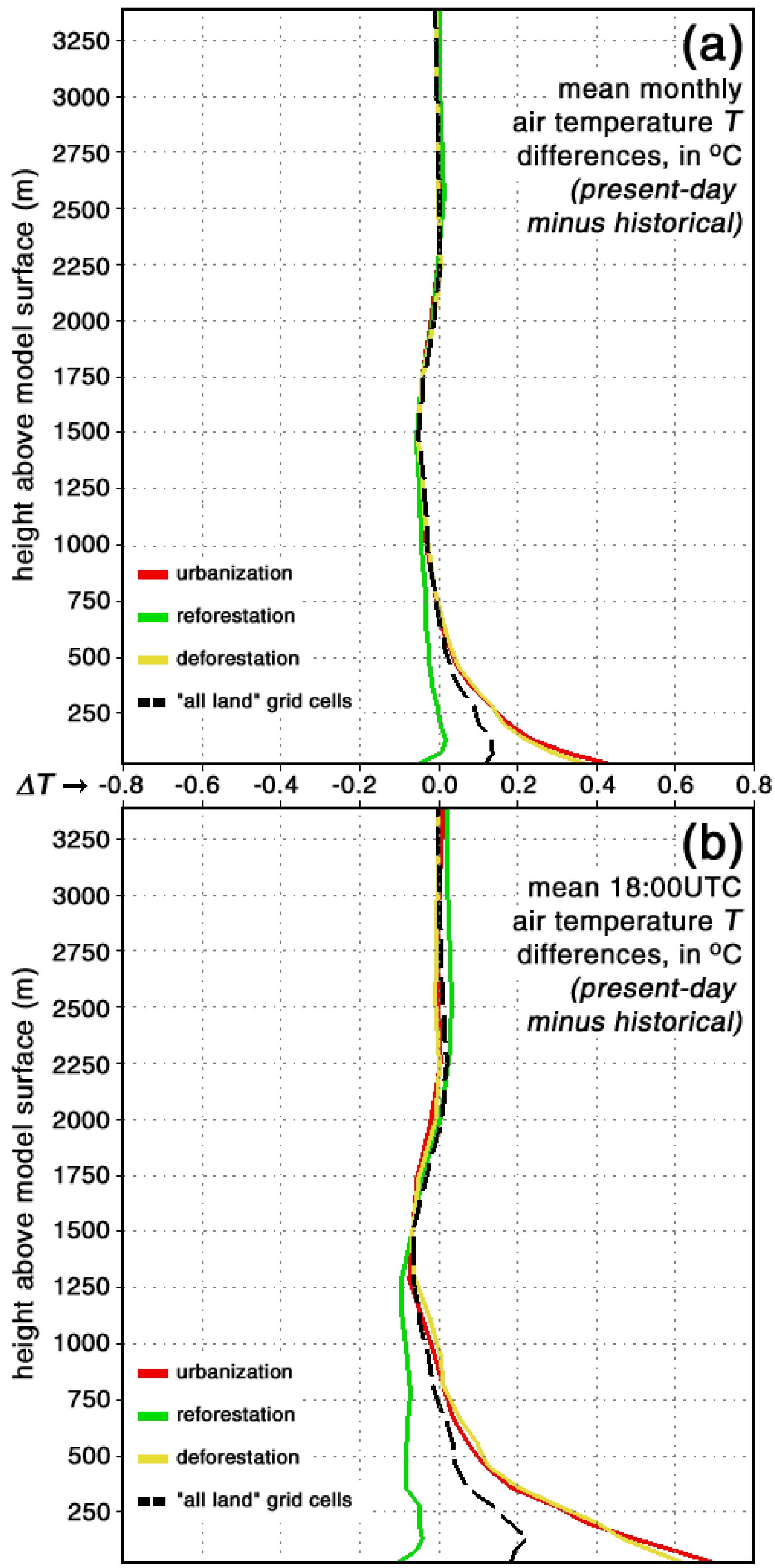
(a)
mean monthly
air temperature T
differences, in °C
(present-day
minus historical)
height above model surface (m)
3250
3000
2750
2500
2250
2000
1750
1500
1250
1000
750
500
250
urbanization
reforestation
deforestation
"all land" grid cells
$\Delta T \rightarrow$
-0.8
-0.6
-0.4
-0.2
0.0
0.2
0.4
0.6
0.8
(b)
mean 18:00UTC
air temperature T
differences, in °C
(present-day
minus historical)
height above model surface (m)
3250
3000
2750
2500
2250
2000
1750
1500
1250
1000
750
500
250
urbanization
reforestation
deforestation
"all land" grid cells

Figure 29 *(continued from previous page)*

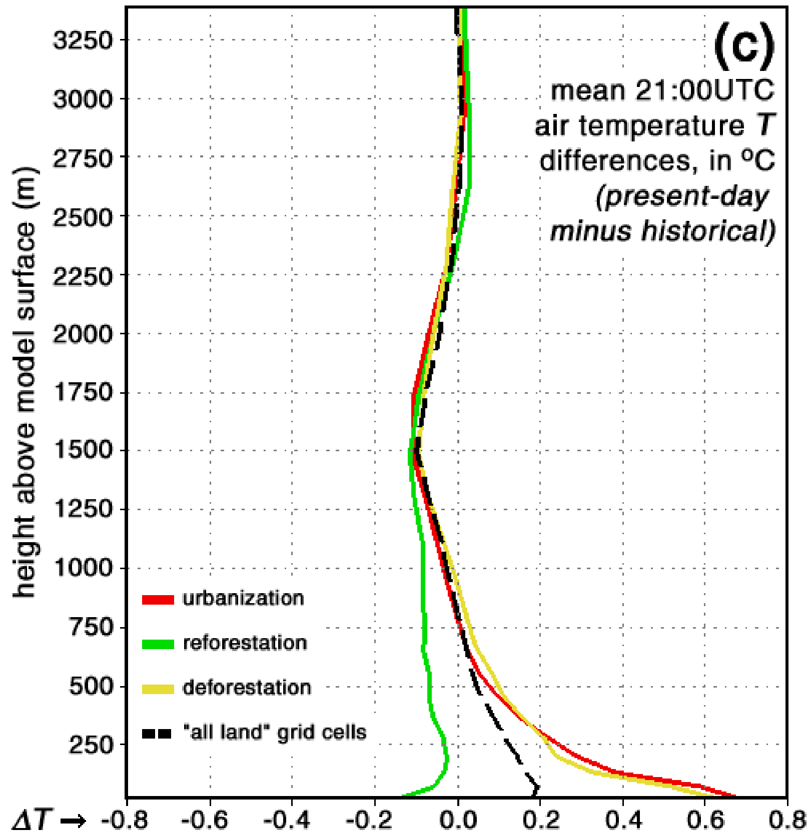

Figure 29. Mean domain-averaged air temperature *T* differences (present-day minus historical land cover), in degrees Celsius, for those grid cells that have experienced a change in dominant land cover resulting from urbanization (red), reforestation (green), deforestation (yellow), and for all land points on grid 3 (dashed black) on the revised grid. The panels show mean monthly *T* differences (a); mean differences at 18:00UTC (b); and mean differences at 21:00UTC (c). The x-axis represents the change in *T*; the y axis represents the height, in m, above the model surface.

Figure 30

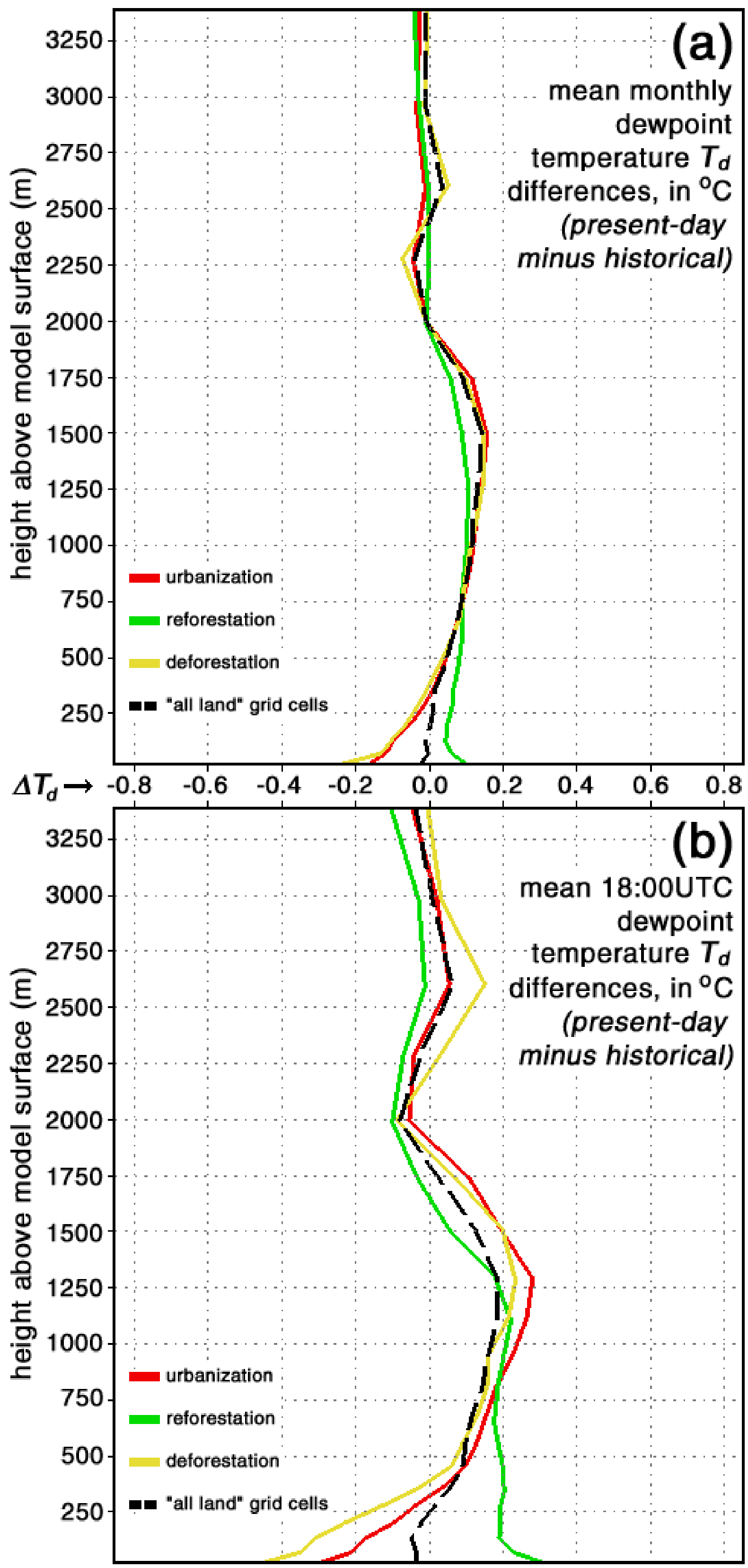

(a)
mean monthly dewpoint temperature T_d differences, in °C (present-day minus historical)
height above model surface (m)
3250
3000
2750
2500
2250
2000
1750
1500
1250
1000
750
500
250
urbanization
reforestation
deforestation
"all land" grid cells
$\Delta T_d \rightarrow$
-0.8
-0.6
-0.4
-0.2
0.0
0.2
0.4
0.6
0.8
(b)
mean 18:00UTC dewpoint temperature T_d differences, in °C (present-day minus historical)

Figure 30 *(continued from previous page)*

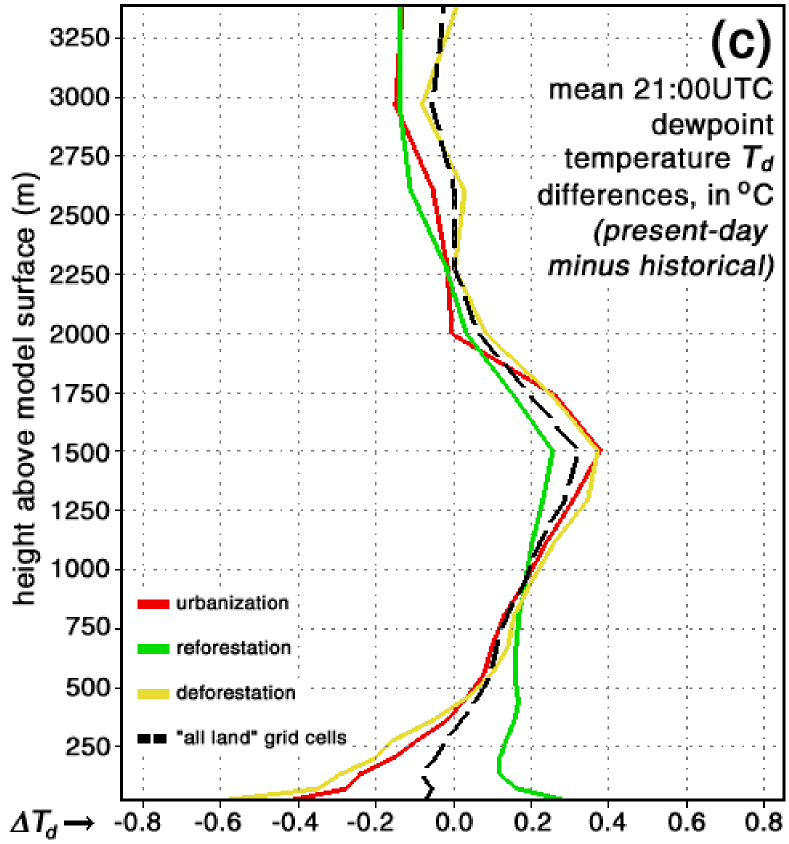

Figure 30. As in Figure 29 except for dewpoint temperatures T_d, in degrees Celsius, for the monthly mean (a); at 18:00UTC (b); and at 21:00UTC (c).

Figure 31

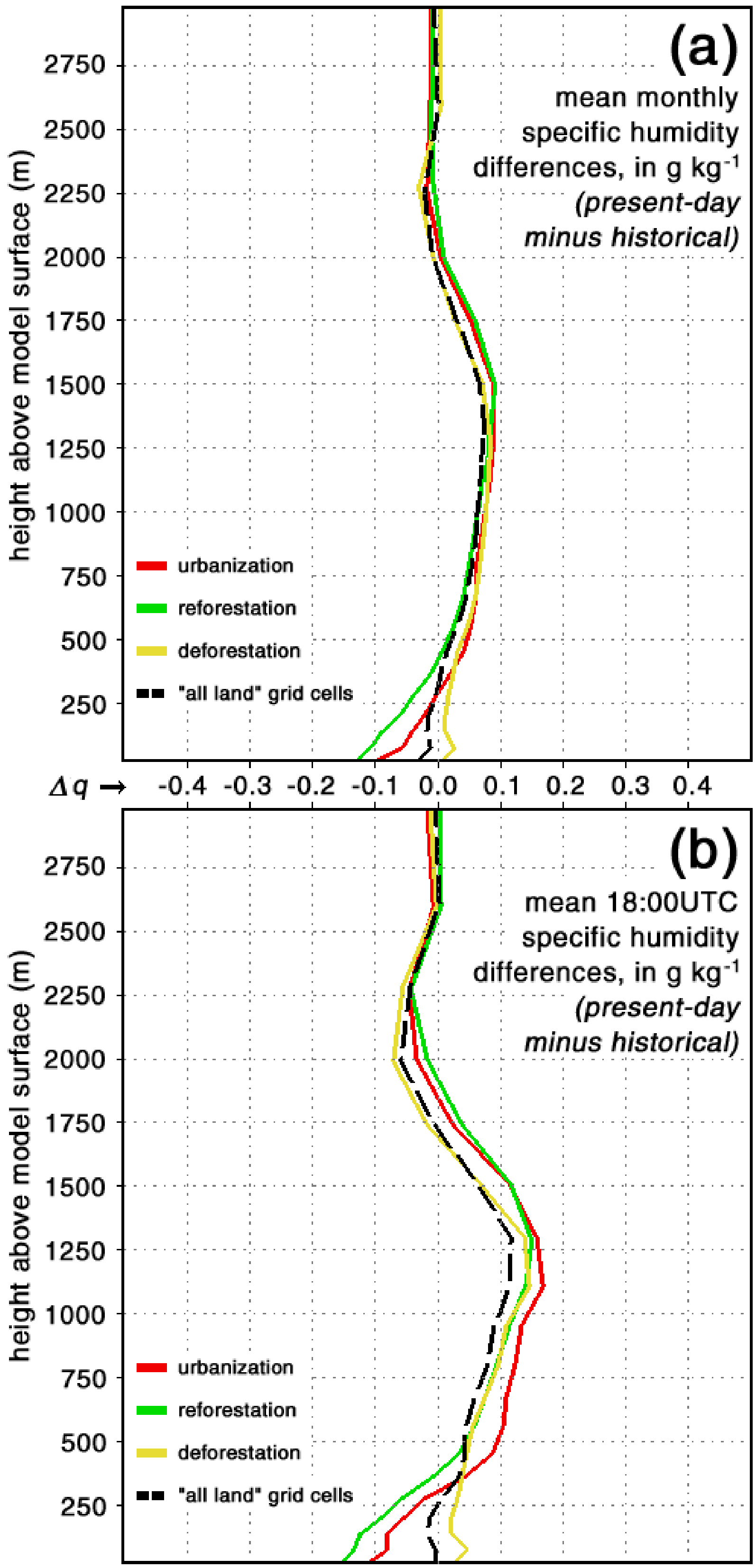
(a)
mean monthly
specific humidity
differences, in g kg-1
(present-day
minus historical)
height above model surface (m)
2750
2500
2250
2000
1750
1500
1250
1000
750
500
250
urbanization
reforestation
deforestation
"all land" grid cells
Δq →
-0.4 -0.3 -0.2 -0.1 0.0 0.1 0.2 0.3 0.4
(b)
mean 18:00UTC
specific humidity
differences, in g kg-1
(present-day
minus historical)
height above model surface (m)
2750
2500
2250
2000
1750
1500
1250
1000
750
500
250
urbanization
reforestation
deforestation
"all land" grid cells

Figure 31 *(continued from previous page)*

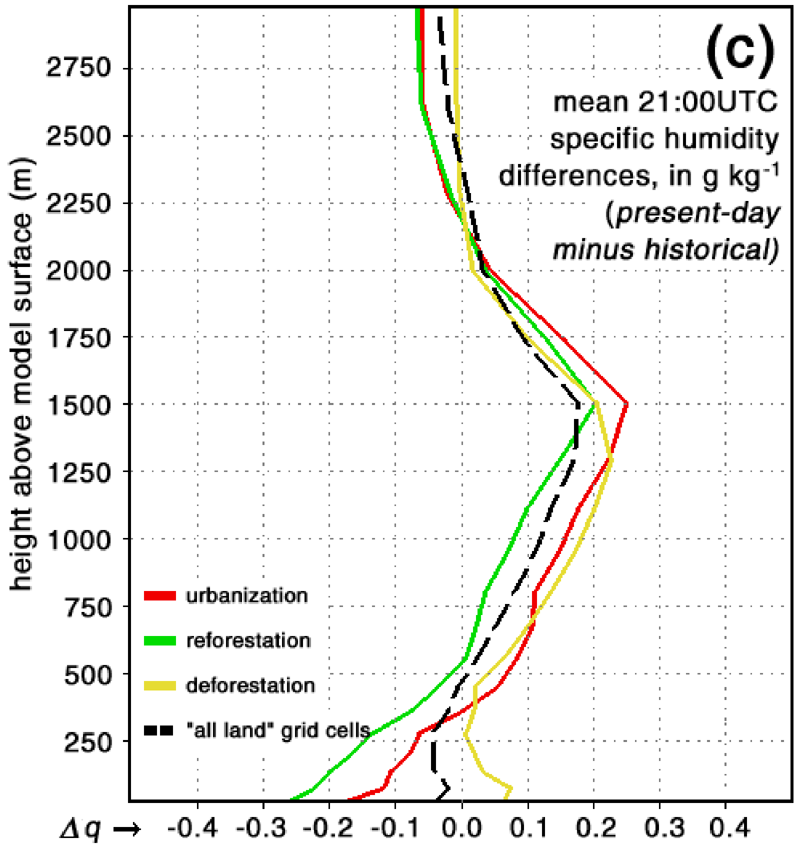

Figure 31. As in Figure 29 except for specific humidity q, in g kg^{-1}, for the monthly mean (a); at 18:00UTC (b); and at 21:00UTC (c).

Figure 32

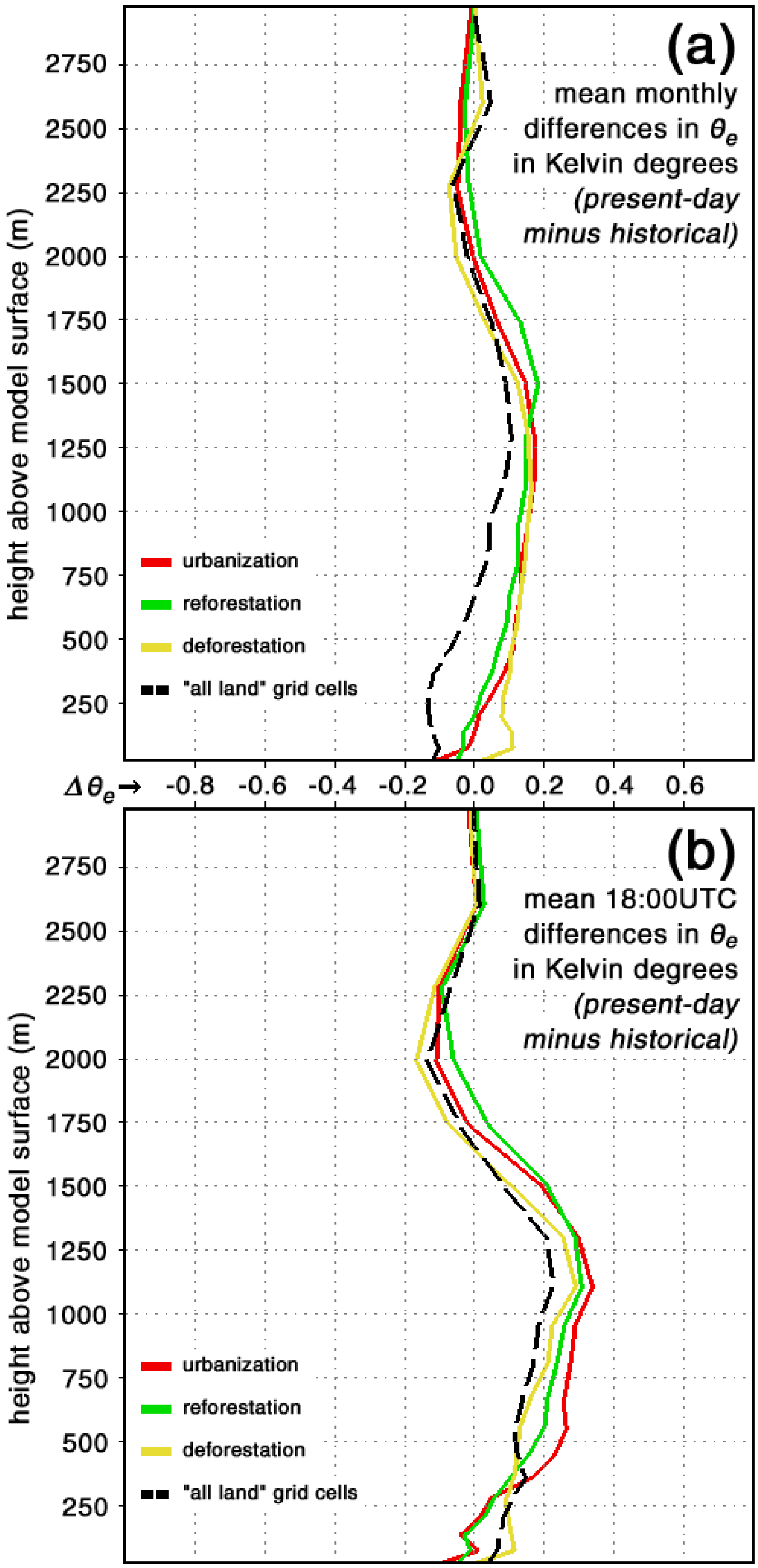
(a)
mean monthly
differences in θ_e
in Kelvin degrees
(present-day
minus historical)
height above model surface (m)
2750
2500
2250
2000
1750
1500
1250
1000
750
500
250
urbanization
reforestation
deforestation
"all land" grid cells
$\Delta\theta_e \rightarrow$
-0.8
-0.6
-0.4
-0.2
0.0
0.2
0.4
0.6
(b)
mean 18:00UTC
differences in θ_e
in Kelvin degrees
(present-day
minus historical)
height above model surface (m)
2750
2500
2250
2000
1750
1500
1250
1000
750
500
250
urbanization
reforestation
deforestation
"all land" grid cells

Figure 32 *(continued from previous page)*

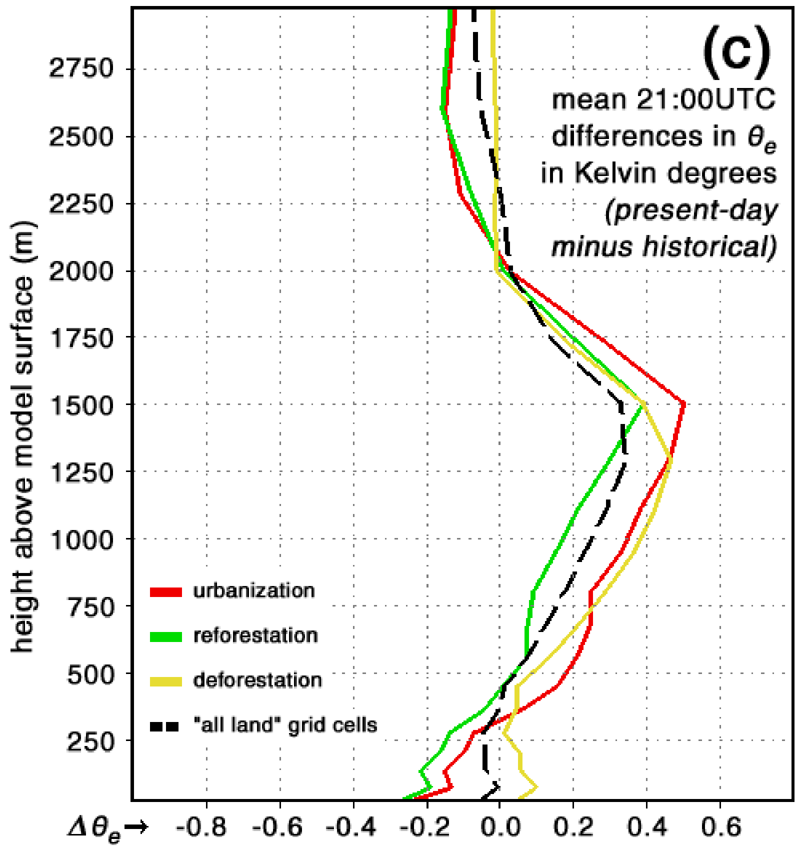

Figure 32. As in Figure 29 except for the differences in θ_e, in Kelvin degrees, for the monthly mean (a); at 18:00UTC (b); and at 21:00UTC (c).

Figure 33

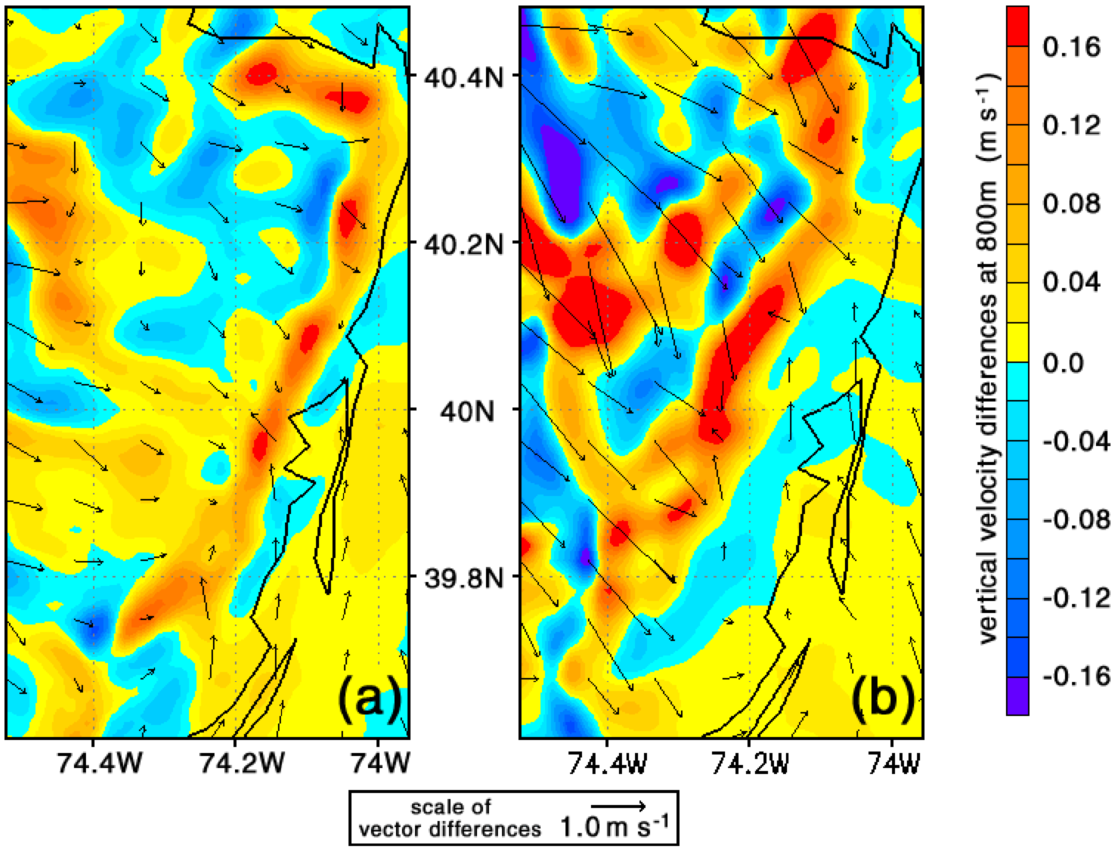

Figure 33. Mean vertical velocity differences (present-day minus historical land cover) at 800m (shaded, in m s^{-1}), shown with the mean horizontal wind vector differences at 360m (also in m s^{-1}), for a composite sea breeze day along the NJ coast, at 18:00UTC (a) and 21:00UTC (b). This is the domain used for the averages shown in Figures 34-35.

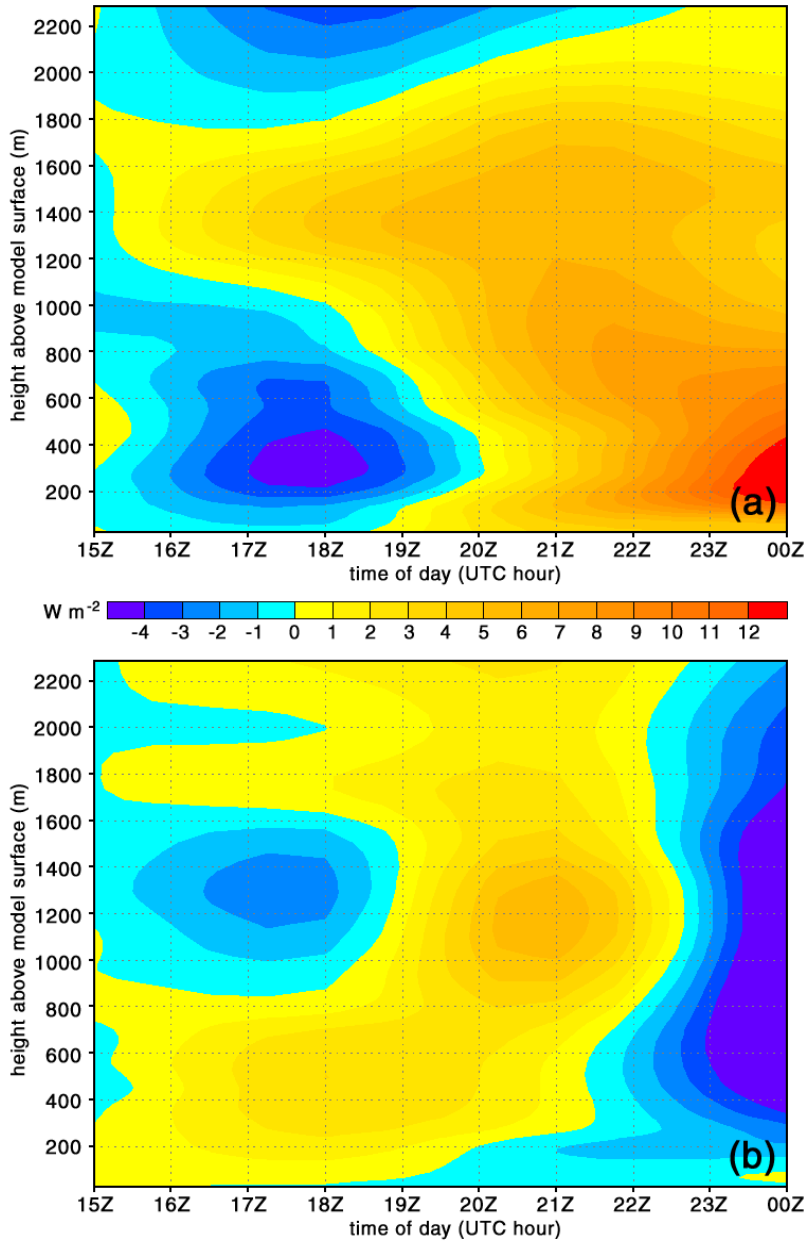

Figure 34. Mean daytime differences in the domain-averaged mesoscale flux of theta *tflux*, in W m^{-2} (a), and the respective differences in the domain-averaged mesoscale flux of water vapor *qflux*, also in W m^{-2} (b), from changes in sea breeze development between the historical and present-day ensembles. The fluxes are averaged over the coastal domain shown in Figure 33. The x-axis represents the time of day (UTC hour), and the y-axis represents the height, in m, above the surface.

Figure 35

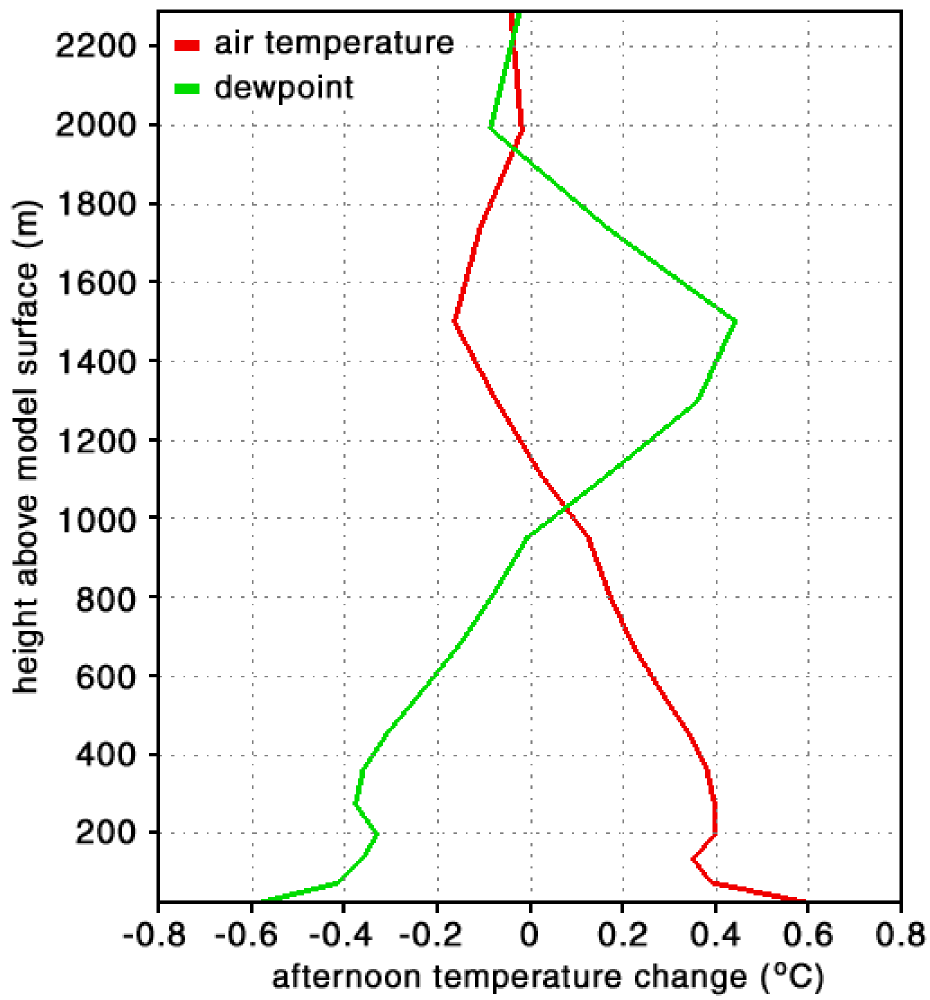

Figure 35. Mean domain-averaged vertical air temperature differences (red line, present-day minus historical land cover) and mean domain-averaged vertical dewpoint differences (green line) during a composite sea breeze afternoon along the NJ coast. This figure represents the mean temperature and dewpoint differences for the times between 18:00 UTC and 00:00 UTC in the region shown in Figure 33. The units for both lines are in degrees Celsius. The y-axis represents the height, in m, above the surface.

TABLES

Table 1. The 1880s-era Land Cover Types Identified on the Cook Map Series

forest type	non-forested wetlands	forested wetlands	other surface types
deciduous forest	cranberry bogs	pine swamp	pasture land
pine forest	freshwater marsh	cedar swamp	short grass
mixed forest	tidewater marsh		beach
	moist swamp		water
	peat		

Table 2. The Historical and Present-day Land Cover Classes and Their Reclassification to a LEAF-2 Category in RAMS

Historical Land Cover Classes	**NLCD Present-day Land Cover Classes**	**LEAF-2 Land Cover Class**
agriculture, pasture land, beach	mixed crop, pasture land, shrubs, grassland, bare rock, sand, other grains	agricultural and pasture land
deciduous forest	deciduous broadleaf forest, orchards	deciduous broadleaf forest
mixed forest	mixed forest	mixed forest with LEAF-2 displacement heights reduced by 5.0 m
evergreen forest	evergreen needleleaf forest	evergreen needleleaf forest
cranberry bogs, tide and freshwater marshes, peat, moist swamps	non-forested wetlands	non-forested wetlands, initialized with fully saturated soil below a 10-cm depth, with 85 percent and 88 percent saturation for the two top soil layers above 10 cm
pine swamp, cedar swamp	forested wetlands	50 percent deciduous shrub and 50 percent modified mixed forest, initialized with fully saturated soil below a 10-cm depth, with 85 percent and 88 percent saturation for the two top soil layers above 10 cm
urban	residential / commercial / industrial area	urban
water	water	water

The historical and present-day land cover classes, as noted in the first two columns, were reclassified to one of the eight LEAF-2 classes that represented a common set of land cover categories applied to both datasets.

Table 3. Land Surface Parameter (LSP) Values Used in the LEAF-2 Model

Land type	albedo[1]	emissivity	LAI	vfrac	z_o	Zdisp	root depth	LEAF-2
water	0.14	0.99	0.0	0.00	0.00	0.1	0.0	0
ENL forest	0.10	0.97	6.0	0.80	1.00	15.0	1.5	3
DBL forest	0.20	0.95	6.0	0.80	0.80	15.0	2.0	5
mixed forest[2]	0.15	0.96	6.0	0.80	0.80	15.0	2.0	38
decid. shrub[3]	0.20	0.97	6.0	0.80	0.10	1.0	1.0	13
agriculture[4]	0.18	0.95	6.0	0.83	0.08	0.8	1.0	15
wetlands[5]	0.12	0.98	6.0	0.80	0.03	1.0	1.0	17
urban	0.15	0.90	4.8	0.74	0.80	6.3	0.8	30

The heading abbreviations in this table are given here in parentheses, followed by the units, if needed: leaf area index (LAI), fractional coverage of vegetation in the grid cell (vfrac, from 0.0 to 1.0), net roughness (z_o, in m), displacement height (Zdisp, in m), rooting depth (root depth, in m), and LEAF-2 class number (LEAF-2).

---

[1] The standard LSP values are used, except that Zdisp has been lowered from 20.0 m to 15.0 m. The surface albedos for the vegetation classes are total solar broadband albedos based on *Lee* [1995] and *Walko et al.* [2000].

[2] The land cover type denoted above as "decid. shrub" represents deciduous shrub. Deciduous shrub was used to represent 50 percent of the surface land type for forested wetlands. The other 50 percent was mixed forest. Refer to Appendix C for additional details.

[3] The LSPs specified for this vegetation class represent an average of the LSPs of mixed cropland (LEAF-2 class 15) and tall grassland (LEAF-2 class 8). Thus, the land cover type denoted above as "agriculture" represents the agricultural and pasture land class I used in the model.

[4] This vegetation class represents non-forested wetlands.

Table 4. Mean Monthly Comparison of Temperatures and Dewpoints between Model and Observations

	July Mean Temperatures		**RMSE**	**July Mean Dewpoints**		**RMSE**
Station	**Observed**	**Simulated**	**Temperatures**	**Observed**	**Simulated**	**Dewpoints**
EWR	27.1	24.4	3.69	17.6	16.0	2.92
TEB	27.1	24.4	3.56	17.3	16.0	3.01
TTN	26.8	26.3	2.83	16.9	16.0	2.66
PNE	27.4	26.5	2.93	19.1	15.7	4.06
LGA	27.5	22.7	5.15	17.5	16.0	2.87
ABE	26.0	27.5	3.00	15.9	15.9	2.48
SMQ	25.9	26.5	3.39	17.4	16.1	2.64
NYC	27.3	22.9	4.77	17.4	16.1	2.62
ACY	26.0	20.9	5.60	18.5	16.1	3.48
ILG	26.8	25.4	3.81	19.1	16.3	3.53
PHL	27.6	26.3	3.15	19.0	16.0	3.81
MIV	25.6	23.0	4.07	19.1	16.2	3.61
VAY	26.7	25.6	3.25	18.6	16.0	3.62
PTW	26.4	27.4	3.19	16.4	16.0	2.54
RDG	26.5	27.6	2.93	16.9	16.0	2.51
Regional Avg	26.7	25.2	3.69	17.8	16.0	3.09

This is a comparison of the mean monthly observed air and dewpoint temperatures with the corresponding model-simulated values along with the respective RMSE for July 1999. The simulated air and dewpoint temperatures represent a mean layer average of the lowest 50m of the model atmosphere. All units are in degrees Celsius.

Table 5. Monthly Mean Percentage Change in Surface Heat and Radiative Flux Components, by Land Cover Conversion

	Q_H	Q_E	Q_N	R_{SW}	R_{LW}	R_N
all land points	1.2	7.5	3.6	0.3	1.8	0.8
urbanization	25.4	- 24.7	5.2	2.4	2.4	3.5
reforestation	-19.8	63.4	5.0	- 0.4	8.1	1.5
deforestation	29.6	- 25.6	- 0.8	1.5	- 4.6	0.8

These values represent the monthly mean percentage change (i.e., present-day land cover minus historical land cover), both for all land points and for each of the land cover conversions, in the surface heat and radiative flux components. These percentages are relative to 100 percent, and are each valid at 18:00UTC local time.

Appendices: Supplementary Information for Land Cover Reconstructions

Appendix A. Cook map series

The Cook map series has detailed land cover classes for the forests and wetlands within the state of New Jersey (NJ), as shown in Table 1. However, the map legend was incomplete and required some interpretation of forest types that were not explicitly identified. I interpreted regions of southern NJ that were depicted with asterisk-shaped symbols to be evergreen needleleaf forest, since these same symbols located within wetlands were clearly labeled as pine swamps. There were other, also apparently forested, areas with numerous cloud-shaped symbols that resembled the crown of a broadleaf deciduous tree; I interpreted these symbols as a deciduous forest cover type. Where these two symbols were numerous and evenly distributed, I assumed a mixed forest of evergreen and deciduous trees. The locations of deciduous, evergreen, and mixed forest types as I identified them are generally consistent with the distribution of these same forest types on a potential natural vegetation map for this region [*Kuchler*, 1964]. In addition, the general locations of the forests also correspond to those of present-day forest types as determined from recent Landsat imagery [*Vogelmann et al.*, 2001].

I used a three-step process to determine the fractional percentages of other historical land cover categories that were not explicitly mapped, including urban areas, pasture land, and mixed agricultural regions. First, I interpreted the extent of urban areas within NJ, and surrounding cities, such as New York and Philadelphia, from the coverage and density of the full road and rail network delineated on each map. Second, I interpreted a map symbol that resembled a few vertical blades of grass as pasture land or open areas dominated by grasses. Some of these areas closely correspond with the distribution of present-day pasture land. Finally, mixed agricultural land was then estimated based on residual fractional percentages within each grid cell once all other types were identified, a reasonable assumption because agriculture is known to have been a dominant land cover type in 19th-century NJ. The validity of this approach was demonstrated by the favorable comparison between my derived estimates and the large fractional percentages of improved agriculture in many NJ counties as documented in the 1880 U.S. Census, as well as from personal communications with county historical commissions across the state. To minimize potential uncertainty, I took the additional step of merging the mixed agriculture and pasture land data for each grid cell and averaging their respective biophysical properties (e.g., surface albedo, roughness, displacement heights) in the Land Ecosystem-Atmosphere Feedback model, version 2 (LEAF-2). The merging of these two land cover types is reasonable because their biophysical properties tend to be very similar during the growing season, especially relative to the biophysical properties of the other land cover classes I have used in my study.

Appendix B. 1880 U.S. Census data

I applied some adjustments and reconciliations to the census-based reconstruction based upon what is known about 19th-century land cover in the states surrounding NJ. The “other” non-farmland category, by default, was assumed to correspond primarily to urban regions, because it was most commonly associated with the locations of known villages and cities. However, in some cases, I assigned a different land cover class where urban land cover was not reasonably consistent with known historical land use. For example, the original forests that covered parts of eastern Pennsylvania (PA) and New York (NY) were repeatedly cleared or logged throughout most of the 1800s to support the demand for wood products for the lumber, fuel for heating, charcoal, and agriculture industries [*Dowhan et al.*, 1997]. By the late 19th century, the barren landscape had regenerated to short scrub oak with a mixed forest component. Since many of the grid cells with this "other" land cover class also covered a small fraction of total grid area, generally 10 percent or less, I reclassified the "other" land cover type within these cells to either deciduous forest or mixed agricultural land in the census dataset. Similar land cover adjustments were necessary within the eastern half of Long Island (LI), in Delaware (DE), and throughout Connecticut (CT).

Appendix C. Modifications to land cover types in LEAF-2

When preparing my surface datasets, I made two modifications to the land cover types in LEAF-2. First, to account for the regrowth of 19th- and 20th-century mixed forests that have occurred in the eastern U.S., I lowered the displacement height for the LEAF-2 mixed forest class by 5.0 m in both land cover datasets. This helped to maintain continuity with the displacement height of the evergreen forests that characterize the Pine Barrens, which are scattered among the mixed forests of southern NJ. The 15.0 m displacement height that I have assigned in LEAF-2 to the mixed forest class is consistent with the 11.0-15.0 m canopies of the pine-oak forests that are predominant in this region [*McCormick and Jones*, 1973].

Since the forested wetlands of NJ are also generally located in the Pine Barrens, I specified this land cover type in LEAF-2 to be a mixture of 50 percent deciduous shrub and 50 percent of my modified mixed forest [*Dowhan et al.*, 1997]. This characterization is consistent with the lowland vegetation of the region, as *McCormick* [1979] and *Olsson* [1979] noted that the forests within these wetlands are usually interspersed among understory shrubs of red maple, scrub oaks, and other broadleaf species. The initial soil water content for these forested wetlands (and for non-forested wetlands as well) was initialized in LEAF-2 as fully saturated for all soil layers below a depth of 10 cm, and with 85 percent and 88 percent of full saturation (~ 0.38 $m^3 m^{-3}$ volumetric soil water content for the silt clay loam soil type used here) at the two top soil layers (from the surface to a depth of 10 cm), with no standing water above the ground surface. This vertical profile of soil wetness reasonably describes the mean hydrology of the forested and non-forested wetlands of NJ during the warm season with little, if any, widespread above-ground inundation [*McCormick*, 1979]. I used the same initial wetland soil moisture conditions for both the historical and present-day simulations, which assumes that the depth of the groundwater table was the same in both periods, although empirical observations have suggested that this might not be true [*Epstein*, 2003; *M. Demitroff*, personal communication, 2004].

Although there was also no change in the LEAF-2 rooting depth for the same tree species between the historical and present-day datasets, I noted differences in the rooting depth by tree species. The trees within deciduous and mixed forests in LEAF-2 had mean rooting depths of 200 cm, while the trees within evergreen forests had shallower rooting depths of 150 cm [*McQuilkin*, 1935; *Little and Garrett*, 1990]. Since observational studies like *Rowe and Reimann* [1961] found that vegetative rooting depth and other factors can influence evapotranspiration (ET) rates, we may expect a change in forest composition between the late 19^{th} and 20^{th} centuries in a given region to have concomitant effects on surface air and dewpoint temperatures.

References

Dowhan, J., T. Halavik, A. Milliken, A. MacLachan, M. Caplis, K. Lima, and A. Zimba (1997), Calcareous habitats and Catskill High Peaks, in *Significant Habitats and Habitat Complexes of the New York Bight Watershed*, pp. 123-130, U.S. Fish and Wildlife Service's Southern New England - New York Bight Coastal Ecosystems Program, Charlestown, Rhode Island.

Epstein, C. M. (2003), Is the Pine Barrens water table declining? What does the record show? In *Periglacial Features of Southern New Jersey: Field Guide and Proceedings of the Geological Association of New Jersey, 20th Annual Meeting, October 10–11, 2003,* edited by M. J. Hozik and M. J. Mihalasky, Richard Stockton College of New Jersey. Pomona, New Jersey, 79–92.

Kuchler, A. W. (1964), The potential natural vegetation of the conterminous United States: New York, American Geographical Society, Special Publication No. 36, scale 1:3,168,000.

Little, S., and P. W. Garrett (1990), Chamaecyparis thyoides (L.) B.S.P: Atlantic white cedar, in Burns, R. M. and B. H. Honkala [tech. coords.], *Silvics of North America, Volume 1, Conifers. Agric. Handb. 654*, U.S. Department of Agriculture and U.S. Forest Service, Washington, D.C., 103-108.

McCormick, J. (1979), The vegetation of the New Jersey Pine Barrens, in *Pine Barrens: Ecosystem and Landscape*, edited by R. T. T. Forman, pp. 229-243, New York Academic Press, New York City, New York.

McCormick, J., and L. Jones (1973), The Pine Barrens: Vegetation geography, in *New Jersey State Museum, Research Report No. 3*, 76 pp., Trenton, New Jersey.

McQuilkin, W. E. (1935), Root development of pitch pine, with some comparative observations on shortleaf pine, *J. Agric. Res.*, *51*, 983-1016.

Olsson, H. (1979), Vegetation of the New Jersey Pine Barrens: A phytosociological classification, in *Pine Barrens: Ecosystem and Landscape*, edited by R. T. T. Forman, pp. 245-263, New York Academic Press, New York City, New York.

Rowe, P. B., and L. F. Reimann (1961), Water use by brush, grass, and grass-forb vegetation. *J. Forestry*, *59*, 175-181.

Vogelmann, J. E., S. M. Howard, L. M. Yang, C. R. Larson, B. K. Wylie, and N. Van Driel (2001), Completion of the 1990s National Land Cover Dataset for the Conterminous United States from Landsat Thematic Mapper Data and Ancillary Data Sources, *Photogrammetric Engineering and Remote Sensing*, *67*, 650-662.

ACKNOWLEDGEMENT OF PREVIOUS PUBLICATIONS

Wichansky, P. S., L. T. Steyaert, R. L. Walko, and C. P. Weaver (2007), Evaluating the effects of historical land cover change on summertime weather and climate in New Jersey: Part I: Land cover and surface energy budget changes. *J. Geophys. Res.*, in press.

Wichansky, P. S., C. P. Weaver, L. T. Steyaert, and R. L. Walko (2006), Evaluating the effects of historical land cover change on summertime weather and climate in New Jersey, p. 128-163, in *New Jersey's Environments: Past, Present, and Future*, edited by Neil M. Maher, Rutgers University Press, New Brunswick, New Jersey.

In the above two publications my first graduate advisor Roni Avissar deserves thanks for suggesting the broad idea, but I fully developed it with C. Weaver (my Ph.D graduate advisor starting in the second year of the Ph.D candidacy). I was fully responsible for the collection, organization, and interpretation of the historical land cover data for NJ. L. Steyaert provided the historical Census data for the surrounding states and assisted with obtaining the proper resolution of the NLCD dataset and suggested land cover reconciliations. I have written most of the text with valuable revisions and refinements by C. Weaver and L. Steyaert, including insightful critiques by L. Steyaert. R. Walko provided programming to use my land cover datasets in RAMS/LEAF-2, suggested valuable insights that allowed us to use the model to its full potential, and explained some of the figure trends that may have initially been confusing. I created all figures using GrADs and Adobe® Photoshop, and was the liaison between my authors and the journal/book. I also co-presented this research with C. Weaver at a Rutgers University conference in 2003, and presented at a NJIT book conference in 2006.

Wichansky, P. S., and R. Harnack (2000), A diagnosis of tropospheric effects upon surface precipitation amount for a sample of East Coast snowstorms. *Wea. and Forecasting*, *15*, 339-348.

This publication was derived from my Masters thesis. The idea for this paper was mine, under the guidance of my graduate advisor R. Harnack. I have written most of the text with edits by R. Harnack. I have performed all data collection, including the organization and extraction of data from LCD reports at 5 stations (which required visits to the NOAA library in Washington D.C.). I also performed all analyses and constructed the figures and enhanced using Adobe® Photoshop. R. Harnack submitted the manuscript to the journal, and I followed up on all required edits.

Wichansky, P. S. (1996), The correlation of upper tropospheric humidity (UTH) with 6.7μm GOES-8 brightness temperatures. *Proc., Fifteenth AMS Conf. On Weather Analysis and Forecasting*, Norfolk, VA, Amer. Meteor. Soc., 44-47.

This preprint was derived from my research during an internship with the National Environmental Satellite, Data, and Information Service (NESDIS). I have written programs using the McIDAS software and collected and organized the data. I wrote the preprint and presented this research at the 1996 AMS conference in Norfolk, Virginia. I have a draft of an unpublished manuscript based on this research, but it was not peer-reviewed. Frances Holt was my immediate supervisor.

CURRICULUM VITAE (C.V.)

Paul Stuart Wichansky

I. EDUCATION

1993 B.S., Meteorology.
Cook College, Rutgers University
Class Rank 43rd of 532. Graduated with Honors.
Recognized by the Dean at the Masters / Ph.D ceremony

1999 M.S., Meteorology.
Rutgers, the State University of New Jersey.

2008 Ph.D, Environmental Sciences, option in Atmospheric Science
Rutgers, the State University of New Jersey.
2001 and 2002 N.J. Agricultural Experiment Station Graduate Scholar

II. EXPERIENCE

1994 to 1996 National Environmental Satellite, Data, & Information Service (NESDIS)
National Oceanic and Atmospheric Administration (NOAA)
Aviation Cooperative Meteorologist

- Developed and refined McIDAS-based software to evaluate the applications of GOES-8 water-vapor imagery in estimating upper tropospheric humidity
- Assisted with the processing of daily Special Sensor Microwave Imager (SSM/I) data from satellites to establish a global soil wetness climatology
- Verified an experimental precipitable water product that combines SSM/I data, GOES-8 soundings, and ETA model guidance to enhance flash flood forecasting
- Participated in explaining features of satellite imagery and model output to students involved in a science awareness program sponsored by N.O.A.A.
- Occasionally hosted daily satellite discussions and model forecast briefings

2001 to present A Vision in Motion Speakers Bureau
Motivational Speaker

- Motivational and keynote speaker specializing in peer leadership, disability and multicultural awareness, character education, self-esteem enhancement, substance abuse prevention, and anti-bullying strategies
- Audiences have covered a broad spectrum that includes K-12 schools, colleges, organizations, and professional companies in 18 U.S. states
- Highlights include keynotes at the United Nations and Special Olympics; numerous youth and peer leadership conferences, and keynotes in the education, medical, social, and human services fields

III. PUBLICATIONS

Wichansky, P. S. (1996), The correlation of upper tropospheric humidity (UTH) with 6.7µm GOES-8 brightness temperatures. *Proc., Fifteenth AMS Conf. On Weather Analysis and Forecasting*, Norfolk, VA, Amer. Meteor. Soc., 44-47.

Wichansky, P. S., and R. Harnack (2000), A diagnosis of tropospheric effects upon surface precipitation amount for a sample of East Coast snowstorms. *Wea. and Forecasting*, *15*, 339-348.

Wichansky, P. S., C. P. Weaver, L. T. Steyaert, and R. L. Walko (2006), Evaluating the effects of historical land cover change on summertime weather and climate in New Jersey, p. 128-163, in *New Jersey's Environments: Past, Present, and Future*, edited by Neil M. Maher, Rutgers University Press, New Brunswick, New Jersey.

Wichansky, P. S. (2007), One man can make a difference: A letter from Paul Stuart Wichansky, in Appendix I of *Don't Hassel the Hoff (David Hasselhoff: The Autobiography)*, edited by P. Thompson, pp. 273-278, St. Martin's Press, New York, New York.

Wichansky, P. S., L. T. Steyaert, R. L. Walko, and C. P. Weaver (2008), Evaluating the effects of historical land cover change on summertime weather and climate in New Jersey: Land cover and surface energy budget changes. *J. Geophys. Res.*, in press.